Alma Mater Studiorum – Università di Bologna

DOTTORATO DI RICERCA IN

Meccanica e Scienze Avanzate dell'Ingegneria

Ciclo XXVIII

Settore Concorsuale di afferenza: Area09/A2

Settore Scientifico disciplinare: ING/IND13

Computational modeling of stability and laxity in the natural and implanted knee joint

Presentata da: Dott. Ing. Irene Sintini

Coordinatore Dottorato — Prof. Ing. Vincenzo Parenti Castelli

Relatore — Prof. Ing. Vincenzo Parenti Castelli

Esame finale anno 2016

Abstract

The knee joint plays a central role in human motion for its dual function: providing a large range of motion in flexion/extension and stability in the other degrees of freedom (DoF). Computational modeling is a powerful tool to deepen our understanding of the joint mechanics, overcoming the main limitations of experimental investigations, i.e. time, cost and impracticability, and providing valuable insights for prosthetic design, rehabilitation and surgical planning. Within this background, the specific aim of this dissertation is threefold.

- The aim of the first study (Chapter 2) to define a predictive kinetostatic model of the tibiofemoral joint by means of a sequential procedure, in order to analyze its behavior both in passive and in loaded conditions. Anatomical surfaces and all the main ligamentous structures are included in the model. To verify the predictive capabilities of the model, no parameter optimization is performed. The model is validated by comparing its motion to experimental data from the literature under several loading conditions. Then anatomical surfaces are replaced with spherical ones in order to evaluate how this simplification affects tibiofemoral motion. Anatomical articular surfaces provide results closer to the reference kinematics, but the accuracy of the two models is comparable. Predictions of the model with spherical surfaces are less accurate when the loads are larger. Ligament and contact forces are also analyzed and they are in reasonable agreement with previous studies. The model proves to effectively replicate the behavior of the human knee in passive and loaded conditions.

- The aim of the second study (Chapter 3) is to develop a dynamic specimen-specific model of the tibiofemoral (TF) and patellofemoral (PF) joint and to validate it by means of *in vitro* experimental data from a squat activity. The kinematic models of the TF and PF joints are developed following the sequential

approach. First, the kinematic model is defined from the passive motion and subsequently the joint compliance is optimized to match laxity tests data from the literature. A computational framework was developed to reproduce the loading conditions of the test rig used to carry out the experimental tests. The quadriceps force needed at the joint to replicate the squat activity is computed in two different ways: in a kinematics-driven simulation, through a static optimization process, and in a 6 DoF force-driven finite-element (FE) simulation, through a proportional-integral (PI) controller. The quadriceps force predicted by the 6 DoF FE model is in good agreement with the one predicted by the static optimization, but both are smaller than the experimental quadriceps force from the test rig. The scope of the FE model was also to analyze quantities not experimentally measurable, such as ligament and contact forces during the squat activity.

- The aim of the third study (Chapter 4) is to introduce a novel method to evaluate TKR by determining the compressive loading required to achieve natural knee stability. Pre-clinical assessment of stability in total knee replacement (TKR) is crucial for developing preferred implant performance. Current TKR patients often experience joint instability that the human body addresses with compensatory strategies. Specifically, an increased quadriceps-hamstrings co-contraction serves to increase joint stability through an increased compressive force across the TF joint. Four current TKR geometries in both their cruciate-retaining and posterior-stabilized forms are modeled in a finite-element (FE) framework. The FE model is initially validated experimentally using traditional knee laxity testing with a constant compressive load and anterior-posterior (A-P) displacement or internal-external (I-E) rotation. Model predictions of constraint are in reasonable agreement with experimental results. The FE model is subsequently interfaced with a feedback controller to vary the compressive force

that the implant requires in order to match experimental natural knee I-E and A-P stability at different flexion angles. Results show that the lower conformity TKR designs require on average 66.7% more compressive load than high conformity designs to achieve natural knee constraint. As expected, TKR stability and compressive load requirements to replicate natural kinematics vary with inclusion of tibiofemoral ligaments. This study represents a new and physiological approach to evaluate stability in existing TKR geometries and to design implants that better restore natural knee mechanics.

Acknowledgements

I am very grateful to all the people that accompanied me during my experience as a PhD student in the past three years.

First, I must thank Prof. Vincenzo Parenti Castelli for his kind support and his professional guidance, and Dr. Nicola Sancisi for his precious help in many of the problems I had to face in my research.

I would like to thank Dr. Peter Laz and Dr. Paul Rullkoetter for giving me the opportunity to work as a visitor scholar at the Computational Biomechanics Lab at the University of Denver.

I want to thank all my friends and fellow graduate students in Bologna and Denver for making my work at Aula Masi-Carducci and MET fun and never boring.

A big thank you goes to my parents, Michele and Rita, for their unconditional support and love, at home and far from it, and to my husband Alessandro, without whom this work would not have been possible.

To my husband Alessandro.

Contents

List of Tables

List of Figures

Contents

Chapter 1

Introduction

In the Introduction, a brief background on the knee joint anatomy, function and common diseases as well as an overview of the state-of-the-art in the healthy and implanted knee modeling will be offered. The objective of the Introduction is to clarify the research rationale behind the studies presented in the following chapters.

1.1 The knee joint

The knee joint consists of two articulations in one: the first articulation is between the condyles of the femur and the corresponding condyles of the tibia, i.e. the tibiofemoral joint (TF) [37]. The second articulation is between the posterior side of the patella and the anterior distal part of the femur (throclea), i.e. the patellofemoral joint (PF) [37]. The TF joint could be thought as a simple hinge, but indeed it allows a 6 degrees of freedom (DoF) motion between the tibia and the femur (Fig. 1.1). The PF joint also allows 6 DoF between the femur and the patella. The knee meets two apparently opposite functional requirements: mobility and stability. It must provide a large range of motion in flexion/extension and stability in the other DoF, in order for the lower limb to properly perform any motor task. In addition, it is subjected to a load of the order of multiple body weight and therefore it must offer extensive

weight-bearing support. As a result, the knee is predisposed to degenerative diseases and commonly injured, and it frequently necessitates surgical interventions. These peculiar features make the knee one of the most complex and fascinating articulations of the human body and justify the great amount of research interest that it raises.

Ligaments and articular surfaces (Fig. 1.2) are the main structures that guide the relative motion between the joint bones and that stabilize the joint. Ligaments are bands of fibrous connective tissue that connect the articular extremities of bones; they are characterized by a force-elongation relationship, therefore a mechanical stiffness, and they exhibit viscoelastic properties. The main ligaments crossing the TF joint are the cruciates and the collaterals. The anterior cruciate and posterior cruciate ligament (ACL and PCL) are the structures that restrain respectively the anterior and posterior displacement of the tibia with respect to the femur. The cruciates originate in between the femoral condyles and have their attachment locations on the very anterior (ACL) and posterior (PCL) part of the tibial plateau. The medial and the lateral collateral ligament (MCL and LCL) are responsible for resisting respectively the internal and external rotation of the tibia and they provide stability in varus-valgus DoF as well. The MCL is on the medial side of the joint and it consists of two bundles, a short deep bundle and a superficial bundle that has its attachment more distally on the tibia. The LCL connects the femur with the fibula, a bone on the lateral side of the tibia that can be thought fixed to the tibia in the biomechanical analysis of the joint. Secondary soft tissue structures, such as the oblique popliteus ligament (OPL), the anterolateral structure (ALS), the posterior capsule (POST CAP) and the oblique posterior ligament (OPL), play a secondary but noteworthy role in stabilizing the joint. In the knee, as in any other human joint, direct bone-to-bone contact is avoided by means of cartilage layers that are on the distal part of the femur, on the proximal part of the tibia and on the posterior face of the patella. Cartilage is made of closely packed collagen fibers whose primary functions are to provide a

bearing surface with extremely low friction, reducing wear and permitting a smooth relative motion between the joint bones, and to distribute the load by increasing the contact area and therefore decreasing stress. Moreover, the knee is a synovial joint, meaning that it is surrounded by a synovial membrane which secretes a lubricating fluid into the joint cavity to facilitate frictionless motion between the bones. Menisci are important structures for the mechanics of the knee joint too (Fig. 1.2). They are two semilunar-shaped mobile pads of fibrocartilaginous tissue mostly made of collagen fibers, as the cartilage is, that provide an extra cushioning essential for one of the main task of the knee joint, which is weight-bearing. Menisci act to spread the load transmitted between the femur and the tibia, increasing the contact area and therefore reducing the average pressure on the articulating surfaces [35] and they also facilitate shock absorption at the joint. Ligaments and articular surfaces can be thought as passive structures of the joint, meaning that they do not actively generate force but they exert force only in response to external loads, determining the mobility of the joint. The mobility of an anatomical joint is defined by the range and pattern of unrestrained movement of the articulating bones [26]. As for the knee, it can be said that its mobility is controlled by the geometrical arrangement of the passive anatomical structures, above all ligaments and articular surfaces [30, 108].

The active structures that play a role in the knee mechanics are the muscles spanning this joint. Muscles are bundles of fibrous tissues that have the ability to contract in order to generate a relative motion or to maintain the relative position of the bones in the joint that they cross. In the case of the knee, the muscles crossing it generate all the forces necessary for the lower limb to perform any dynamic activity. Knee muscles can be divided in two groups: flexors and extensor. Flexor muscles are the hamstrings, namely the biceps femoris, the semimembranosus, the semitendinosus (Fig. 1.3), and they are responsible for the tibia to flex with respect to the femur. Extensor muscles are the quadriceps (rectus femoris, vastus medialis, lateralis and

intermedius) and the medial and lateral gastrocnemius, and they are responsible for the tibia to extend with respect to the femur. Flexion-extension mechanism is completed by the patellar ligament (Fig. 1.3), that connect the distal part of the patella to the anterior part of the tibia, permitting the quadriceps force to be transferred to it. Muscles are attached to the joint bones through tendons, which are cords of tough fibrous tissue capable of transmitting force. Together with the patellar ligament, the quadriceps tendon is part of the extensor mechanism of the knee, and it connects the quadriceps muscle group to the patellar bone (Fig. 1.3).

1.2 The Total Knee Arthroplasty

As mentioned before, the knee is particularly susceptible to various injures, such as ligament or meniscus tears, and diseases, the most common of which is osteoarthritis. Osteoarthritis (OA) is a degeneration of joint cartilage and the underlying bone and it affects weight-bearing articulations. OA, also known as the inflammatory form of the osteoarthrosis, causes pain and loss of mobility at the joint and it is a primary cause of disability in the elderly population. Many are the factors that can lead to this disease, such as age, injury, obesity and genetic predisposition. So far no cure exists for OA and the only known working procedure to restore joint mobility and functionality and to relieve pain is the total knee arthroplasty (TKA) or replacement (TKR). TKA is a surgical intervention consisting in the substitution of the damaged articular surfaces of tibia, femur and possibly patella with artificial devices (Fig. 1.4). Its incidence is estimated to reach 3.5 million of case in the United States of America by 2030 [56], without considering the surgical revision that many times is needed after the intervention because of infection, wear or loosening of the implant. TKA surgical procedure has a high successful rate, with typical 10-year survivorship near 95% [36, 88]. In most of the cases, TKA involves the resection of the

ACL and, in some cases, depending on the implant design, also the resection of the PCL. It is clear then that this surgical procedure deprives the knee of its key stability structures, namely the articular surfaces, the menisci and one or both the cruciate ligaments. Therefore the ultimate goal of the TKR components must be to restore normal knee mechanics, meaning that the implants must be capable of transmitting load, providing sufficient stability and allowing enough mobility at the joint, properly interacting with the soft tissue surrounding it, in a similar way to what the healthy knee does. In other words, according to [106] TKR aims to offer to the implanted joint the proper balance between stability and laxity. The femoral component and the tibial tray are generally made of a cobalt chromium molybdenum alloy. The tibial insert and the patella component are instead made of ultra-high-molecular-weight polyethylene (UHMWPE), a polymer that offers high abrasion resistance and superior wear properties. Both cobalt chromium molybdenum alloys and UHMWPE are biocompatible and yield a low coefficient of friction, though higher than the one that the cartilage provides. Various designs have been developed through the years, since the first TKA were performed in the 1960s: fixed or mobile-bearing, cemented or uncemented, with or without patellar resurfacing, with different degrees of conformity between the tibial and femoral components, all-polyethylene or metal-back, symmetrical or asymmetrical. The asymmetrical TKR design deserves some attention. It consists in a conforming medial side and a low constraint lateral side, in the attempt to replicate the natural asymmetrical morphology of the knee: despite that, this design struggles to raise a real interest in the biomechanical world [106]. Differences exist also in the surgical approach chosen for the implant procedure, namely the mechanical alignment and the kinematic alignment approach [14]. The intent of kinematic alignment is the restoration of the normal three-dimensional orientation of the knee, permitting some degrees of varus-valgus between the femur and the tibia, while the mechanical alignment consists in having the hip, the knee and the ankle

joint centers positioned along a straight line. The two most noticeable groups of TKR designs are cruciate retaining (CR) and PCL sacrificing or posterior-stabilized (PS) implants. The CR design takes advantage of the PCL to limit the anterior sliding of the femoral component on the tibial insert. However, in some OA knees, the PCL is damaged along with the cartilage, or the surgeon determines that its function cannot be retained with TKA. In such cases, the PCL is resected and the PS implant is used. The PS design typically incorporates a cam in the tibial insert and a post mechanism in the femoral component to restrict the tibial posterior displacement, in the attempt to artificially replace the function of the PCL.

1.3 Why modeling the knee?

Despite the high success rate of the TKA procedure, persistence of pain after the surgery [15] and knee instability, particularly during high-demand activities [74, 76], remain a common complaint of TKR patients. Investigating the mechanics of the bones, articular cartilage, menisci, ligaments, as well as the kinematics of the TF and PF joints and the muscular loads is crucial to effectively improve the TKR design and surgical procedure. Some of the joint mechanical quantities are relatively straightforward to measure either *in vivo* or *in vitro*, such as the TF and PF relative motion. Instead, it is problematic to experimentally assess the loads through the joint structures, such as muscles, ligaments and contact surfaces, particularly *in vivo*. For this reason, the development and validation of reliable computational models of the joint is essential [109]. Biomechanical models are a useful tool to understand the mechanical behavior of the knee, allowing the quantification of the key factors influencing it and, therefore, the prediction of the functional capabilities of the natural and implanted joints. Models can complement experimental testing and provide a cost and time-efficient framework to investigate the interactions between the implant

and the bone, the contact loads acting at the joint, the joint kinematics and the constraints offered by the soft tissue. When modeling the knee joint, a certain level of approximation must be tolerated, given the complexity of the anatomical structures involved. A relevant source of uncertainty comes from the large variability of mechanical and geometrical properties in any biological tissue. Subject-specific and specimen-specific models try to reduce this variability by identifying as many parameters as possible and replicating a specific patient or experiment. However, some level of uncertainty can never be eliminated, because of the impossibility to directly measure certain properties. For example, when *in vitro* laxity tests are performed on cadaveric knees to measure the restrain offered by the ligaments, the mechanical properties of single ligaments cannot be measured without compromising the integrity of the joint. When direct measurements are not available, averaged data from the literature are often used in place of them. A fundamental step to develope a reliable biomechanical model is its validation, which is particularly challenging because of the already mentioned difficulties in obtaining *in vivo* or *in vitro* data. An example of the challenges in the validation process is the lack of muscle forces measurements: electromyography (EMG) signals and instrumented implants are the only available tools that allow a qualitative or indirect comparison of computational estimates to *in vivo* data. Several approaches have been used to develop computational models of healthy and TKA knees: the two most common approaches, i.e. multibody and finite element modeling, are presented hereafter.

1.3.1 Multibody modeling

A multibody dynamic system consists of solid bodies, or links, connected to each other by joints that limit their relative motion. Multibody models can be used for both forward and inverse dynamic analysis, depending on the goal of the computational simulation. When a forward dynamics simulation is performed, boundary conditions

are applied to the model and its motion is forward-integrated and predicted; on the other hand, an inverse dynamics analysis calculates the loads needed at the joints to generate a certain motion. In the past, musculoskeletal models of the knee primarily consisted of analytical rigid body representations with simplified geometry, ligaments modeling and contact definitions. Some models were limited to the sagittal plane [18, 79, 97], while others were three-dimensional [12, 108]. These models, in their simplicity and within the limited computational power that was available at the time, could still claim a good accuracy in predicting joint kinematics, ligament and contact forces. A noteworthy modeling approach is the sequential procedure [30]: this approach relies on the notion that isometric ligaments and articular contact guide passive flexion and that the other five DoF are coupled to flexion during the passive motion [108, 109]. It is a three-step procedure that starts from the definition of a kinematic model of the joint, i.e. a model of the passive motion, used then as a starting point for the kinetostatic and dynamic models (second and third step, respectively). The advantage of the procedure is that each step does not invalidate the previous ones, preserving their capabilities. It is worth notice that the kinematic model developed through the sequential procedure is accurate and simple at the same time, and it can easily be included in more complex musculoskeletal models of the lower limb [70]. The sequential approach is the one adopted for the two studies on the natural knee presented in this dissertation (Chapter 2 and Chapter 3). Multibody modeling evolved as more powerful software became available. Bloemker et al. [13] used Adams (MSC Software Corporation, Santa Ana, CA) to develop a computational model of the knee and of a dynamic knee simulator, in order to validate the joint model. Adams is used in Chapter 2 of this dissertation for the development of a kinetostatic model of the knee. Opensim, an open source multibody code specifically designed for the musculoskeletal modeling, was introduced in 2007 by researchers at Stanford University and it is now worldwide spread [19]. Opensim offers specific tools for computing inverse kinematics,

inverse dynamic and forward dynamic analysis on musculoskeletal models. It also has the capabilities to estimate muscular forces for a given motion, by performing a static optimization that minimizes the sum of the squared muscular activation at each time frame to solve for the muscle redundancy [19]. Muscle redundancy is due to the fact that in the human body there are more muscles than DoF therefore there are infinite combinations of muscle forces that result in the same joint motion. One of the advantages of Opensim is that it allows different levels of complexity in the model: for example, the knee joint can be modeled as a simple hinge, as a one DoF mechanism in which translations and rotations are coupled to the flexion, or as a 6 DoF mechanism that includes ligaments [111] and contact forces [60]. Opensim is used in Chapter 3 of this dissertation to compute the quadriceps force during a squat activity.

1.3.2 Finite element modeling

The finite element (FE) analysis is a well-known and broad used tool in the biomechanical world, because it provides the right platform to overcome the difficulties related to the computing of stress, strain and contact areas of complex shapes such as the anatomical and prosthetic surfaces [24]. For this reason, FE models of both the natural [7] and the TKR joint [33, 46] have been and are successfully developed by many biomechanical researchers, and they are used to predict joint kinematics and contact mechanics, as well as ligament forces. The capability to estimate stress and contact pressure in the healthy and TKR joint makes the finite element technique a significantly valuable tool for implant design. Moreover, ligaments [7], menisci [83] and cartilage [53] can be efficiently and effectively modeled in the FE platform. While recent advances in model development and simulation platforms offer a wide range of tools to investigators, the decision making process during modeling and simulation has become more opaque [24]. The risk is that FE modelers are often uninformed about the limitations of their models and the simulation software and therefore they

compromise the goodness of their own results not knowing the boundaries of their trustworthiness. In order for a FE model to be reliable, some precautions have to be taken into account, such as having a refined enough mesh, i.e. small enough element, and using a small enough time increment to run the analysis. In fact, a convergence study on these two quantities is always suggested for the output quantities to be reliable. These rules become clearer once the mathematical process behind a FE simulation is explained. The healthy and implanted knee models presented in this dissertation in Chapter 3 and Chapter 4 were developed using Abaqus/Explicit (Abaqus, Inc., Providence, RI). Abaqus/Explicit uses a central difference rule to integrate equations of motion "explicitly" through time, using the kinematic conditions at one increment to calculate the kinematic conditions at the next increment. At the beginning of an increment the program solves for dynamic equilibrium. The accelerations are integrated through time using the central difference rule, which calculates the change in velocity assuming that the acceleration is constant. Thus, satisfying dynamic equilibrium at the beginning of the increment provides the accelerations. Knowing the accelerations, the velocities and displacements are advanced "explicitly" through time. The term "explicit" refers to the fact that the state at the end of the increment is based on the displacements, velocities, and accelerations at the beginning of the increment. It is important to note that the explicit method is based on the assumption that the nodal accelerations are constant during an increment. For the method to produce accurate results, the time increments must be quite small, and, as a result, analyses typically require many thousands of increments. However, unlike the traditional implicit FE method, solving each iteration in explicit is computationally inexpensive. In the case of rigid-body analyses, the internal stresses and strains are not computed, and the problem is simplified to the calculation of just the nodal displacements under specified contact definitions. This represents a substantial saving in computational time.

1.4 Purpose of this work

The overall purpose of the research presented in this dissertation is to possibly advance the current knowledge on the modeling of the natural and implanted knee, with particular focus on the factors that influence its stability and laxity. Each one of the three studies presented in the following chapters has a specific aim, as listed below.

- The aim of the study presented in Chapter 2 is twofold. The first goal is to assess if a sequentially-defined kinetostatic model of the TF joint, featuring anatomical surfaces and a complete representation of the joint soft tissue, could be exempt from optimization, and therefore claim predictive capabilities. The second goal of this study is to evaluate the performance of spherical contact surfaces, when they are used in place of anatomical surfaces, in kinetostatic conditions.

- The aim of of the study presented in Chapter 3 is to develop a dynamic specimen-specific sequentially-defined model of the TF and PF joint, starting from the findings of Chapter 2, and to validate it by means of *in vitro* experimental data from a squat activity. Another goal of this study is to compare different techniques to predict the muscular force necessary to perform the squat activity and to understand to to which extent the knee representation influences these predictions.

- The aim of of the study presented in Chapter 4 is to introduce a novel method to evaluate TKR joint by determining the compressive loading required to achieve natural knee stability. The goal of the study is also to understand to which extent implant geometry influences such compressive load.

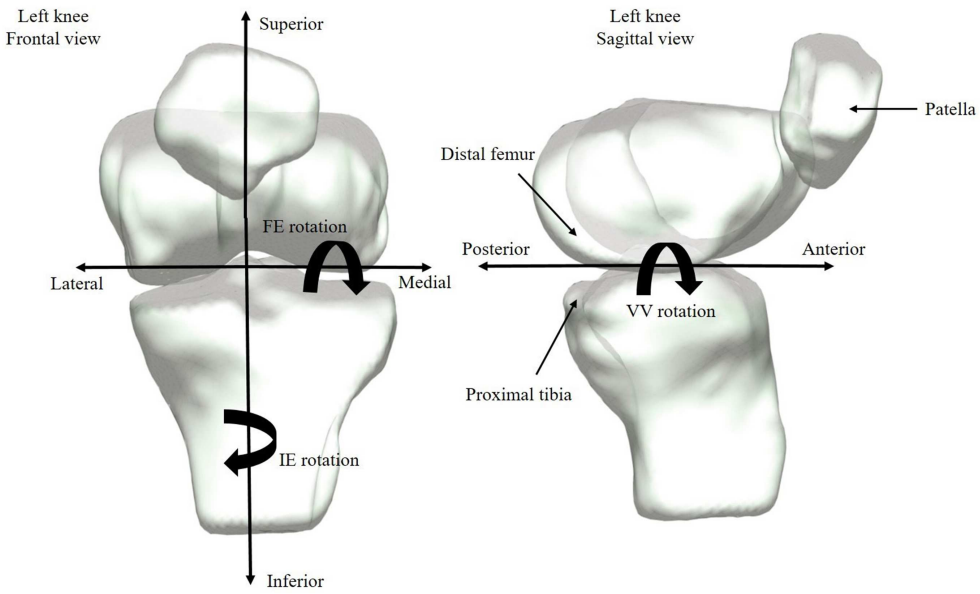

Figure 1.1: Tibiofemoral (TF) and patellofemoral (PF) joints. The 6 degrees of freedom (DoF) of the tibia and the patella with respect to the femur are: flexion-extension (FE), internal-external (IE) and varus-valgus (VV) rotation, medial-lateral (ML), superior-inferior (SI) and anterior-posterior (AP) translation.

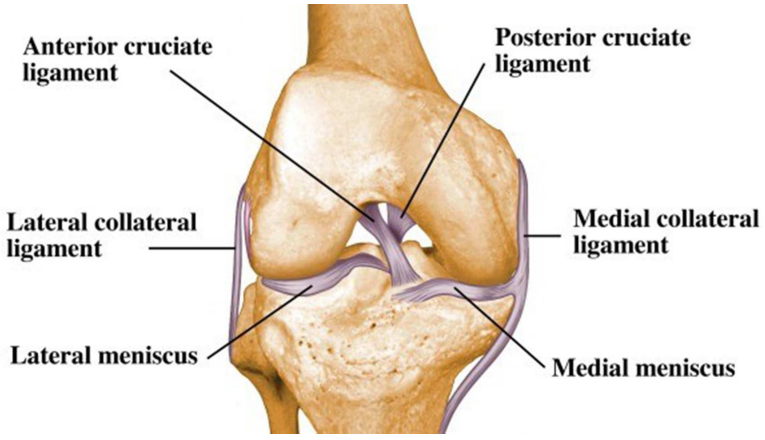

Figure 1.2: Soft tissue in the TF joint. Anterior cruciate ligament (ACL), posterior cruciate ligament (PCL), medial collateral ligament (MCL), lateral collateral ligament (LCL), medial and lateral menisci.

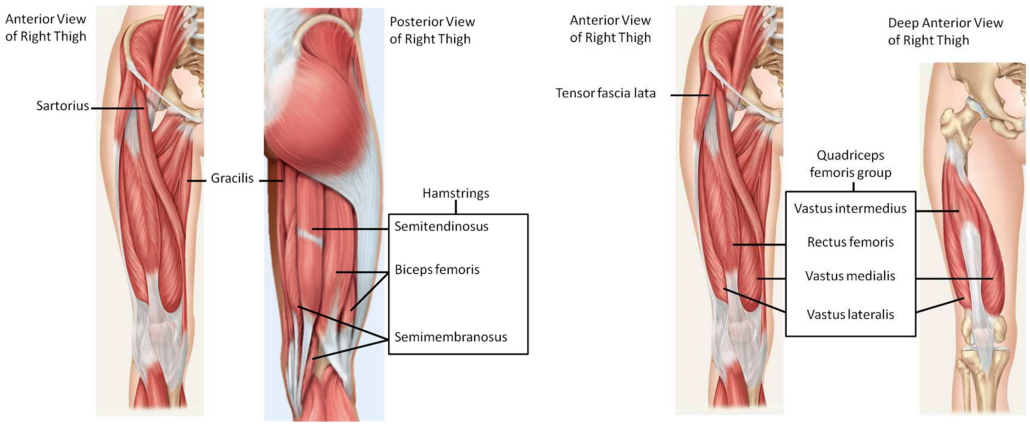

Figure 1.3: Main muscles crossing the knee joint: hamstrings (biceps femoris, semimembranosus, and semitendinosus) and quadriceps (rectus femoris, vastus medialis, vastus lateralis and vastus intermedius).

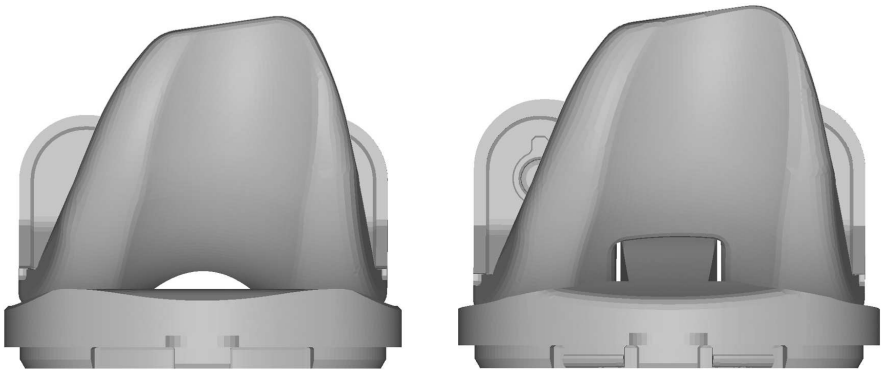

Figure 1.4: Femoral component and tibial insert of P.F.C. Sigma®, a TKR design from DePuy Synthes Inc., Warsaw, IN: cruciate retaining (CR) design (left) and posterior stabilizer (PS) design (right).

Chapter 2

Sequentially-defined kinetostatic models of the knee with anatomical and spherical surfaces

2.1 Introduction

The knee joint has always played a central role in the human motion for its dual function: it provides a large range of motion in flexion/extension and stability in the other degrees of freedom (DoF). Many mathematical models have been presented in the literature to investigate the dynamic behavior of the knee and two main approaches can be identified. The first one is the simultaneous approach, which does not separate the analyses of joint mobility and stability, solving the kinematic and dynamic analyses of the joint in a single step [1, 13, 49]. The second method is the sequential approach, which considers the kinematic, kinetostatic and dynamic analyses in subsequential steps. First, a model that solves only the kinematic analysis is defined. This model replicates the passive motion of the knee and it includes only the structures involved in this type of motion (ligaments and articular surfaces). Then, based on this first

step, two more models are defined [30,81,82,93,110]. The second model replicates the behavior of the joint in kinetostatic conditions by including the compliance properties of the articular structures. The third model includes the muscle actions and it solves the dynamic analysis of the joint. Through the sequential approach, joint mobility is addressed in the first step with the kinematic model, whereas joint stability is modeled in the following two steps with the kinetostatic and dynamic models. This approach allows a step-by-step identification of the model parameters by including in each step only the structures involved in the current analysis [30, 93]. For this reason the sequential approach preserves the role played by the passive structures for both the mobility and the stability of the joint. In other words, it ensures that the kinetostatic and dynamic models are still able to replicate the passive motion, in addition to the the loaded motion.

A sequentially-defined kinetostatic model of the knee has been previously presented [93]. This model included the main ligamentous structures and a spherical approximation of the articular surfaces. The mechanical characteristics of the ligaments were found in the literature and then optimized to fit the reference experimental kinematics. The spherical approximation simplified the definition of the articular surfaces and the contact representation. The model proved to correctly replicate both passive and loaded motion. However, the optimization of the elastic parameters may be an issue in some applications because it is a time consuming process and it requires a target loaded motion that, unlike the passive motion, is hardly achievable *in vivo*.

The main purpose of this study is to verify whether the model parameter optimization can be avoided by using the sequential approach and by including a more detailed and complete representation of the passive structures of the knee. This would allow predictive potentialities for the model in loaded conditions and it could free from technical issues related to the optimization procedure. Therefore, a new kinetostatic model of the knee is defined in this study, according to the sequential

approach. This model is based on an extension of a preliminary work [100] and it is consistent with many previous studies [22, 29, 51, 90, 93] which emphasize an accurate replication of the passive motion as a key point for a precise description of the human joints kinematics. Articular anatomical surfaces and almost all the ligamentous structures of the knee are included in the new kinetostatic model in such a way that does not alter the passive motion of the preliminary kinematic model. Assessment of the model behavior is performed by comparing its motion during standard laxity tests to target kinematics from the literature [31, 41, 55, 85]. In addition, as a further validation, ligament and contact forces are analyzed for selected loading conditions and qualitatively compared to previous studies [1, 7, 34, 40, 47, 65, 66, 80].

A limitation of several subject-specific models of the knee is that anatomical geometries are needed to model the tibiofemoral (TF) contact [61] and the segmentation from MRI images is a time consuming process that requires manual work. Spherical approximations of the contact surfaces are instead quickly obtainable from anthropometric measurements and they closely replicate the anatomical surfaces during passive motion [93], with the advantage of a simpler contact representation. The second goal of the present work is then to evaluate the performance of spherical contact surfaces in kinetostatic conditions by assessing their influence on the TF motion when they are used in place of anatomical surfaces. Therefore, articular surfaces are replaced in the model by spherical surfaces and the motions resulting from the two models are compared. This analysis shows to which extent a simplified surface representation can be reliable.

2.2 Methods

The kinetostatic model presented in this study is developed as the second step of a procedure which includes three sequential steps [30]. A kinematic model (M1)

of the knee with the main passive structures of the joint was defined to accurately reproduce the passive motion. Then the kinetostatic model (M2) was defined as a generalization of the kinematic model by adding the remaining passive structures to it and by including the viscoelastic properties of all the structures. M2 replicated the joint behavior when external loads are applied, but it did not involve muscle forces. In the generalization from M1 to M2, the parameters of the kinematic model were not changed and the newly added structures must not alter the passive motion. With a proper identification of the model parameters, all the structures added in M2 remain almost slack during the passive motion. For this reason M2 could replicate the knee passive motion as well as M1, in addition to the joint loaded motion.

2.2.1 Experimental Session

Experimental data collected in previous investigations were used for the model definition [91, 93]. Geometries of a right knee specimen were obtained with a stereophotogrammetric system (Stryker Navigation System, Stryker-Leibinger): anatomical landmarks, TF articular surfaces, origin and insertion areas of the main knee ligaments, namely anterior cruciate ligament (ACL), posterior cruciate ligament (PCL), medial collateral ligament (MCL), lateral collateral ligament (LCL), were digitized as point clouds. Bone geometries were segmented from a CT scan of the joint. The combination of bone geometries and digitized point clouds allowed an accurate reconstruction of the joint surfaces. Anatomical landmarks were used to define two anatomical coordinate systems, $\mathcal{S}_f$ for the femur and $\mathcal{S}_t$ for the tibia. The origin of $\mathcal{S}_t$ is located at the center of the tibia, i.e. the deepest point in the sulcus between the medial and lateral tibial intercondylar tubercles. The x-axis is orthogonal to the plane defined by the two malleoli and the center, anteriorly directed. The y-axis is directed from the mid-point between the malleoli to the tibia center. The z-axis is consequently defined according to the right hand rule. The origin of $\mathcal{S}_f$ is located at

the mid-point between the lateral and medial epicondyles. The x-axis is orthogonal to the plane defined by the two epicondyles and the femoral head center, directed anteriorly. The y-axis is directed from the origin to the femoral head center. The z-axis is consequently defined to form a right-handed triad of axes.

2.2.2 Kinematic Model

The kinematic model is based on an equivalent mechanism presented in previous studies [21, 78, 81, 82]. It replicates the passive motion of the knee, which is guided by two articular contacts and three isometric ligament fibers [110]: one fiber of the ACL, one of the PCL and one of the MCL. In this step, the knee was modeled as a one DoF mechanism (Fig. 2.1) composed by two rigid bodies, i.e. the femur and tibia, connected by three rigid links, i.e. the isometric fibers, and two sphere-on-sphere pairs that represent the contacts between the two femoral condyles and the tibial plateau [78,81,82]. The geometrical parameters of the model were the location of the origins and insertions of isometric fibers and sphere centers, the ligament lengths and the sphere center distances, i.e. the sum of the radii of the lateral pair spheres and the difference of the radii of the medial pair spheres. Once the geometrical parameters are identified on the specimen, the passive motion can be calculated by solving the loop closure equations of the mechanism. The full identification procedure is described in previous studies [82, 91]. The articular surfaces were approximated by best-fitting spheres and the attachment sites of the isometric fibers are determined according to origin and insertion areas. This preliminary estimates were then optimized to best replicate passive motion of the specimen.

2.2.3 New Kinetostatic Model

The second step of the sequential approach is the definition of the kinetostatic model M2 as a generalization of the kinematic model M1. M2 included anatomical articular surfaces and a detailed representation of the ligamentous structures.

Articular Surfaces

The femoral and tibial surface point clouds, previously obtained by the stereophotogrammetric system and used for the kinematic model definition, were aligned and merged with CT scans, in order to combine the geometrical accuracy of the first method to the completeness of the second one. The alignment was performed with the software Rhinoceros 3D (Robert McNeel and Associates) (Fig. 2.2). However, according to the sequential approach definition, the anatomical contact surfaces must not alter the passive motion of the knee. Therefore, the constraints provided by the anatomical surfaces during the passive motion must be kinematically equivalent to the two sphere-on-sphere contacts of the kinematic model. The envelope procedure was used for this purpose. The aligned femoral surfaces were moved using the kinematic model in order to obtain their conjugated surfaces on the tibia during a passive flexion arc. Two relevant sections of the conjugated surfaces around the contact areas were isolated (in green in Fig. 2.3). These sections were then merged with the aligned experimental surfaces of the tibia (in red in Fig. 2.3). The surfaces of the tibia obtained with this method were very similar to the experimental ones, thanks to the accuracy of the kinematic model. The tibial and femoral surfaces obtained with this method were then imported as triangular meshes in Adams (MSC Software Corporation), the multibody dynamics software where the new M2 model is implemented. Rigid contact with a stiffness coefficient of 10^5 $N/mm^{2.2}$ and a damping coefficient of 10 Ns/mm was imposed between the surfaces.

To study the influence of surface approximation on the joint behavior, a second model (M2s) was developed by replacing the anatomical surfaces with the spherical surfaces of the kinematic model. M2s is exactly the same as M2, except for the surface definition. Rigid contacts was then imposed between the spheres.

Ligament Modeling

Each ligament was represented in the model by a group of fibers, for a total of thirty-five fibers. Origin and insertion of each fiber were determined on the bone surfaces according to measurements on the specimen and to data from the literature. Attachment areas of ACL, PCL, MCL and LCL were measured on the specimen. Origins and insertions were then chosen inside the areas according to descriptions in the literature [32,48,64,72]. The ACL, PCL and MCL featured, among the others, one isometric fiber, i.e. ACL iso, PCL iso, MCL iso, which represented the corresponding rigid link in the kinematic model. These fibers were modeled as elastic elements in the kinetostatic model, but they were still called isometric to distinguish them from the fibers not included in the kinematic model. The popliteal tendon (PT) was modeled with two fibers whose origin and insertion coordinates were chosen according to [64]. The oblique popliteal ligament (OPL) was modeled with three fibers, two medial and one lateral, as described in [57]. The origins of the three fibers were located in the proximal lateral aspect of the joint, on the fabella, which can be thought as rigidly coupled to the femur. The insertion of the OPL lateral fiber was just lateral to the PCL insertion; the two medial fibers had their insertions on the medial aspect of the tibia. The posterior oblique ligament (POL) was included in the model although its existence as a distinct ligament is still debated [52, 57, 59, 84]. According to [52], the POL was modeled with two fibers as a stand-alone ligamentous structure. It can be thought as a thickening of the capsular ligament which extends obliquely and posterior from the femoral adductor tubercle to the posteromedial part of the tibia,

with a length of about 50 mm when the knee is fully extended. Its the tibial insertion was located approximately 15 mm under the joint line. The fabellofibular ligament (FFL) [23, 67] was modeled with two fibers that originated on the fabella, close to the OPL origin. Their insertions were located on the fibular styloid, close to the LCL insertion area, and the distance between the LCL and FFL origins was set to 20 mm [34]. Some authors pointed out a negative correlation between the FFL and the arcuate ligament [47, 67], therefore, only the FFL was considered in the model. The choice was based on the larger amount of accurate information on the geometry of the FFL compared to the few available data on the arcuate ligament [23,38,47,58,64,67]. Two capsular structures were included in the model: the posterior capsule (CAP) and the mid-third lateral capsular ligament (MLCL). The CAP was modeled with three fibers: medial, intermedial and lateral [86]. The origins of the three fibers were proximal to the articular margin of the femoral condyles and their insertions were near the tibial articular margin. In particular, the lateral fiber origin was 19 mm proximal to the origin of the OPL, while its insertion is lateral to the insertion of the PCL [57]. The MLCL is an anterolateral structure which can be described as a thickening of the lateral capsule and it is also known as anterolateral structure or anterolateral capsule [6, 54, 98]. Its origin starts anterior and proximal to the lateral epicondyle and ends near the attachment of the lateral gastrocnemius tendon. The insertion extends from the Gerdy's tubercle to the popliteal hiatus [23, 47, 101]. The MLCL was modeled with four fibers. Literature data were used to set the stiffness of each fiber of ACL and PCL [72], MCL, OPL and FFL [11, 64, 72, 80], LCL and PT [64], CAP [86]. The stiffness of the FFL was obtained by data on the arcuate ligament, since no specific information were found in the literature. Experimental data were not available for the POL either, therefore its stiffness was set according to the mechanical properties of the posteromedial capsule [89], because of the similarity of these two ligaments. The MLCL stiffness was chosen within the minimum and the

maximum boundaries presented in [6] for the anterolateral capsule. All the fibers were modeled as one-dimensional nonlinear springs. The force-strain curve was assumed to be parabolic-linear (Eqn. 2.1) and it was imposed to each fiber by a user function in Adams [13]:

$$\begin{aligned} F &= \frac{1}{4}k\frac{\epsilon^2}{\epsilon_l} \qquad 0 < \epsilon \leq 2\epsilon_l \\ F &= k(\epsilon - \epsilon_l) \qquad \epsilon > 2\epsilon_l \\ F &= 0 \qquad \epsilon \leq 0 \end{aligned} \tag{2.1}$$

In Eqn. 2.1, k is the fiber stiffness and ϵ is the strain of the fiber defined as $\epsilon = \frac{L-L_0}{L_0}$, where L and L_0 are respectively the length and the zero-load length of the fiber; ϵ_l is assumed to be 0.03 [13]. The zero-load lengths of the isometric fibers were the same used in kinematic model, consistently with the sequential approach. As regards the other fibers, they must be slack or just slightly tight during passive motion not to alter it. Therefore, their zero-load lengths should be greater than the maximum origin-to-insertion distances obtained during the passive flexion arc. However, this inferior bound for each fiber was reduced by 1% to simulate a minimal fiber tightening (that is possible for small ligaments) during the passive motion that cannot be measured experimentally. A damping coefficient of 1 Ns/mm was used in parallel to each fiber in order to reach the static equilibrium and avoid dynamic instabilities. The geometrical and mechanical characteristics of all the ligamentous fibers of M2 and M2s are reported in Appendix A (Tab. A.1).

Loading Conditions

M2 and M2s were tested in several clinically significant loading conditions. Specifically, anterior-posterior (AP) tests, ab/adduction (AA) tests, internal-external (IE) torsion tests were performed. The relative motion between the femur and the tibia under each loading condition was measured [42] and compared to the results presented

in a reference study [41]. This work was chosen because of the accurate description of the loading conditions and of the TF reference systems, as well as because results from all the performed clinical tests were available both in passive and in loaded conditions at various flexion angles. To be consistent with the testing conditions of the reference study, the femur was fixed and the tibia was allowed to move freely under the effect of its own weight (50 N) and of external forces (100 N along the anteroposterior axis, 20 Nm about the anteroposterior axis, 5 Nm about the superior-inferior axis). The mediolateral rotation of the tibia was fixed at the desired flexion angle during each test as in the experimental session [41], therefore the model had five DoF. AP tests were also performed with various loads from 50 N up to 350 N at 90° of flexion, in order to evaluate the influence of articular shape at high loads.

2.3 Results

The motion of both M2 and M2s replicated the experimental reference kinematics [41] with good accuracy (Fig. 2.4). For further validation, the motion of the models was also compared to more recent experimental data [31, 55, 85] and it was in good agreement with them as well (Fig. 2.4). Fig. 2.4a shows the results of AP tests: top and bottom curves represent respectively the anterior and posterior displacements of the origin of $\mathcal{S}_t$ with respect to $\mathcal{S}_f$. At each flexion angle, displacements are measured from the corresponding relative pose when only the weight of the tibia is applied [41]. Likewise, Fig. 2.4b and Fig. 2.4c show respectively the results of IE and AA tests: bottom curves represent the variation in abduction and in internal rotation angles, while top curves represent the variation in adduction and in external rotation angles, with respect to the corresponding pose of the joint when only the weight of the tibia is applied. The mean absolute differences between the reference motion ([41]) and the simulated motion, expressed as percent values with respect to

the maximum range of the corresponding motion, were 12.21% (AP test), 7.99% (IE test), 10.16% (AA test) for M2 and 19.07% (AP test), 7.22% (IE test), 22.45% (AA test) for M2s. The comparison between the motion of M2 and M2s in the AP test at 90° of flexion showed that, as the load increases, spherical surfaces become less effective in providing a sufficient constraint to the joint motion (Fig. 2.5).

As a further validation, M2 ligament and contact forces for selected loading conditions are reported in Fig. 2.6 and Fig. 2.7. Fig. 2.6 shows the contribution of each structure to the anterior-posterior stability in the AP test. The displayed forces are the projections of passive structure forces,i.e. ligaments and contact forces, along the direction of the applied external load, therefore their sum is always equal and opposite to the external force (100 N). Fig. 2.7 shows the resultant forces of each passive structure for IE and AA tests at 0°, 45° and 90° of flexion. Contact forces were generally high (up to 500 N), but for several loading conditions they were either in the lateral or in the medial compartment (Fig. 2.7). Despite their large magnitude, the contact forces did not always play a central role to balance the applied external load: for instance, the projection of the lateral contact force during the anterior drawer at 0° is quite low (Fig. 2.6), even if the force itself has a high amplitude (Fig. 2.7). All the ligaments, including the secondary ones, played a structural role in every clinical test simulated in this study, in particular at full extension (Fig. 2.7). The number of ligaments involved always increased near full extension (Fig. 2.7). In fact, the knee is much more constrained and stiffer at full extension than at higher flexion angles. The CAP significantly constrained the fully extended knee, providing the greatest constraint in the abduction test, but it was almost unloaded at 45° and 90° of flexion (Fig. 2.7). The OPL and FFL presented the same behavior (Fig. 2.7). As expected, the ACL was the structure that exerted the highest force in the anterior drawer test, regardless the flexion angle (Fig. 2.6, Fig. 2.7). Similarly, the PCL provided the greatest constraint in the posterior test (Fig. 2.7). The LCL restrained both the anterior

and posterior drawer tests at full extension, but its contribution was negligible when the knee was flexed (Fig. 2.6, Fig. 2.7). The MCL constrained both the anterior and posterior drawer tests at 45° and 90° of flexion (Fig. 2.6). Other ligaments exerted significant forces as well, such as the POL in the posterior drawer test, the MLCL in the anterior and posterior drawer tests and the PT in the anterior drawer test. All these structures provided both positive and negative contributions to the joint equilibrium (Fig. 2.6). The most loaded ligaments in the AA tests were the ACL and PCL (Fig. 2.7), together with the LCL and PT (adduction) and the MCL and POL (abduction). In the external torsion test, the CAP, the LCL, the OPL, the ACL and the PT were the most important constraints when the knee is fully extended, while the PT and the MCL exerted the highest forces at 90° of flexion (Fig. 2.7). In the internal torsion test, the ACL and the MCL were generally the most involved ligaments, while the CAP and PCL exerted considerable forces at 0° and 90° of flexion, respectively (Fig. 2.7). The POL played an important role to stabilize the internal torsion when the knee was fully extended but its importance was reduced as the knee was flexed (Fig. 2.7). On the contrary, the MLCL force increased with flexion (Fig. 2.7).

2.4 Discussion

A new kinetostatic model of the knee was defined in this study to predict the behavior of the joint both in passive and loaded conditions. The model included the anatomical articular surfaces and a detailed set of the knee ligamentous structures, thanks to a deep literature investigation. The model was developed by means of the generalization of a kinematic model of the joint passive motion. This generalization process followed a sequential approach, that allows joint mobility and stability to be sequentially analyzed. The mechanical and geometrical parameters of the model were determined from a specimen and from the literature. The results proved that the model accurately

replicated the motion of the joint both in passive and loaded conditions (Fig. 2.4), when compared to experimental data from the literature [31, 41, 55, 85]. Although the model included the optimized parameters of the kinematic model [93], a full optimization was not performed: this suggested a potentially predictive ability of the model.

The kinematic model on which M2 is based was a spatial mechanism proposed, discussed in detail in previous investigations [21, 78, 81, 82]. The kinematic model accurately replicated the knee passive motion, reproducing the role that some passive structures play in guiding this motion. This mechanism included a spherical approximation of the articular surfaces instead of anatomical surfaces because previous investigations showed that numerical instabilities and a high model sensitivity are associated to equivalent mechanisms with complex surfaces [78]. Therefore the anatomical surfaces were used only during the generalization from the kinematic model to the kinetostatic one. After the generalization, the kinematic model corresponding to the new kinetostatic model was no longer the mechanism in Fig. 2.1 but it was kinematically equivalent to it, thanks to the procedure used to generate the surfaces described in Sect. 2.2.3. However, it would provide different results in terms of contact paths and articular forces, since the contact surfaces were no longer spheres.

Besides anatomical surfaces, the model proposed in this study included a complete representation of almost all the knee ligaments. Since the attachments of some ligamentous structures were not digitized during the experimental session, their location on the specimen surfaces was chosen according to their anatomical descriptions in the literature. The very existence of some structures is still discussed in the literature, such as the existence of the POL as a distinct ligament or as a part of the deep MCL [52, 57, 59, 84], or the possible negative correlation between the FFL and the arcuate ligament [47,67]. Therefore the choices made in this study may not represent

the real anatomy of the specific specimen. However, this limitation did not compromise the accuracy of the model because of the small influence of these ligaments in comparison to the main structures that constrain the joint. Ligamentous forces were generally in good agreement with the literature [1, 7, 34, 40, 47, 65, 66, 80], therefore they provided a further validation of the model and made it possible to understand the role of all passive structures in giving stability to the joint (Fig. 2.6, Fig. 2.7). In accordance with [1,7,80], at full extension, the most involved ACL fibers for the anterior drawer test were the posterolateral ones, while the most involved PCL fibers for the posterior drawer test were the posteromedial ones. On the contrary, the anteromedial ACL fibers (in the anterior drawer test) and all the PCL fibers (in the posterior drawer test) were involved at 90° of flexion ([7]). During the anterior drawer test, the resultant force on the ACL was always greater than the applied external force, in accordance with [80]. This is a consequence of the rotations coupled with the joint translations. The MCL posterior deep fiber played a significant constraining role during the posterior drawer test [1]. In accordance with [80], results show that the ACL and the MCL are the most involved ligaments in the internal torsion test. Besides the MCL, on the medial aspect of the knee, the POL played an important role to stabilize the internal torsion when the joint was fully extended, but its importance was reduced as the knee flexed [40]. On the lateral side, the LCL acted in accordance with [1], restraining both the anterior and posterior drawer test at full extension and giving almost no contribution to the joint stability when the knee was flexed. The MLCL was actually an important constraint of the joint in adduction [34, 47, 65, 66], when the knee was either flexed or extended, and it could be considered the lateral counterpart of the deep MCL. The analysis of the ligaments forces pointed out some apparently paradoxical behaviors of the joint: an increasing force in posterior drawer test at 90 degrees reduced the posterior translation, that became even positive (i.e. anterior) with spherical surfaces at high loads (Fig. 2.5). However, these behaviors can

be explained in the context of joint equilibrium, considering the rotations generally coupled to translations during the drawer test.

The comparison between the results of M2 and M2s suggests that, even if the anatomical surfaces provided a higher model accuracy, spherical surfaces can still predict the joint behavior when the applied loads are not too high. However, despite the mean absolute differences between the model and the reference results were comparable (less than 12.21% for M2 and less than 22.45% for M2s), the behavior of the two models was similar, but not always the same for each considered loading condition. The shape of articular surfaces caused differences mainly in the posterior drawer and in the abduction tests while internal and external rotations were quite similar regardless the type of articular surfaces considered (Fig. 2.4). The differences between M2 and M2s motion increased as the load increased (Fig. 2.5) and in these conditions M2s showed a overall lower stiffness. Moreover, spherical surfaces could not represent more than one contact point for each pair of contact surfaces, unlike the anatomical surfaces. Thus, it may be inferred that the model with spherical surfaces is a trustworthy tool to qualitatively predict the motion of the knee with some advantages over the model with anatomical surfaces. Spherical surfaces allows a simple but effective contact model [93] that reduces computational time and avoids the laborious process of anatomical surface design. However, when the loads increase, the articular contact is on areas where the spherical approximation is less effective. In this case, the anatomical surface geometry provides secondary constraints that make the joint stiffer.

A previous kinetostatic model with spherical surfaces and only the main ligamentous structures showed slightly lower mean absolute differences with respect to the same reference motion, because a systematic optimization on the mechanical characteristics of the ligamentous fibers was performed [93]. Even if the new model is not entirely exempt from an optimization procedure, no systematic optimization was

performed on it in order to verify if a more accurate and complete representation of the articular surfaces and ligaments improved the predictive capabilities of the model. Although the results of the new model could benefit from an optimization procedure, the present accuracy can be considered acceptable in several practical applications, where optimization time could be saved. The reference experimental kinematics for the present study was taken from the literature [41], therefore the specimen used to develop the model and the ones used to measure experimental motion were different. For this reason, it is not surprising that largest differences with respect to the reference motion were found in the drawer tests: the amount of translation actually depends on the reference point chosen to measure translations, due to the effect of coupled rotations. Although a stronger validation will be required with laxity tests performed on the same specimen, the accuracy showed by the model when compared to several literature data confirms its predictive capabilities.

The development of this work will be the inclusion of the main muscular structures that cross the knee joint and of the patellofemoral articulation. In other words, the natural continuation of this study is the definition of the dynamic model of the knee joint, which is the last step of the sequential procedure [30]. This will be presented in Chapter 3.

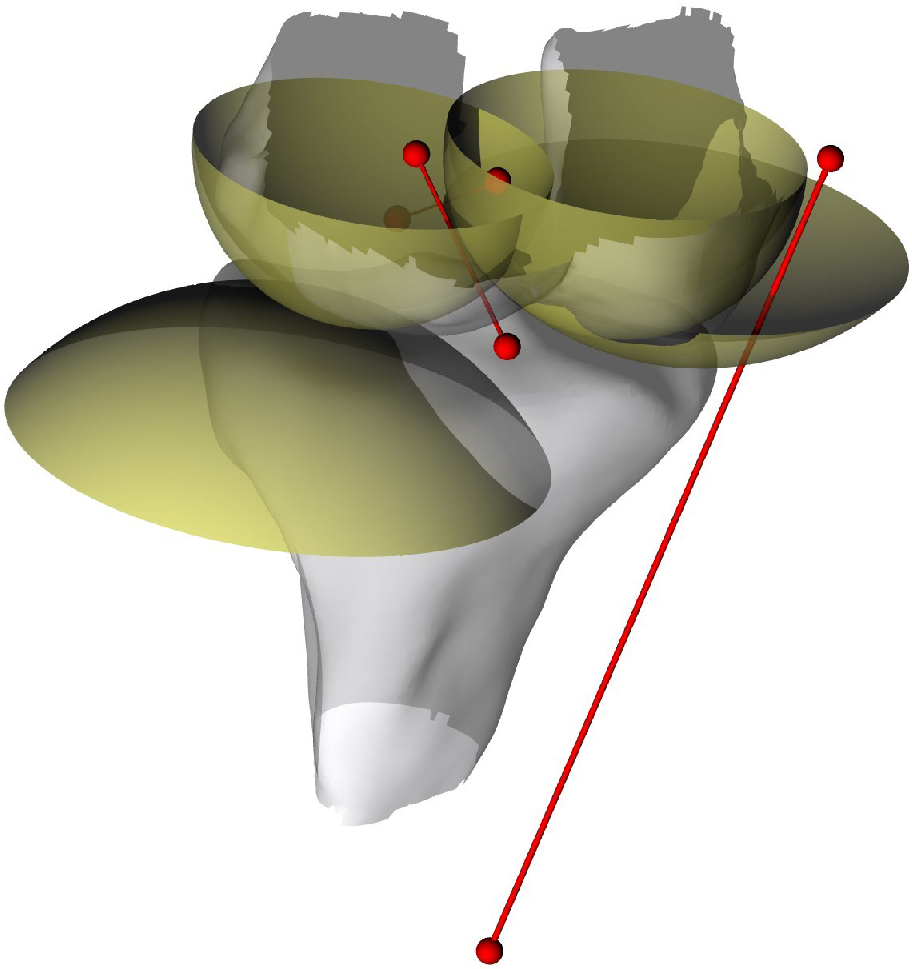

Figure 2.1: Kinematic model: spherical surfaces (yellow) approximate the anatomical articular surfaces (grey); ACL, PCL, MCL isometric fibers are represented as rigid links (red).

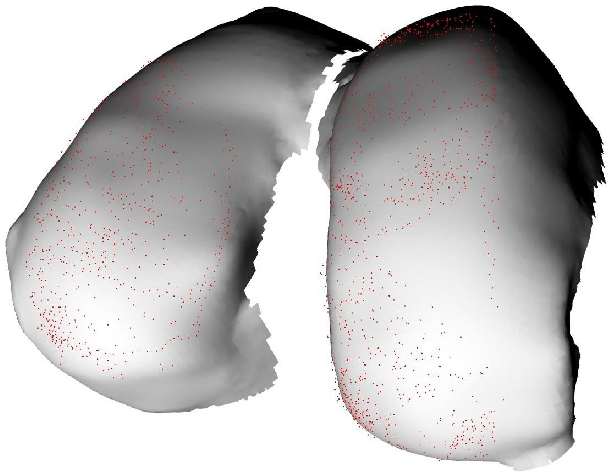

Figure 2.2: Femoral surfaces (grey) after the alignment and the merging of CT scans with point clouds (red) from the stereophotogrammetric system were performed.

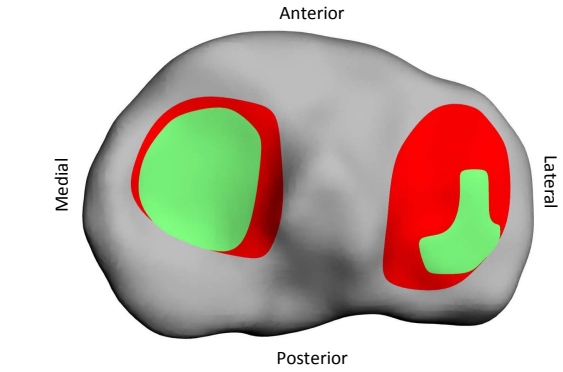

(a)

(b)

Figure 2.3: Conjugated surfaces and final tibial and femoral surfaces after the alignment and the merging of CT scans with stereophotogrammetric data were performed. The relative position of the surfaces at full passive flexion (a) and the tibia surface (b) are showed. Different contributions to the design of the anatomical surfaces are shown in different colors: CT scans (grey), stereophotogrammetric data (red), contact areas on the tibia during passive motion (green).

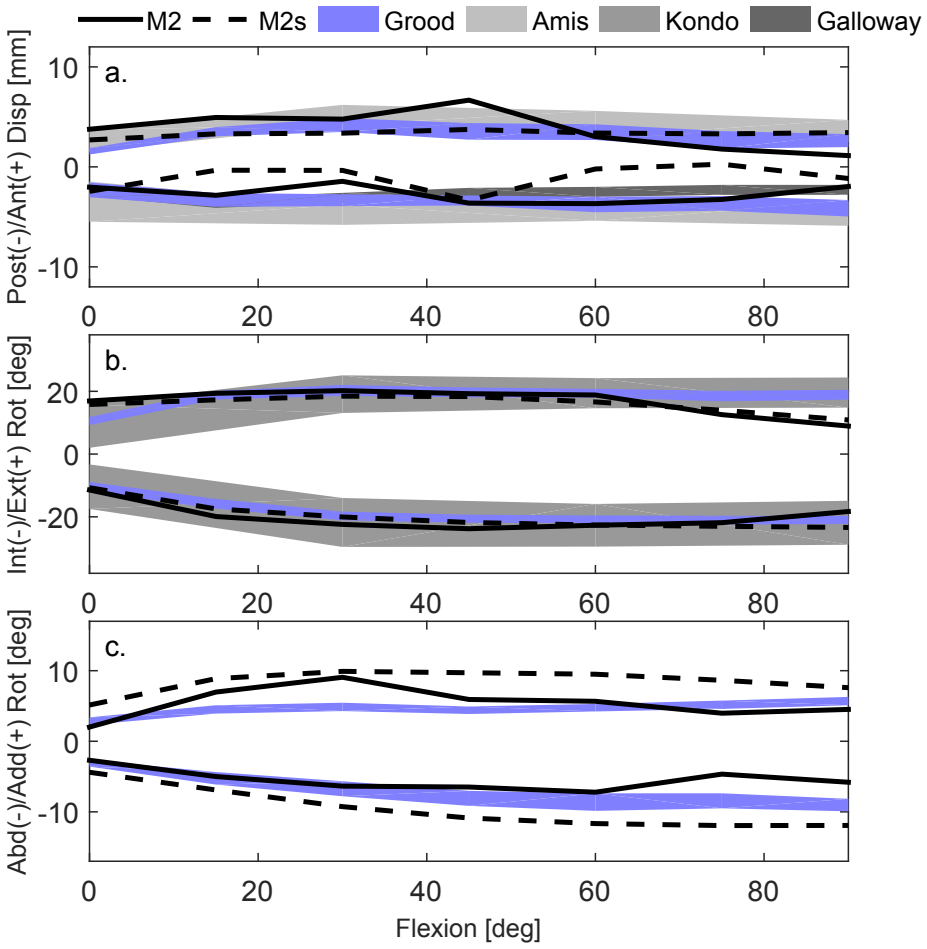

Figure 2.4: Motion obtained with M2 and M2s is compared to the reference data from [31,41,55,85]. The shaded regions represent the mean ± one standard deviation.

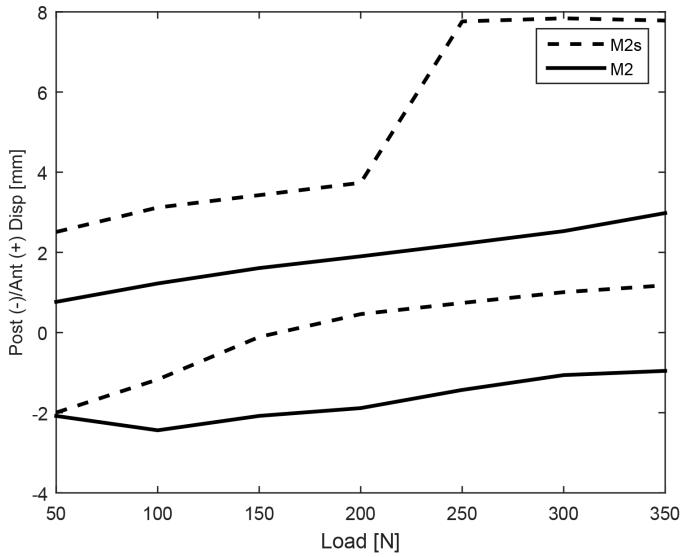

Figure 2.5: Anterior and posterior drawer tests: comparison between M2 and M2s at 90° of flexion.

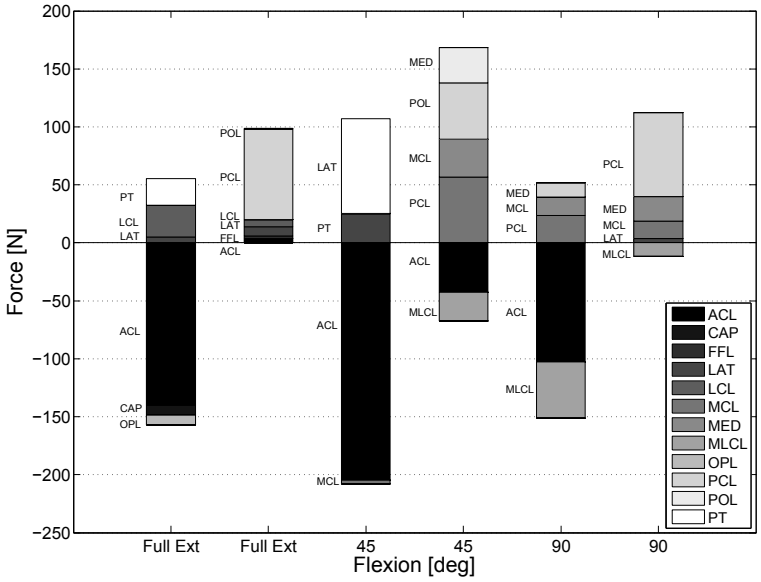

Figure 2.6: Projection of passive structure resultant forces in the direction of the external applied load, during the AP test at 0°, 45° and 90° of flexion. For each flexion angle, forces from the anterior test are on the left, and forces from the posterior test are on the right.

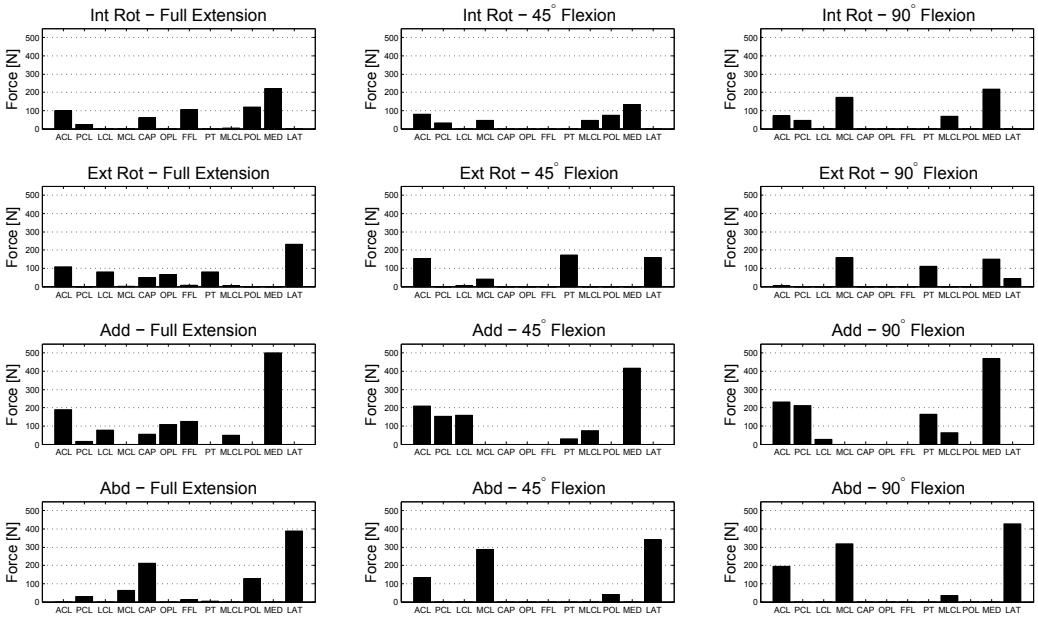

Figure 2.7: Ligament and contact forces during IE and AA tests at 0°, 45° and 90° of flexion.

Chapter 3

Specimen-specific dynamic model of the knee to estimate squat quadriceps force

3.1 Introduction

Computational models of the knee are powerful tools to evaluate the behavior of the joint in different conditions and to estimate forces and variables that cannot be measured. In order to be fully predictive, a joint model must be tested and validated in several static and dynamic conditions, in which both internal and external loads are applied. The sequential procedure proved to be an efficient and effective method to design kinematic and kinetostatic models of both the tibiofemoral (TF) and the patellofemoral (PF) knee joint [92, 93] The last step of the procedure consists in the development of the dynamic model of the knee, whose objective is to estimate the muscle load at the joint in any dynamic activity, starting from the previously optimized kinematic and kinetostatic models [30]. Quantifying muscular forces is crucial for the estimate of the joint loads and therefore it would benefit many aspects

of the orthopaedic medicine, such as prosthetic design [8], rehabilitation strategies or surgical procedures [87, 96]. Since non-invasive *in vivo* experimental measurements of muscular forces are not possible, computational models are necessary in order to estimate these loads [103]. Most of the musculoskeletal models simplify the knee joint representing it as a 1 degree of freedom (DoF) mechanism [70], in which rotations and translations of the tibia with respect to the femur are coupled to flexion. Moreover, the vast majority of the available models are not subject or specimen-specific, meaning that they use generic passive motion data [107, 112] to define the law of motion for the knee mechanism [102]. This approach is certainly efficient but does not lead to a deep understanding of the knee mechanics under dynamic loading conditions. Recently, more interest has been directed towards the representation of the knee as it is in the human body, i.e. a 6 DoF joint [103], but defining subject-specific joint models that capture the complex three-dimensional knee laxity remains a challenge for many reasons. Most of the mechanical and geometrical properties of the knee soft tissue, such as the ligaments, need to be calibrated against joint laxity data, which is a time-consuming process, especially if contact is included in the model. Moreover, it is crucial that the knee model tested under static or dynamic conditions is able to preserve the passive motion of the joint [30]. The sequential procedure offers a quick and efficient way to design such a model for both the TF and the PF articulation.

The primary objective of this study is to validate the 6 DoF specimen-specific model of the joint derived with the sequential approach by comparing the experimental and model-predicted motion and quadriceps force for a squat activity. The experimental data were previously collected from an *in vitro* experiment performed with test rig [28]. Specifically, a finite element (FE) model of the joint is developed and quadriceps force is estimated by means of a proportional-integral (PI) controller that tracked knee flexion. This computational representation of the experiment provides also an estimate of quantities that cannot be measured neither *in vivo* nor *in*

vitro, like ligament and contact forces [5, 33]. Musculoskeletal models are commonly used to estimate muscle forces using an inverse dynamics approach, in which the muscle redundancy of the human body is solved with optimization techniques that minimize some kind of energy cost [4]. OpenSim is a freely available multibody dynamics software that allows to perform inverse dynamics from *in vivo* experimental kinematics and to estimate muscle forces needed to achieve the measured motion by means of a static optimization technique [19]. Another goal of the present study is to replicate the *in vitro* squat experiment in OpenSim and to estimate the quadriceps force needed to actuate the model with two different sets of kinematic data: first, TF and PF rotations and translations are expressed as a function of flexion derived from the squat kinematics; then TF and PF rotations and translations are replaced with the same DoF from passive motion. A comparison between quadriceps forces estimated with loaded and passive motion will allow to verify if passive motion is a viable alternative to measured kinematics for the prediction of muscular loads. To summarize, the objective of this study is threefold:

- To design a specimen-specific dynamic model of the joint and to validate it against results from an *in vitro* squat activity.
- To analyze joint quantities not experimentally measurable, such as ligament and contact forces, during the squat activity, in a FE framework.
- To understand to which extent the knee model affects the prediction of muscular quantities in a dynamic activity like the squat.

3.2 Methods

3.2.1 *In vitro* testing

Both unloaded (passive motion) and loaded (squat) tests were performed on the left knee of an 80 year old male specimen with no previous condition at the joint, as declared by the surgeon. A detailed description of the experimental procedure as well as of the test rig used to perform the experiment can be found in [28]. Briefly, the foot and the soft tissue were removed and the knee capsule was left intact. The leg was mounted on the rig with its anatomical flexion axis (transepycondilar femoral axis) coincident to the revolute joint axis between the portal and the base of the testing machine. The passive motion of the TF and PF joints was recorded at several degrees of flexion, from full extension to deep flexion (over 120 °). A tracker directly fixed to each bone, i.e. introducing no soft tissue artifact, and a stereophotogrammetric system (Vicon Motion Systems Ltd., nominal accuracy 0.5 $Nm/0.5°$) were used to measure the relative motion between femur, tibia and patella. Then the knee was tested in a common daily task: a squat. Ground reaction forces and torques recorded during a squat activity were taken from the literature [43] and applied to the tibia by means of a cable driven parallel manipulator included in the test rig. At each considered angle of flexion (from 7° to 94°), the test rig applied the quadriceps force that was necessary to equilibrate the external load. Since the rig does not allow co-contraction of flexor and extensor muscles, it was assumed that the net torque at the knee was generated by the quadriceps only. TF and PF joint motion was recorded for the squat activity in the same way it was done for the passive motion. Magnetic resonance imaging (MRI) was performed on the specimen lower limb.

3.2.2 Computational modeling

The computational modeling is divided in subsequential steps (Fig. 3.1). First, the knee kinematic and kinetostatic models were defined starting from experimental passive data and laxity tests data, similarly to what was done in Chapter 2. Then a dynamic model was implemented both in a multibody software (Opensim, Stanford University) and in a FE software (Abaqus/Explicit, SIMULIA, Providence, RI) in order to estimate the quadriceps force during the squat activity and compare it to the experimental force as a validation.

Kinematic model

The kinematic model of the TF joint is a 1 DoF mechanism able to replicate the passive motion [81, 109]. It is defined as a 5-5 fully parallel mechanism, as in [93]. The five rigid links of the mechanism represent the passive structures that guide the passive motion of the joint, i.e. three isometric ligamentous fibers, whose lengths do not change during the passive flexion arc [109], and the medial and lateral articular contacts, which are model as spherical contacts (Fig. 3.2). To define the initial geometrical parameters of the mechanism, the articular surfaces were approximated by best-fitting spheres and the femoral and tibial attachment sites of three isometric fibers were chosen inside the insertions areas of ACL, PCL and MCL. In the definition of the mechanism proposed in [93], the medial contact is represented by a ball and socket joint while the lateral contact is modeled as a sphere-on-sphere joint. This explains why the center of the tibial sphere is above the center of the femoral sphere in the medial contact representation, while the opposite happens in the lateral contact representation (Fig. 3.2). The isometric fibers were selected among the entire ligament bundles as those fibers whose lengths remain almost constant during the passive flexion arc of the knee. An optimization procedure was implemented to find the parameters of the mechanism that best replicate experimental passive motion.

The design variables were the spatial coordinates of the tibial and femoral insertions of the isometric fibers (ACL, PCL, MCL) and of the centers of the spheres that approximate the condyles (Fig. 3.2). The tibial quantities were expressed in the tibial anatomical coordinate system $\mathcal{S}_t$ and femoral quantities were expressed in the femoral anatomical coordinate system $\mathcal{S}_f$. A global optimization method, namely the genetic algorithm available in Matlab 2015 Global Toolbox (The MathWorks, Natick, MA), was used to find the design vector that minimizes the difference between the experimental passive motion and the motion produced by the mechanism throughout the flexion arc. The motion was evaluated at 31 different flexion angles, from 5° to 123°, i.e. the limits of the available experimental motion. The motion of the mechanism was obtained by solving its loop closure equations at each flexion angle. The loop closure equations enforced that the length of each one of the five links must be equal to the distance between the corresponding origin and insertion at each pose [93]. If the flexion angle was imposed, the loop closure equations consisted in a set of five equations in five unknowns, which were the parameters that define the relative position and orientation of the femur and the tibia. The transformation matrix between $\mathcal{S}_f$ and $\mathcal{S}_t$ was parametrized according to Grood and Suntay [42]: internal-external (IE) and ab-adduction (AA) rotations, anterior-posterior (AP), superior-inferior (SI) and medial-lateral (ML) translations. If the design vector satisfied the loop closure equations, then the error between each parameter of the mechanism motion and the correspondent experimental parameter was calculated and normalized with respect to the maximum range of motion in that particular DoF. At each iteration, the output of the objective function was the sum of the error at each flexion angle for each DoF. If, for a particular design vector, the solution of the loop closure equations could be found, the output of the objective function was set to an extremely large number. The solution was considered feasible if the current design variables were inside a sphere of radius equal to either 2.5 mm for the links representing the ligament fibers, or 2

mm for the links representing the contacts. The centers of these spheres were defined according to the initial geometry of the mechanism. This was done by means of a nonlinear constraints function. After the global optimization was performed, a local optimization method, namely the interior-point algorithm, available in Matlab 2015 Optimization Toolbox, was used to refine the result. Details of the code are reported in Appendix B.

In the passive motion of the knee, all DoF of the PF joint are coupled to TF flexion [92]. The patella can slide on the femoral distal surfaces (trochlea and condyles) while it is connected to the tibia through the patellar ligament and to the femur through the quadriceps. Since this muscle is not tight during passive motion, the patella moves on the femur surfaces being trailed just by the patellar ligament. In particular, the tibia and femur relative motion is not constrained by the PF joint during passive motion if knee flexion is imposed. In other words, TF kinematics does not depend on PF joint during passive motion. For this reason, the PF joint is modeled as a zero DoF mechanism, as in [92]. To define the initial geometry of the mechanism, the femoral trochlea was approximated by a best-fitting cylinder and the isometric fiber of the patellar ligament was selected in a similar way to what was done for the TF joint. In the kinematic PF model, the relative motion between the femur and the patella is constrained with a hinge joint (Fig. 3.2) and the direction of the hinge axis, i.e. the axis of the cylinder that approximates the trochlea, was chosen through an optimization procedure. The tibial and patellar attachment sites of the patellar ligament were optimization variables as well. The objective of the optimization was to minimize the difference between the experimental PF passive motion and the motion produced by the PF mechanism, at each TF flexion angle. At each iteration, the loop closure equations of the PF mechanism must be satisfied [92] and, in case they were not, the value of the objective function was automatically set to an extremely large number. If the solution of the loop closure equations existed, the difference between

the mechanism motion and the experimental motion was calculated as it was done for the TF mechanism. A nonlinear constraint function was included in the optimization algorithm to force the cylinder axis to be no more than 5 mm distant and no more than pi/10 radians rotated with respect to the initial axis. The patellar ligament attachments were constrained to be inside a sphere of 3.0 mm radius. For the PF mechanism optimization, the use of a global technique was not needed because the initial geometry of the mechanism was close enough to the optimal one. Therefore the problem was solved with a local optimization technique, namely the interior-point algorithm, available in Matlab 2015 Optimization Toolbox. Details of the code are reported in Appendix B.

Kinetostatic model

A TF kinetostatic model was developed consistently with the sequential approach (Fig. 3.3). The model was developed in a similar way to what was presented in Chapter 2 of this dissertation. Origin and insertion areas of the cruciate (ACL, PCL) and the collateral (MCL, LCL) ligaments were estimated from the MRI of the joint. Specifically, the ACL was modeled by means of three fibers (anteromedial, posterolateral and isometric), the PCL was modeled by means of three fibers (posteromedial, anterolateral and isometric), the MCL was modeled by means of three fibers (deep, superficial and isometric), and the LCL was modeled by means of two fibers (anterior and posterior). The attachment sites of the secondary passive structure of the knee joint were estimated from the literature, according to the results of Chapter 2. The posterior capsule (PCAP) was modeled with a medial, a lateral and an intermediate fiber. The posterior oblique ligament (POL) was model with an anterior and a posterior fiber, the oblique popliteus ligament (OPL) was model with three fibers. The popliteus tendon (PT) was represented by an anterior and a posterior fiber. The anterolateral structure (ALS) and the fabellofibular ligament (FFL) were each one

represented by a single fiber. Each fiber was modeled as one-dimensional parabolic-linear spring [13]. A Matlab code was developed to optimize the laxity properties of the joint, minimizing the RMS differences between the model-predicted and the experimentally measured laxity at various DoF. The stiffness of each ligament was varied within boundaries reported in the literature [7, 39, 64, 71]. The resting length of each fiber was chosen according to the maximum distance between the origin and the insertion of the fiber during the passive flexion arc [92]. The lengths found with this process were then shorten by 1% or 2% to account for some possible tightening of the ligament fibers during the passive flexion and to help stabilizing the simulations when the applied load is low. The ligament resting lengths determined in this way were not optimized. Although the specimen-specific ACL, PCL, LCL and MCL tibial and femoral attachment sites were identified by means of MRI, errors within this process are likely. Hence, the attachment locations were included in the optimization. Collaterals and cruciates attachment sites were allowed to vary inside a sphere of respectively 3 mm ad 1 mm radius by means of a nonlinear constraint function included in the optimization algorithm. Isometric fibers geometry was left unmodified from the kinematic model, to be consistent with the sequential procedure. The genetic algorithm available in Matlab 2015 Global Toolbox was used to minimize differences between model-predicted and experimental [41] laxity responses at 0°, 15°, 30°, 45°, 60°, 75° and 90° of flexion for various external loads, namely IE torque (10 Nm), AA torque (20 Nm) and AP force (100 N). In the optimization process, the laxity of the model under different types of external load was always normalized with respect to the laxity in the DoF of interest when only the tibial weight was applied. Consequently, the experimental laxity taken as a reference was normalized too. As in the study presented in Chapter 2, the experimental data for the laxity tests were taken from [41] despite more recent work available in the literature because the completeness of the results presented allowed to set up an optimization process

that could capture the laxity of the knee in all the main DoF at all flexion angles and the knee passive behavior as well. The optimization process had a design vector containing 19 stiffness values; the total number of fibers present in the model was 23 but some secondary structures, such as the POL or the PT, were modeled with multiple fibers constrained to have the same stiffness value to decrease computational time. Moreover, the attachment sites of cruciates and collaterals (all the fibers except the isometric ones) had to be included in the design vector, making a total of 67 parameters to optimize. The optimization process was set up so that at each iteration the equilibrium equations of the system were numerically solved, meaning that the sum of the forces, namely ligament forces, contact forces, weight and external load, if present, and the sum of the moments acting on the femur with respect to the tibia must be equal to zero. Since each laxity test was performed at a fixed flexion angle, a counter force was introduced: its magnitude was obtained at each iteration so that the sum of the moments produced by all the other forces about the flexion axis was zero and its direction was anteroposterior in $\mathcal{S}_t$, at a fixed distance from the origin. If for a particular value of the design vector, the solution to the equilibrium equations could not be found, the output of the objective function was automatically set to an extremely large number. Details of the code are reported in Appendix B.

Dynamic model

The knee dynamic model was developed both in Opensim and in Abaqus/Explicit, as follows.

- One of the limitation of the test rig used in the experiment is that it does not allow co-contraction of flexor and extensor muscles crossing the knee joint. To understand to which extent co-contraction could affect quadriceps force prediction in the squat, Opensim [19] was use to reproduce the experiment and to estimate the muscular force necessary to generate the needed torque at the knee

joint for this activity. Opensim models are designed in a similar way to serial robots: each body is defined by means of a mass and an inertia matrix and it is connected to the previous body in the chain (parent body) by means of a customizable joint. In the Opensim model developed for this study, the TF and PF joints were model in two different ways, and then muscular forces and joint torque prediction were compared. First, the TF joint was modeled as a 1 DoF joint in which IE and VV rotations and AP, SI and ML translations were coupled to flexion by means of splines defined from the experimental squat kinematics (Fig. 3.4). This ensures a perfect replication of the knee motion from the squat test. The PF joint was modeled in the same way, but PF flexion was coupled to TF flexion, leaving zero DoF at the patella. In a second version of the model, the TF and PF joints were modeled assigning splines to each DoF according to the joint passive kinematics, as it is typically done in most of the published models [70, 102]. The splines used for the knee kinematics were calculated extracting the Cardan angles from the transformation matrices between the bones in their anatomical coordinate systems. Opensim uses the X-Y-Z Cardan angle sequence, therefore the rotation about Z axis is the first one to be performed, followed by the rotations about Y and X axis. Translations are then performed after rotations. The hip was modeled as a spherical joint between the femur and the pelvis. No foot, i.e. no ankle joint, was present in the model since it was not present in the experiment either. Four muscles were included to model the quadriceps: vastus medialis, vastus lateralis, vastus intermedius and rectus femoris. The hamstrings (biceps femoris long head, biceps femoris short head, semitendinosus and semimembranosus) and the gastrocnemii (gastrocnemius medial and gastrocnemius lateralis) were included in a second model, almost identical to the first except for the presence of these muscles. The attachment sites of the muscles were derived from previous work [18] and manually adapted

to the current bone geometry. Wrapping surfaces were included in the model for the flexor and the extensor muscles and for the gastrocnemii in order to allow physiological wrapping to the underlying bones, i.e. the posterior and anterior part of the femoral condyles. Muscles were treated as linear actuators in order to be as consistent as possible with the experiment and to avoid uncertainty generated by the parameters that characterize the Hill-type model [113], also available in Opensim. The Hill-type model is certainly more a physiological representation of the muscular unit but it adds a complexity to the model that exempts from the purpose of this study. In the model with only the quadriceps group, the femur flexed and extended with respect to the tibia, which always remained in vertical position, consistently with the experiment. In the model including the hamstrings and the gastrocnemii, both the knee and the hip joints were present and the squat motion was achieved with an extension moment about both joints. The extension moment at the hip causes the activation of the hamstrings. However, the hamstrings are biarticular muscles that also generate a flexion moment at the knee. Therefore, co-contraction of antagonistic muscles at the knee takes place during the squat activity. Hip kinematics profile was taken from the same literature data as the ground reaction forces [43] for consistency. Muscle forces were computed solving the redundancy problem, i.e. more actuators than DoF, through a static optimization procedure available in Opensim, which minimizes the sum of the activation squared at each instant of time [19]. Inverse dynamics was performed on the model as well in order to calculate the net joint torque during the squat activity. The geometries from the segmented MRI of the joint were included in the model only for visual purpose (Fig. 3.4).

- A dynamic FE model of the TF and PF joint was developed, starting from the previously defined kinematic and kinetostatic models. The model included

bones, ligaments and flexor/extensor muscles crossing the knee and it was implemented in Abaqus/Explicit (Fig. 3.5). The complexity of the TF articular surfaces representation was increased from spherical approximation to anatomical-based shapes. The tibial contact surfaces were altered in such a way that the passive motion was not modified from the one predicted by the kinematic model. Details of the procedure were already presented in Chapter 2. Briefly, the conjugate surfaces of the femur were generated from the TF kinematic model. Then the contact areas at each pose were identified as those points on the tibia (represented as a point cloud) whose distance from at least one point of the femoral surface (represented as a point cloud) was less than 0.5 mm. This threshold was chosen after different values were evaluated, based on the goodness of the final result. These tibial points were substituted with the correspondent section of the envelope of the conjugates in Rhinoceros 3D (Robert McNeel and Associates). This process ensures that the constraints provide by the contact surfaces during the passive motion remained consistent with the kinematic model and it can also make up for possible errors during the segmentation process. The tibia, the femur and the patella were meshed with two-dimensional triangular element in Hypermesh (Altair, Troy MI) and treated as rigid bodies in the simulation to reduce the computational cost without sacrificing the accuracy of the kinematics prediction. The average edge length for each element was set to 2 mm: mesh refinement was proved not to influence kinematics [33], therefore a finer mesh would have been an unjustified cause of increase in computational time. A coefficient of 3.2 was used to define the contact stiffness and the coefficient of friction between bones was set to 0.0025 [73] to replicate the one of cartilage-on-cartilage. A contact damping coefficient of 0.01 Ns/m was add to the contact definition in order to increase the stability of the simulation. TF ligaments were defined as axial connectors with a nonlinear force-displacement

relationship. The stiffness and zero-load length were assigned to each connector representing a ligament fiber according to the results of the optimization previously performed. TF kinematics was measured by three connectors at the joint, defined according to [42]. The squat activity performed on the test rig was replicated in the FE framework with objective to estimate the quadriceps force and compare it to the experimental one and to the one obtained with Opensim through the static optimization. The PF joint was modeled both as the zero DoF mechanism previously optimized and as a 6 DoF joint with a two-dimensional membrane-like patellofemoral ligament [3] and results from the two models were compared. In order to represent the zero DoF PF mechanism in the FE framework, a hinge joint was built between the femur and the patella, with the hinge axis direction coincident to the one found in the PF model optimization process, and the patellar ligament was treated as isometric. The ground reaction force measured during the squat activity [43] was applied to the tibia at each degree of flexion (from 7° to 94°) by means of three concentrated loads and three pure torques, properly transformed to the global coordinate system of the FE model, i.e. the femoral anatomical coordinate system. The quadriceps muscle was modeled with three axial connectors representing the vastus medialis, vastus lateralis and vastus intermedius. The connectors were directed as the global (femoral) SI axis. The patellar attachments for the vastus intermedius was set on the most superior point of the patella, while the patellar attachments for the vastus medialis and lateralis were defined according to the [18]. Besides the connectors, a two-dimensional membrane was integrated in the quadriceps muscle in order to let it to wrap around the frontal surface of the distal femur (Fig. 3.5). Two hamstring muscles were included in the model as well, namely the semimembranosus and the biceps femoris: the axial connectors representing the hamstring were directed as the global SI axis and their tibial attachment

sites were defined according to [18], consistently with the Opensim model. A proportional-integral (PI)-control was integrated into the model to drive the muscular actuators. A sensor measuring knee flexion was incorporated into the FE model, and instantaneous measurements from the sensor were fed to the controller, implemented within an Abaqus/Explicit user subroutine VUMAP. The control system was used to calculate the instantaneous flexor or extensor force required to match the target knee flexion profile, which was the same as the experiment. The flexor and extensor force computed at each instant with the controller was divided between each muscular unit to match the proportions of the Opensim results. Therefore 70% of the flexor force was assigned to the semimembranosus (30% to the biceps femoris), 60% of the extensor force was assigned to the vastus lateralis (25% to the vastus medialis and 15% to the vastus intermedius). This distribution respected the proportion between the physiological cross sectional areas (PCSA) of the muscles. Model verification was performed by comparing the model-predicted TF kinematics and quadriceps force to the corresponding experimental quantities. The quadriceps force predicted by the FE model was also compared to the muscular forces obtained with Opensim. The simulation time was 1.5 second, with a time increment of 1e-5 second. The simulation was divided in two subsequential steps: first (step 1, 0.5 second long) tibia, femur and patella were bring into contact by applying a small load to the quadriceps, then (step 2, 1 second long) the feedback controlled squat activity was performed. As was previously proved [33], the kinematic results from an explicit FE analysis are independent from the time step size when the activity or test that are being replicated are quasi-static.

3.3 Results

Kinematic and kinetostatic model optimization

The root mean square (RMS) differences between the experimental TF passive motion and the TF mechanism motion were 2.24° (IE), 0.4° (AA), 2.77 *mm* (AP), 0.78 *mm* (SI), 1.19 *mm* (ML) (Fig. 3.6 (a)). The root mean square (RMS) differences between the experimental PF passive motion and the PF mechanism motion were 20.04° (FE), 2.54° (AA), 2.79° (IE), 7.58 *mm* (AP), 7.18 *mm* (SI), and 2.09 *mm* (ML) (Fig. 3.6 (b)). The genetic algorithm combined with the interior-point method found the optimized parameters of the TF mechanism in less than 5 hours (15579 seconds) and the interior-point algorithm found the optimized parameters of the PF mechanism in less than 10 minutes (483 seconds), using one CPU. The RMS differences between the experimental TF laxity tests [41] and the same tests simulated with the kinetostatic model were 2.7° (IE), 1.2° (VV) and for 0.8 *mm* (AP). The genetic algorithm found the global optimal solution for the problem in about 50 hours, using 1 CPU. When only the tibia weight was applied, the kinetostatic model was able to replicate the passive motion without significant alterations with respect to the motion of the kinematic model (Fig. 3.7 (a)), ensuring that ligament forces remained extremely low (Fig. 3.7 (b)).

Opensim muscular force prediction

Inverse dynamics was performed in Opensim and the net joint torque necessary for the squat activity is shown in Fig. 3.8. The torque was not significantly affected by the type of model adopted at the knee joint. The muscular force necessary to generate such a torque was computed in Opensim through a static optimization process and it is shown in Fig. 3.9. If co-contraction was allowed, the total quadriceps force was on average 85% more than in case of no-contraction, i.e. only the extensor muscles

generated the torque at the joint. In both cases, the quadriceps force predicted by the Opensim model was smaller than the experimental one. The average RMS difference between the moment arms calculated with the squat kinematics and the passive kinematics was 15.4 mm, averaged across the three vasti muscles.

FE model prediction

The quadriceps force that the PI controller calculated at each instant of the simulation in order to guarantee equilibrium at the desired flexion angle was close to the one obtained with the Opensim model (Fig. 3.10). RMS difference between the two was 126 N. When the zero DoF mechanism was used in place of the 6 DoF PF joint, the quadriceps force necessary for the squat activity was smaller by 21% on average. The average RMS difference between the target flexion profile and the model flexion profile was 1.32°, which suggests that the PI controller gains were correctly tuned. TF rotations and translation predicted by the FE model were extracted and compared to the experimental ones, using the Cardan angle sequence Z-Y-X (Fig. 3.11). Ligament and contact forces predicted by the FE model are shown in Fig. 3.12 (a). The FE model correctly identifies the ACL as the tightest structure in full extension and the PCL as the tightest structure when the joint is flexed (Fig. 3.12 (a)). The contact forces predicted by the model for the TF and PF joint were respectively almost 1200 N and over 600 N when the knee is flexed (Fig. 3.12 (b)). The FE simulation ran in about 45 minutes, using 4 CPU.

3.4 Discussion

The purpose of this work was to develop and validate a computational framework to replicate an *in vitro* experiment performed of the knee, namely a squat activity. This was done in subsequential steps: first, the kinematic model of both TF and PF

joint was defined and then compliance was added, optimizing the geometrical and mechanical parameters of the TF ligaments in order for the model to correctly match the experimental motion during several laxity tests (IE, AP, and VV). This joint model was then integrated in a more complex FE musculoskeletal model, which included quadriceps and hamstrings muscles, and in which the spherical approximation of the condyles, used in the optimization procedure for efficiency, were replaced with anatomical-based geometries. The FE model was tested in a force-driven simulation, where the TF flexion was feedback controlled through flexor and extensor muscular forces in order to match the experimental flexion from the squat activity, and all the other TF and PF DoF were left free. The quadriceps force estimated with the feedback-controlled FE model was then compared to the one obtained with Opensim static optimization for the same squat activity.

3.4.1 Findings

The comparison between the experimental and FE model-predicted quadriceps force showed large differences. Specifically, a RMS difference of 1397 N between the two force profiles was calculated. A possible explanation for this difference could be that the moment arm of the quadriceps in the FE model was much larger than the actual moment arm in the specimen. Another difference between the experiment and the model that possibly affected the results is that a dynamic simulation across the range of flexion was performed with the model, whereas several static tests at various flexion angles were performed in the experiment. Yet, these differences can hardly explain why the peak quadriceps force needed in the experiment was twice as large as the muscle load in the model. However, the musculoskeletal simulations performed in OpenSim and data from the literature [44] favorably compared to the results obtained with the FE model. This suggests that quadriceps forces reasonably consistent with the applied external forces and with the simulated activity were predicted by the FE

model. It is worth noting that, without some flexor muscle force, the tibia would not have been able to follow the squat flexion profile in the very first part of the simulation. In fact, at the beginning of the activity, the tibia tended to extend under the effect of the ground reaction force, causing the hamstrings to activate.

Opensim proved to be a proper tool to model a dynamic experiment and to compute muscle forces. Static optimization is a validated technique that proved to be equivalent to dynamic optimization for gait [4] and was used for more challenging activities such as step down and chair rising on TKR patients, predicting contact loads consistent with data from instrumented implants [75]. Moment arms represent the effectiveness of a muscle in generating a torque about a joint of interest, while in a given configuration [99]. Moment arms mainly depend on the muscle geometry. However, the results presented in this study prove that joint kinematics can also influence them, since they are estimated with respect to the instantaneous helical axis. In fact, when the kinematics measured in the experiment and passive motion of the joint were implemented in the knee model, significantly different moment arms were calculated (average RMS difference: 15.4 mm). Therefore, the predicted muscular forces were also different (RMS difference: 145 N in the case without co-contraction), although similar net torques were estimated by performing inverse dynamics (Fig. 3.8). The analysis of the ligament forces throughout the squat cycle proved that the mechanical properties optimized by the sequential approach were consistent with the modeled specimen. Specifically, the ACL was active at the beginning of the simulation (close to full extension) to prevent hyperextension of the tibia, whereas PCL and MCL generated force at deep flexion angles. Most of the other ligaments were only slightly tight throughout the flexion range and did not significantly influence the motion of the joint.

The model-predicted TF and PF kinematics were moderately different from the experimental ones (Fig. 3.11). This does not surprise mainly because the quadriceps

force applied in the experiment was significantly larger (average RMS difference: 1397 N) than the one obtained with the PI controller in the FE model. The difference in the quadriceps force certainly affects the motion of the joint. For instance, the internal rotation of the tibia in the experimental session was at most 5°, while the model predicted an internal rotation up to 11° throughout the squat cycle. Moreover, the ligaments calibration performed against literature data could have produced soft tissue mechanical properties that did not perfectly match the ones of the specimen. Generally, the prediction of all the DoF in a complex joint such as the knee is one of the greatest challenges in the biomechanical world. Therefore the FE-predicted kinematics, although it does not perfectly match the experimental measurements, could still be positively interpreted as a validation of the model.

This work shows that the FE modeling is a powerful and efficient tool to estimate all those quantities not easily measurable during an experiment but crucial for the prosthetic design and the surgical planning, such as contact and ligament loads. In this study, the prediction of TF and PF contact forces has a limited meaning because of the experiment itself. *In vitro* estimates of contact forces are certainly not comparable to *in vivo* ones. However, the computational framework developed in this study could easily be adapted to *in vivo* experiments, which offer more interesting and meaningful data in terms of muscular forces and joint loads.

3.4.2 Limitations

The limitations within the current study are several, but they do not invalidate the main findings of this work. Ideally, the laxity properties of the TF joint would have to be calibrated against tests performed on the same specimen. In absence of those tests, literature data are a valid option, as it was showed in Chapter 2 of this dissertation, but still a source of errors. For example, the definition of the coordinate systems used to record the joint relative motion could be not exactly the same between the model

and the experiment. Moreover, the patellar ligament mechanical properties are taken from the literature [3] and not calibrated on the current specimen. The muscles are modeled as simple linear actuators, while in reality the muscular forces are length- and velocity-dependent [113]. This simplification is acceptable here because in the *in vitro* experiment against which the model predictions are validated, a hydraulic cylinder is used in place of the quadriceps. If the computational framework designed in this study will be used to replicate an *in vivo* experiment, a more physiological representation of the muscles will have to be adopted. In the FE model of the knee joint, one-dimensional ligaments are an acceptable approximation within the scope of this work. One-dimensional ligaments are a reliable and computationally efficient representation of the effect of the soft tissue constraints on the joint motion [5]. However, in order to extract more detailed information on ligament length patterns or loading conditions, a two- or three-dimensional representation would be more appropriate.

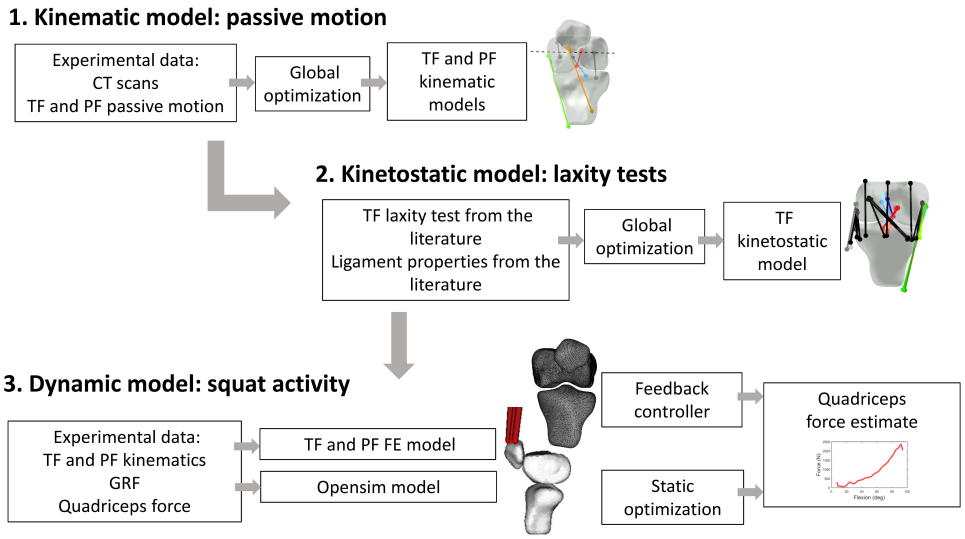

Figure 3.1: Workflow. The TF and PF kinematic models are designed and then included in the kinetostatic model. The last step is the design of the dynamic (muscular) model of the knee.

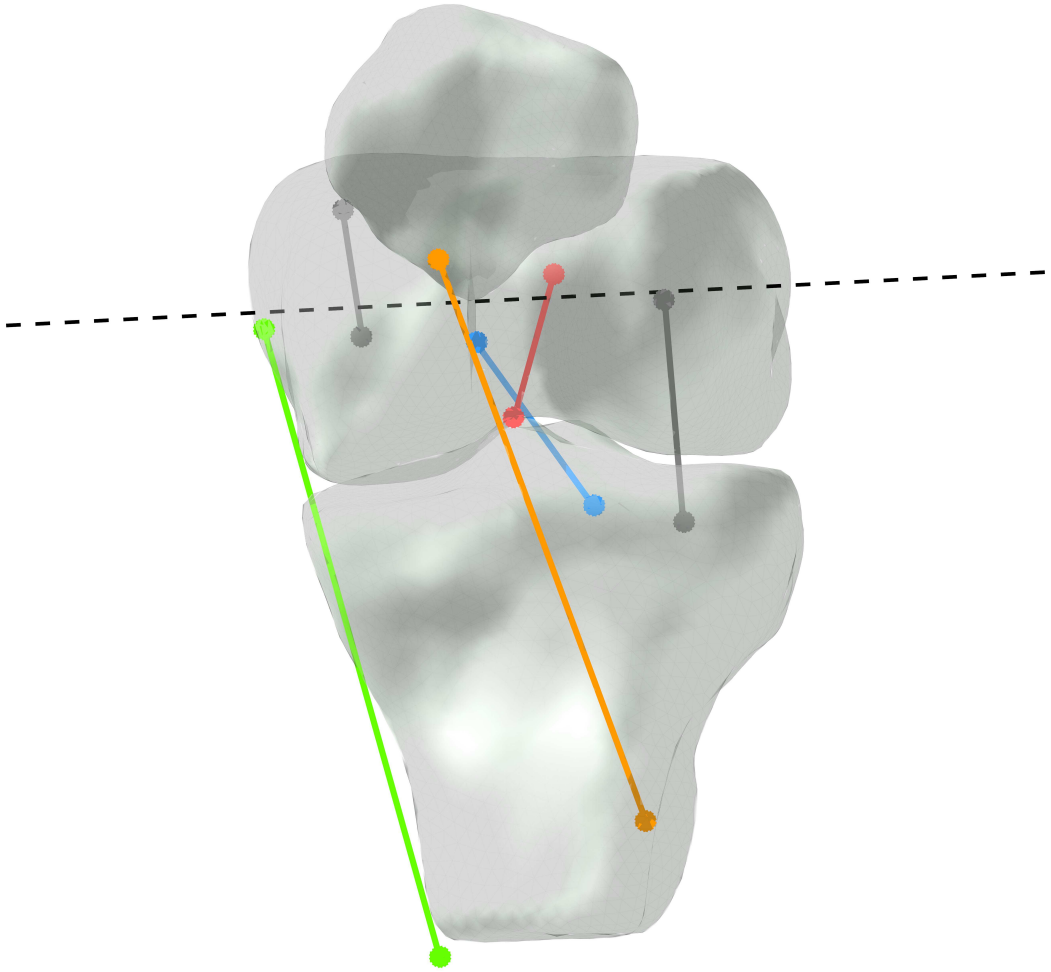

Figure 3.2: Kinematic model of the TF and PF joint. ACL (red), PCL (blue), MCL (green) and patellar ligament (orange) isometric fibers are represented as rigid links. The black lines are the rigid links that connect the centers of the medial and lateral spheres approximating the condyles. The axis of the cylinder approximating the femoral trochlea in the PF mechanism is represented as a black dotted line.

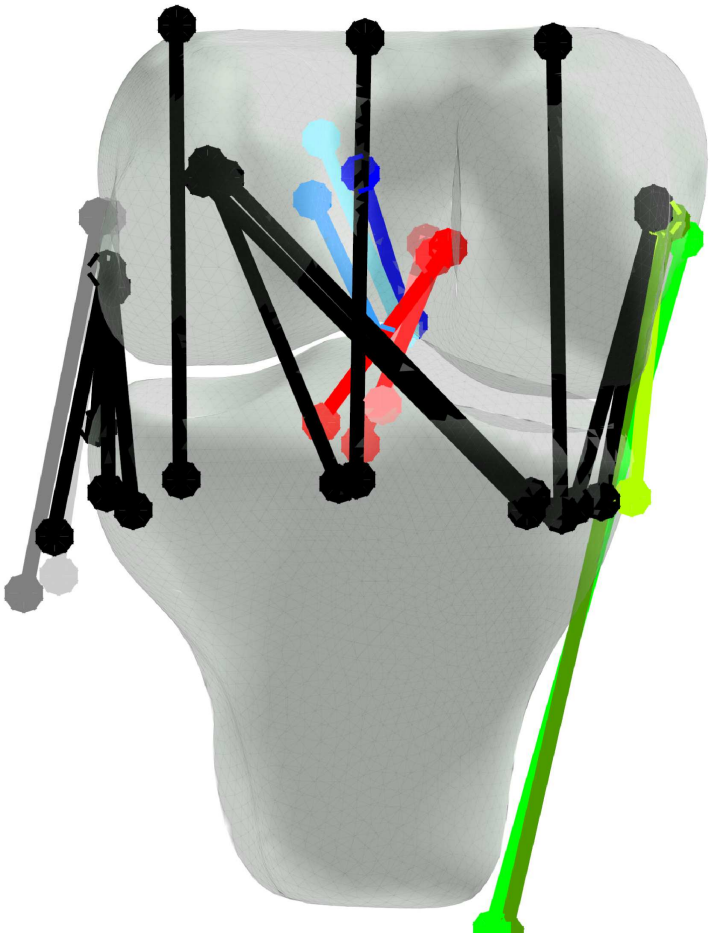

Figure 3.3: Kinetostatic model of the TF joint (posterior view). ACL (blue), PCL (red), MCL (green), LCL (grey) and secondary structures (black) with anatomical surfaces are shown.

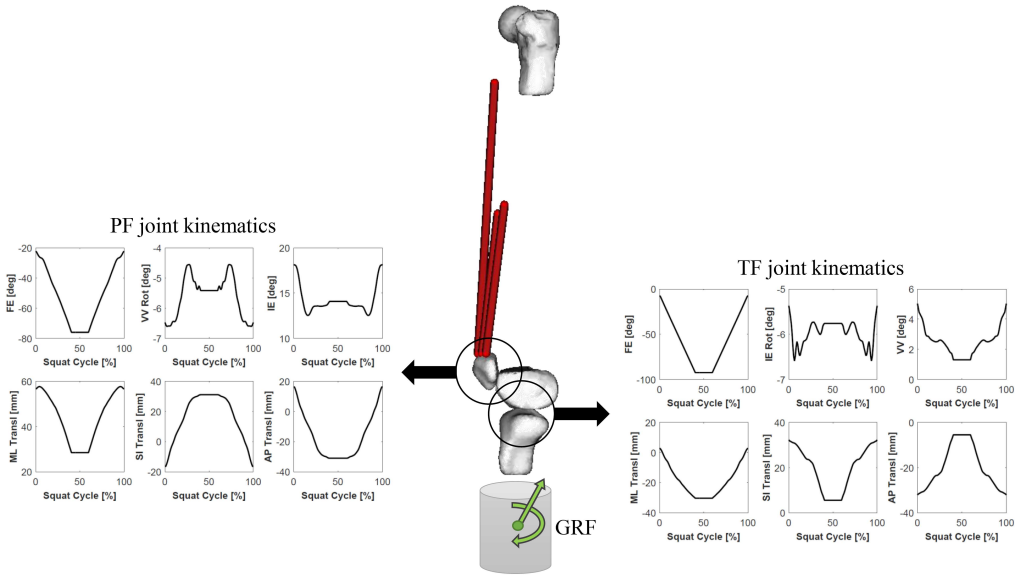

Figure 3.4: Opensim model. TF and PF experimental motions are assigned to the joint by means of splines and the ground reaction forces and torques are applied to the tibia in the same way as the test rig does, i.e. by means of a ring. The model represented in this picture is the one with only the vasti muscles.

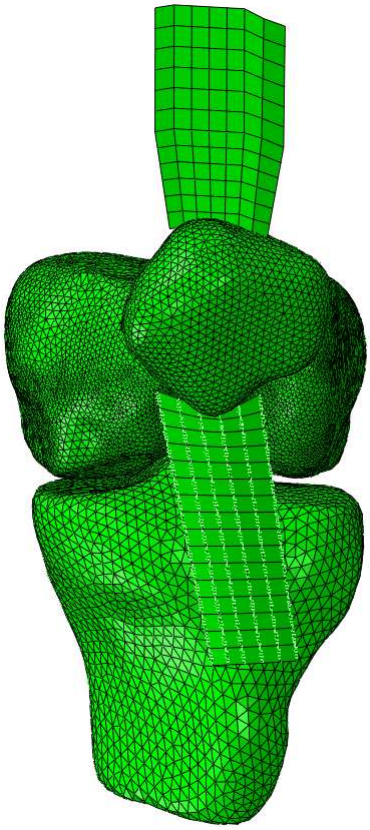

Figure 3.5: FE model of the TF and PF joints (Abaqus/Explicit). Quadriceps and patellar tendon are represented as two-dimensional membranes while ligaments (not visible) are represented as one-dimensional springs. Bones are meshed with triangular elements.

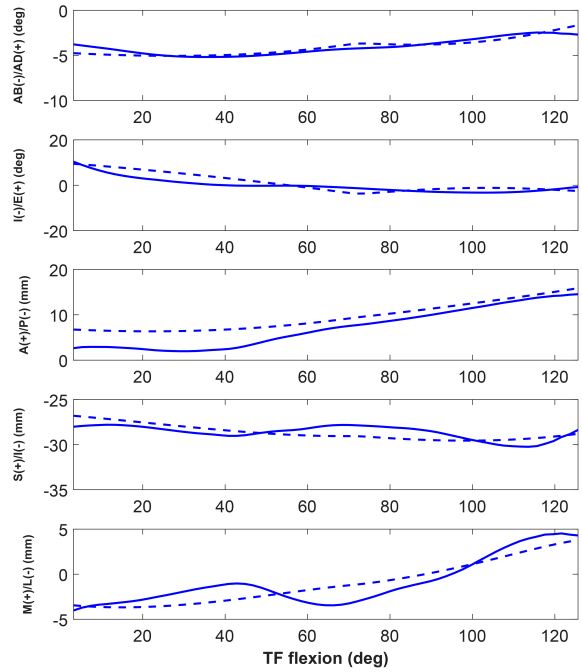

(a)

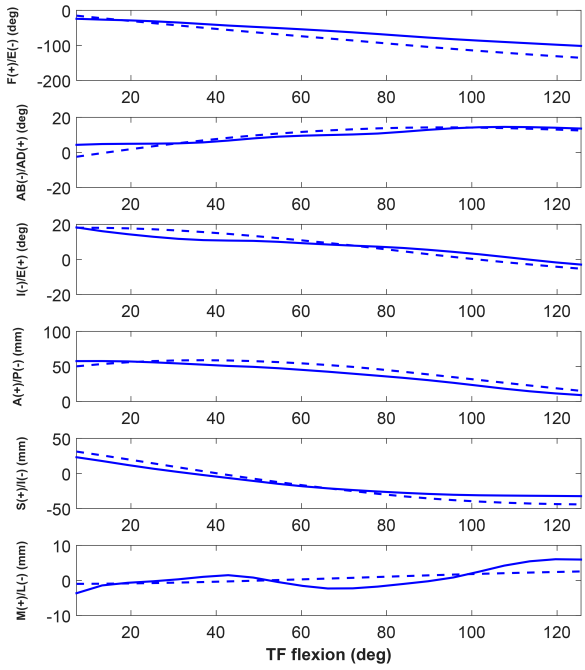

(b)

Figure 3.6: TF (a) and PF (b) passive motion: model-predicted motion against experimental results.

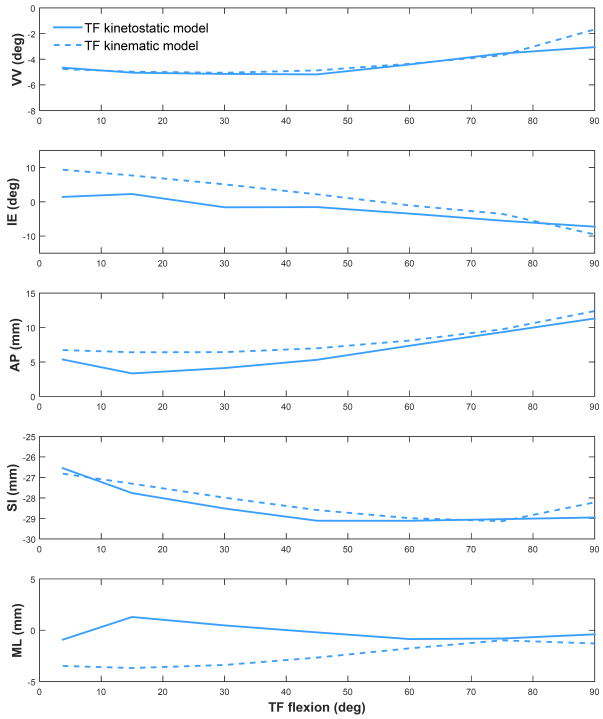

(a)

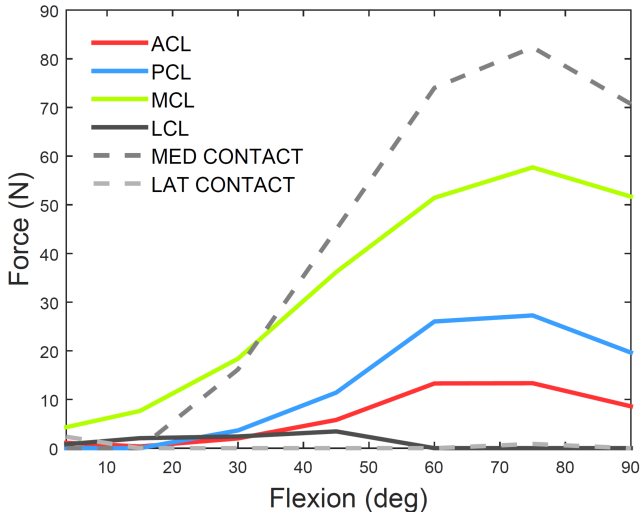

(b)

Figure 3.7: Passive motion of the kinematic and kinetostatic model (a). Ligament and contact forces in the kinetostatic model during passive flexion (b). Ligament forces are not small but not quite zero because their resting lengths was shorten by 1% to 2% with respect to the one obtained from the kinematics model.

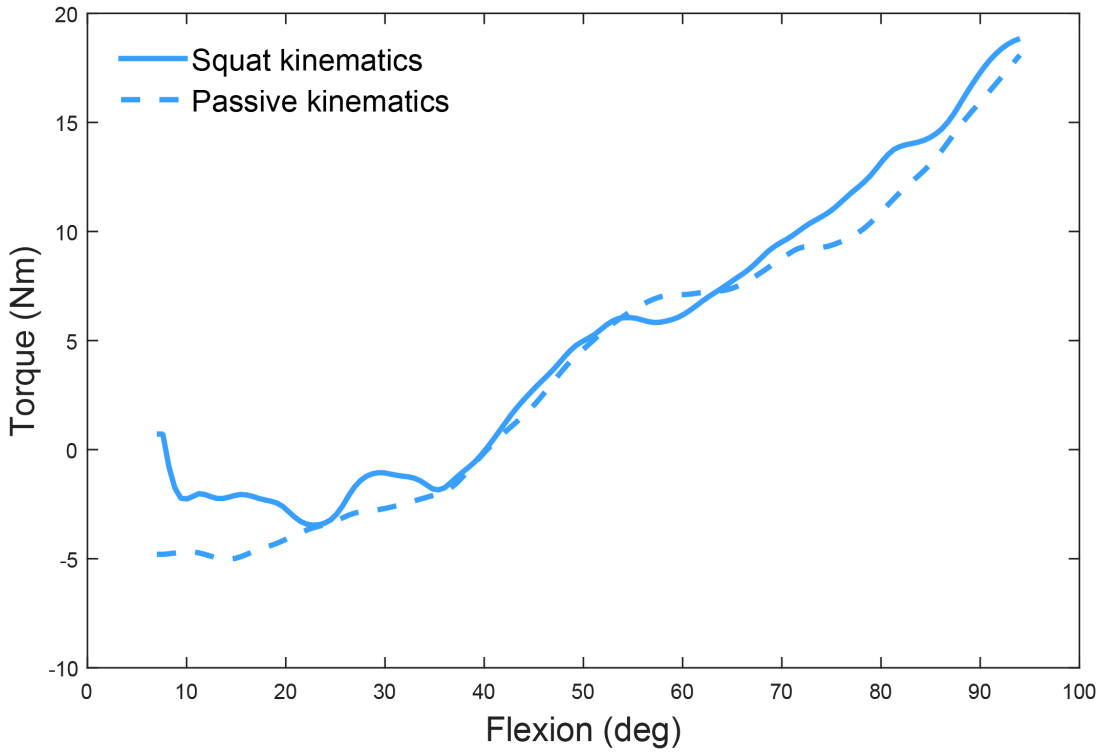

Figure 3.8: Joint torque needed to perform the squat activity in Opensim. The TF and PF joints are modeled respectively as 1 DoF (TF) and zero DoF (PF) joint whose rotations and translations are expressed as a function of TF flexion derived from the passive motion (dotted lines) or from the squat kinematics (continuous lines).

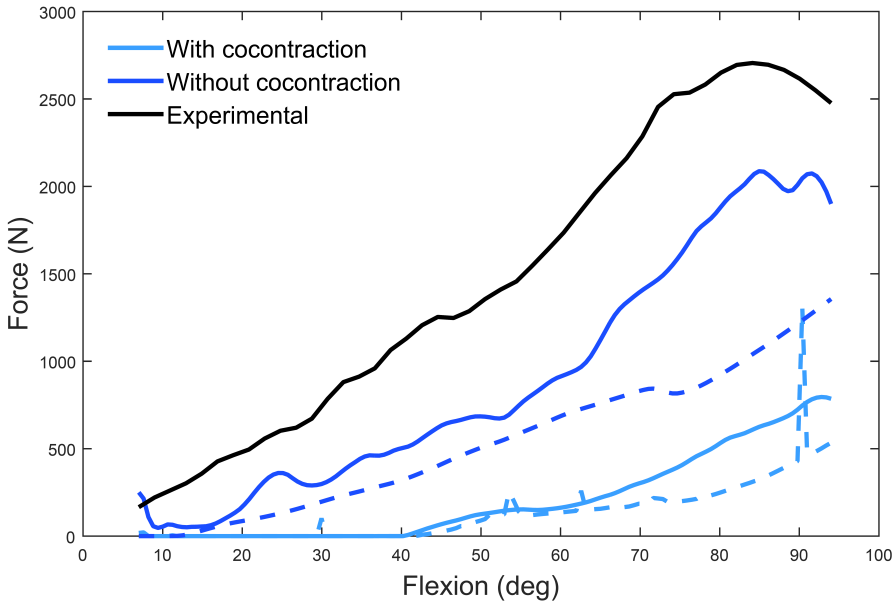

Figure 3.9: Quadriceps (vastus medialis, vastus lateralis and vastus intermedius) force to perform the squat activity obtained with Opensim static optimization, compared to the experimental force. The TF and PF joints are modeled as 1 DoF (TF) and zero DoF (PF) joint whose rotations and translations are expressed as a function of TF flexion derived from the passive motion (dotted lines) or from the squat kinematics (continuous lines).

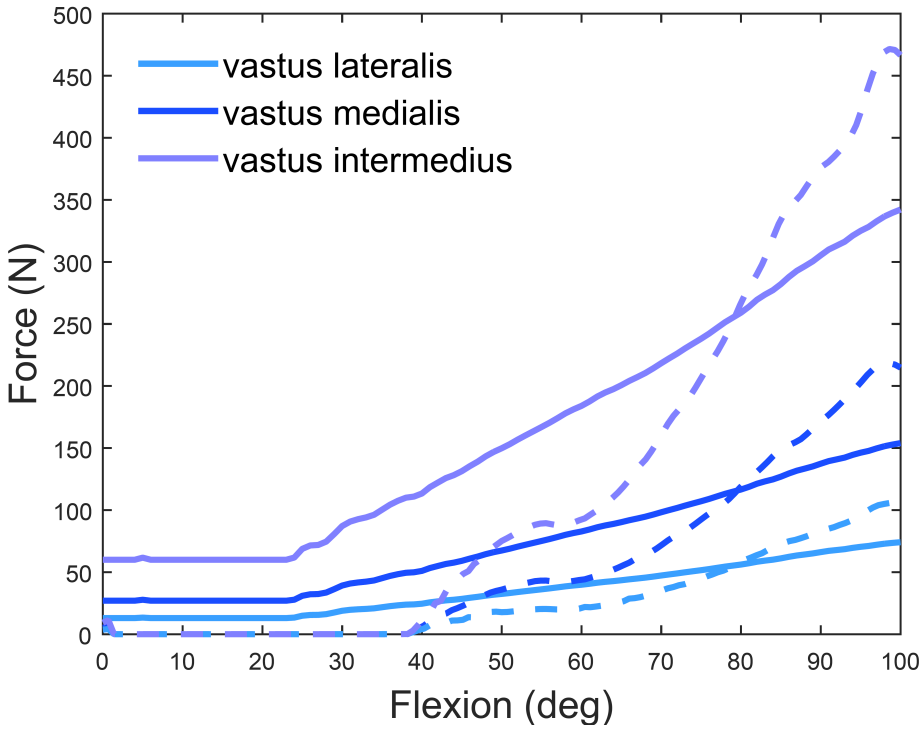

Figure 3.10: Quadriceps force obtained with the feedback controlled FE model (continuous line), compared to Opensim prediction (dotted line).

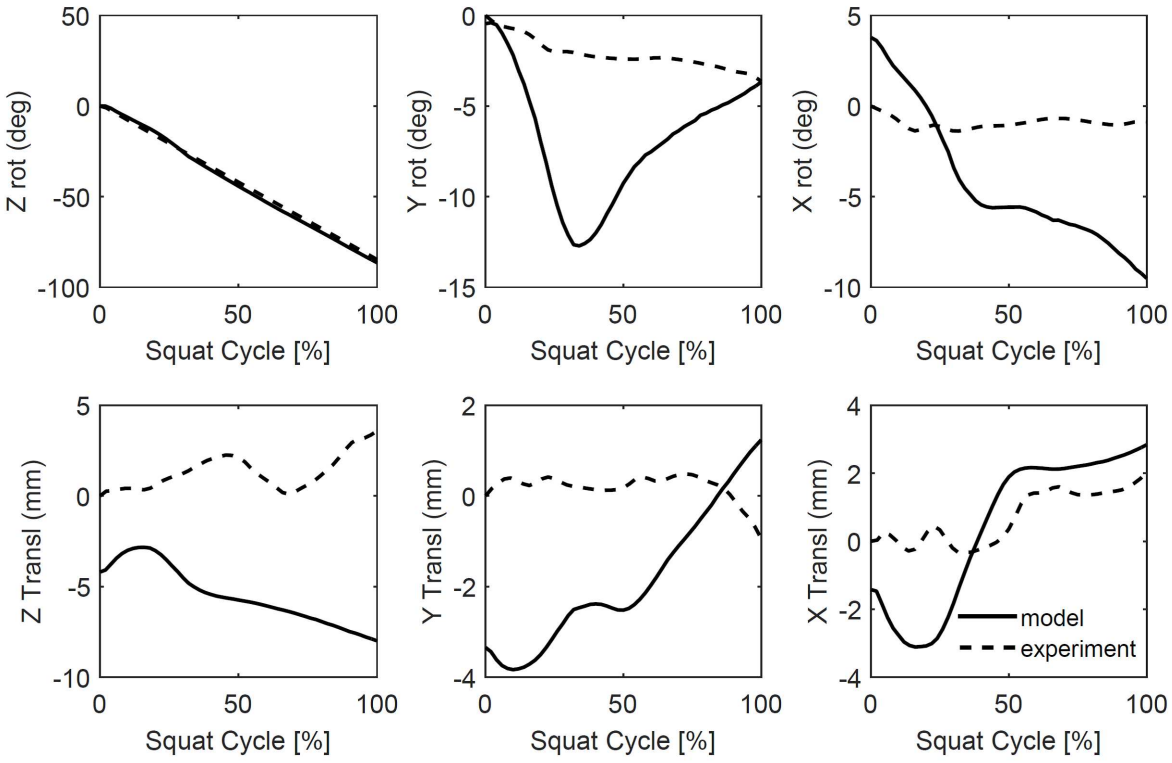

Figure 3.11: FE model-predicted and experimental Cardan angles (Z-Y-X sequence) and translations for the TF joint during feedback controlled squat activity, in the femoral anatomical coordinate system.

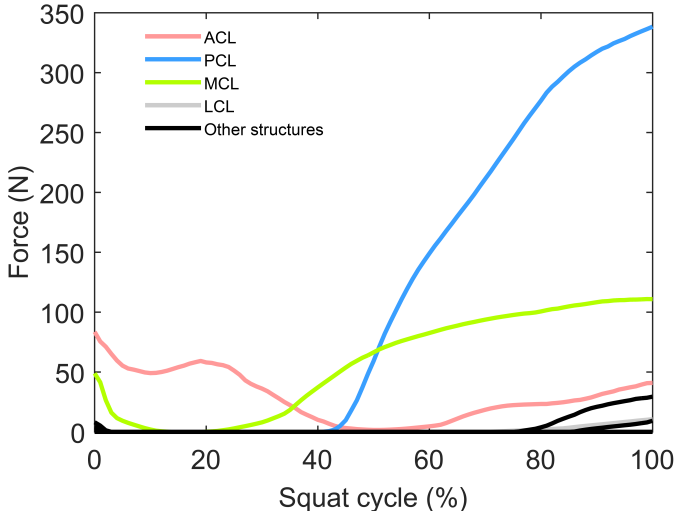

(a)

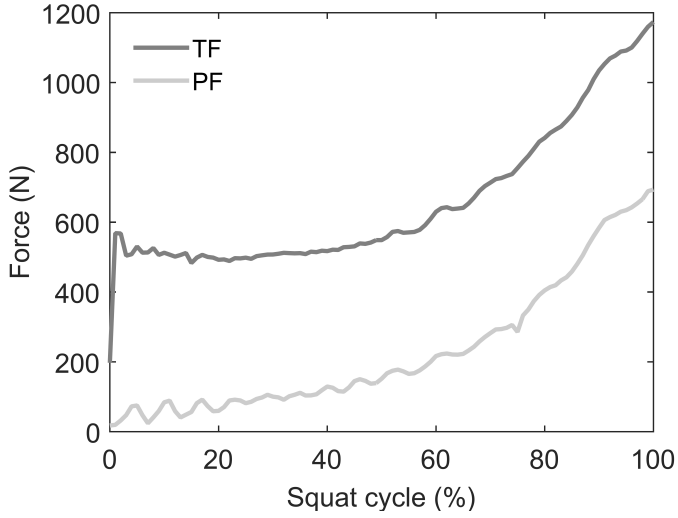

(b)

Figure 3.12: Ligament forces (a) and contact forces (b) obtained with the FE model simulating the squat activity.

Chapter 4

TKR compressive load to reproduce natural joint stability

4.1 Introduction

Total knee replacement (TKR) is a common and effective procedure in reducing or eliminating joint pain and restoring joint function, with typical 10-year survivorship near 95% [36, 88]. The procedure involves removing a number of structures which provide restraint in the natural knee, including the articular surfaces of the bones, menisci and one or both cruciate ligaments. The implanted components aim to restore joint stability provided by the sacrificed structures; however, knee instability remains a common complaint of TKR patients, particularly during high-demand activities such as stair ascent/descent [17, 69, 74, 76].

A number of studies have compared tibiofemoral (TF) laxity/stability characteristics of the natural knee with a variety of available implant designs. Various experimental studies [45, 94] compared the laxity of multiple TKR designs of varying sagittal radius in the absence of any soft-tissue, reporting substantial differences in anterior-posterior (AP) and internal-external (IE) range of motion between compo-

nents. Luger et al. [62] used an experimental knee simulator to apply compressive force plus cyclic AP force and IE torque to cadaveric natural and implanted knees, reporting that for low conforming devices, soft-tissue restraint was required at low compressive loads in order to avoid anterior tibial subluxation, while at higher compressive force, sufficient stability was provided by the component geometry alone.

These traditional laxity tests are based on evaluating the differences in joint motions under an applied out-of-plane load for different designs; for example, they demonstrate that a low conformity design will achieve greater IE range of motion under the same applied IE torque as a high conformity design. However, it is difficult to interpret the resulting differences in laxity, across implants or compared with the natural knee, in millimeters or degrees, and the potential impact to the joint replacement patient directly. In addition, the human body is effective at adopting compensatory strategies in response to surgical trauma, injury or degeneration. Notably, adaptation of muscle recruitment patterns and forces to counteract sensations of joint instability is commonly reported in clinical electromyography (EMG) studies, with increased quadriceps-hamstrings co-contraction shown to enhance TF joint stability after TKR [9, 10, 16, 25, 63, 104]. Benedetti et al. [9, 10] reported a high level of coactivation of hamstrings and quadriceps in the stance phase of gait for patients with low conformity TKR, two years after surgery. Lunderberg et al. [63] showed similar findings, specifically a prolonged co-contraction of antagonistic muscles in the TKR subjects compared to the healthy group. In sight of this, some studies [104] pointed out that to minimize compensatory movement strategies and optimize muscle-firing patterns should be the focus for clinicians treating TKR patients. Mitchell et al. [68] suggested that intrinsic stability in TKR design may be one of the factor that provides for efficient muscle recruitment. With respect to the TF articular surfaces, muscle co-contraction is primarily experienced as an increase in the compressive force on the joint, i.e. the contact force across the joint, as this is an important factor in stabi-

lization [8, 77]. Hsieh and Walker [50] reported a marked increase in stability with an increase in compressive load, and believed geometrical conformity of the condyles to be the most important factor in decreasing laxity under load-bearing conditions. The compressive force across the joint has been identified as one of the key factor influencing TKR motion, together with friction and condylar conformity [94].

As an appropriate goal for TKR is to restore the natural mechanics of the TF joint [20, 95, 105, 106], we aim to evaluate TKR stability in a novel, more physiological way, through incorporating adaptation in compressive load via feedback control. Specifically, the objective of the current study is to estimate compressive load requirements necessary to achieve natural stability/laxity for current TKR designs, and we hypothesize that these load requirements will vary as a function of the constraint inherently provided by the geometry of the TKR components.

4.2 Methods

4.2.1 Model Validation

Two cruciate-retaining fixed-bearing TKR (Attune® and P.F.C. Sigma®, DePuy Synthes Inc., Warsaw, IN) were tested in a tension-torsion Instron (Norwood, MA) servohydraulic test frame with custom fixturing (Fig. 4.1). Prior to testing, the joint was lubricated with Vaseline. A constant compressive load of 667 N was applied to the implant. At different flexion angles (0°, 15°), experimental trials were run under displacement control, applying either IE rotation (up to 20°) or AP translation (up to 10 mm), while the corresponding load in the same degree of freedom (DoF) was measured. During testing, femoral varus-valgus and vertical translation were free, with all other DoF fixed except for the DoF under evaluation. AP translation was applied to the insert via a side actuator during the AP constraint testing. A finite-element (FE) model of the implant (Fig. 4.1) was developed in Abaqus/Explicit (SIMULIA,

Providence, RI): the model consisted of the femoral component and the tibial insert. Both the polyethylene insert and the femoral component were meshed with triangular surface elements and were modeled as rigid bodies for computational efficiency. A rigid contact definition with a pressure-overclosure relationship optimized to replicate the deformable behavior [46] was used together with a friction coefficient of 0.04 appropriate for metal-polyethylene interaction [33]. The model was evaluated under the same conditions as the experiments. Response loads were measured in the DoF of interest and compared to the experimental data.

4.2.2 Conformity Ratio Measurement

Before simulation, conformity ratios were computed to quantify the geometry of four current TKR designs in posterior-stabilized (PS) and cruciate-retaining (CR) configurations: Triathlon® (Stryker, Kalamazoo, MI), NexGen® (Zimmer, Warsaw IN), Attune® (DePuy, Warsaw, IN) and P.F.C. Sigma® (DePuy Warsaw, IN). Conformity ratio was calculated by dividing the femoral sagittal radius of curvature by the insert radius of curvature at the dwell point at 0°, 30°, 60°, and 90° of flexion. The utilized implants intentionally represent a range of available conformity (Fig. 4.2).

4.2.3 Feedback-Controlled Model Development

Data from experimental *in vitro* laxity tests of the natural knee were obtained from published literature [2,50]. Specifically, torque-rotation and force-displacement curves from the following tests were obtained:

- Anterior tibial translation under an increasing AP load from 0 to 200 N at 40° and 90° of flexion with a compressive load of 900 N [2].
- Internal and external tibial rotation under an increasing IE torque from 0 to 15 Nm or 20 Nm at 40° and 90° of flexion with a compressive load of 900 N [2].

- Internal-external rotation under a cyclic IE torque from 0 to 4.903 Nm at full extension with a compressive load of 734 N [50].

A FE model of the implanted TF joint as described above was used. The primary ligaments crossing the joint were also included (Fig. 4.3). Specifically, two-dimensional representations of the posterior capsule (PCAP), medial collateral ligament (MCL), lateral collateral ligament (LCL), antero-lateral structure (ALS), popliteofibular ligament (PFL), and posterior cruciate ligament (PCL) (with CR designs) were included in the model, and have been previously calibrated to reproduce measured knee constraint [5]. The boundary conditions of the experimental testing were replicated. The implant components were positioned according to the initial flexion angle of the specific test and in neutral mechanical alignment. Preliminary simulations were performed as traditional laxity tests. Load profiles (either IE torque or AP force), as per the *in vitro* tests, and compressive force were applied to the tibial component and relative TF joint motions were recorded. TF joint kinematics and loads were applied and measured via a Grood and Suntay joint coordinate system [42]. The step size time was 1 second: previous work showed that if the FE model is meant to replicate quasi-static activity/test, the step length does not affect kinematics prediction [33]. The time increment was chosen after a convergence analysis and set to 1e-5 second. Laxity properties of the four TKR designs were evaluated. One of the CR devices (P.F.C Sigma®) was evaluated in two states: with a normal posterior cruciate ligament (PCL) and in a worst-case scenario, i.e. with the PCL removed. All the evaluated TKR designs were the same size (equivalent to P.F.C. Sigma® size 3). Subsequently, simulations which allowed adaptation of the applied compressive load in response to implant laxity were performed; that is, the compressive force was calculated based on the force required to match the target IE torque or AP force profiles of the cadaveric tests. This was implemented through a proportional-integral (PI) control system which was coded in FORTRAN language and interfaced with the

FE models through an Abaqus user subroutine [27]. Details of the subroutine are reported in Appendix C. A sensor in the Abaqus/Explicit model was used to pass the instantaneous load of the tibial component (either torque or force, depending on the test) to the PI controller at each increment of time during the simulation, while the natural knee kinematics (either IE rotation or AP translation) was applied to the insert (Fig. 4.4). The purpose of the controller is to adjust the compressive load active on the tibial component, so that, for an instantaneous kinematic pose, joint load in the corresponding DoF matched that of the natural knee. For example, if the measured IE torque in the model is greater than the target IE torque (i.e. the natural knee IE torque), the compressive load applied to the implant decreases to reduce IE torque, while if the measured IE torque is less than the target torque, the compressive load increases. The proportional and integral gains in the PI controller were manually tuned for each laxity test in order to minimize the error between the target profile and the sensor value. The compressive load required for each implant during each simulation was recorded and compared to the compressive force applied in the natural knee cadaveric tests. Compressive load requirements were also compared between implant designs, implant types (CR or PS), and between models tested with and without ligament structures. To evaluate the most efficient FE solution, results from Abaqus/Explicit (dynamic) and Abaqus/Standard (both static and quasi-static) models were compared in terms of required compressive load and target matching as well as analysis time. Abaqus/Explicit was faster than Standard (20 min. vs. 2 hrs. simulation), obviously an important characteristic in the control tuning process, providing comparable results, and hence was adopted for the analyses shown herein.

4.3 Results

The FE model predictions of TKR constraint in IE and AP were in good overall agreement (Fig. 4.5) with the experimentally measured displacements in the same DoF (average root mean square (RMS) error = 0.39 Nm and 79.6 N, respectively), and appropriately differentiated the two implant designs. Because of the rigid body assumption, deviation from the experiment began upon edge loading of the insert, as can occur toward the extents of motion (Fig. 4.5). The feedback-controller was able to effectively match the natural knee stability after an adequate tuning of the gains of the control system. RMS differences between the simulations and the target kinematic profiles were on average 0.52 Nm for the IE tests (4.41% with respect to the load range) and 8.17 N for the AP test (4.09% with respect to the load range).

Traditional laxity testing with the same constant compressive force applied on the intact natural knee during the experimental testing, resulted in substantially different measured behaviors at full extension (Fig. 4.6) as well as at 40° and 90° of flexion (Fig. 4.6). Many of the tested implant designs dislocated (interrupted plots in Fig. 4.6b) when subjected to the same loads applied to the natural knee. The TKR IE laxity was in general greater than the natural knee when the same compressive force was applied (Fig. 4.6a). Conformity ratios ranged from 0.22 to 0.88 (Fig. 4.2). P.F.C. Sigma® and Attune® showed a higher conformity ratio than Nexgen® and Triathlon® at each of the evaluated degrees of flexion.

With the feedback-controlled FE models, the lower conformity implants (as defined by the conformity ratios) generally required a higher compressive force than higher conformity geometries regardless of the flexion angle at which the laxity test was performed (Fig. 4.7, Fig. 4.9, Fig. 4.8, Fig. 4.10). The two lower conformity designs overall required an average of 66.7% more compressive force than the high conformity designs to maintain stability equivalent to that of the natural knee (at peak applied AP/IE loading). The two groups (two lower and two higher conformity

implants) were statistically different ($p \leq 0.001$) by means of an unpaired two-tailed Student's t-test. Simulation was also performed in IE without the soft tissues present, which quantifies to what extent the implant surfaces contribute to the stability of the joint (Fig. 4.7, Fig. 4.9). When the implants were tested without the soft tissue, differences in the required compressive force to match natural stability were found, although not always substantial, which indicates that the articular surfaces of TKR are the main contribution to the joint stability. On average, at the peak IE load, the device tested without ligaments required 28.2% more compressive force. Implants overall were much more similar to natural stability in AP loading than IE loading. On average, over all the tests performed, the PS designs required 2.6% more compressive force than CR, at the peak AP or IE load; the two groups proved to be not statistically different when subjected to a paired Student's t-test. On average, cruciate-retaining P.F.C. Sigma® tested without PCL required 37.7% more compressive force at the peak IE torque, with respect to the same implant evaluated with the ligament.

4.4 Discussion

Current TKR designs demonstrate wide variation in the level of geometric constraint provided at the TF joint. Under a constant compressive load, the most constrained device, evaluated with soft tissue, provided similar AP and IE laxity to that reported in the natural knee during cadaveric testing, while the least constrained device resulted in AP and IE motions up to 5X greater than the natural knee. These traditional laxity tests assume that the loading condition at the joint remains consistent and variation in component design is reflected through variation in joint motion and ligament forces. It is somewhat difficult to interpret the impact to the patient of greater motion in the implanted knee under consistent loading. The method described in this paper is a novel approach to assessing joint constraint in the implanted knee.

Implant stability is described in terms of the physiological requirements to reproduce stability equivalent to that of the natural knee. EMG studies have demonstrated that the body adopts alternative muscle loading strategies to try to maintain the stability of the joint, with higher levels of quadriceps-hamstrings coactivation frequently reported after TKR than in an intact control group [9, 10, 16, 25, 63, 104]. While it is most likely that the *in vivo* joint will incorporate a combination of increased muscle force and increased joint laxity, rather than purely one or the other, the current study provides an interesting complement to traditional laxity assessments and illustrates the levels of compressive load required to achieve stability on par with the natural knee for different TKR designs. Given that patients commonly suffer from muscle activation deficit, implant designs which aim to reduce the compressive force requirements (and hence muscle force requirements) to maintain a stable knee have potential for improving efficiency and function for the TKR patient.

This work presented an extended comparison between TKR designs with different level of conformity in their cruciate-retaining and posterior-stabilized configurations. In general terms, all of the implants required more compressive load in order to maintain natural stability, which demonstrates the complexity of reproducing the combined contribution of the articular surfaces and stabilizing structures of the natural knee. The higher conformity designs with soft tissue reasonably reproduced measured natural stability, while the lower conformity implants required greater compressive loading to maintain stability. Implants were much closer to natural mechanics during anterior tibial loading than during internal-external loading, which is primarily a reflection of different design philosophies. Many implants have intentionally reduced IE constraint in an attempt to allow or encourage a more natural kinematic response with substantial IE rotation during flexion. As seen with rotating-platform designs, IE constraint is not a requirement for clinical success; however, as both the understanding of natural knee mechanics and implant design become more sophisticated,

reproducing combined stability and mobility requirements will be more accessible, and the method developed herein will be useful in iterative design.

There are limitations in the present study that should be considered. First, the reference natural knee data were taken from previously published work and therefore minor differences between the computational model boundary conditions and the experimental setup could be present. However, the authors believe that this limitation does not significantly affect the main findings of the study and it certainly does not affect the validity of the proposed method for implant evaluation. A second limitation is that the mechanical and geometrical properties of the ligaments included in the FE model derive from a previous work [5] and therefore do not match the specific *in vitro* experiment or the range of patient soft-tissue balance post-operatively. However, the experimental data used here as a reference were averaged over more than one subject therefore the effect of the ligament properties on the knee joint laxity were averaged as well. In addition, under compressive load, the conformity of the condylar surfaces is a more critical factor for the TKR stability than the surrounding soft tissue [50]. A last limitation of the study is that only the main DoF, i.e. IE and AP, and only some flexion angles, i.e. 0°, 40°, 90°, were considered currently, primarily due to absence of a comprehensive experimental dataset published in the literature or elsewhere.

The current study comprises of a reasonably straightforward approach to joint stability; increased or decreased stability is directly created through modification of the compressive force acting at the joint. For a patient, the compressive force across the joint is driven by the muscle forces acting across the knee; additional co-contraction of the quadriceps and hamstrings serve to increase the compressive force and reduce joint motion under external loads. However, despite the simple implementation, this study demonstrates the influence of implant design, and ranks TKR components, in isolation of confounding patient-specific factors (ligament tension, body weight, etc.), in terms of the compressive load requirements to maintain a level of stability mea-

sured in the natural knee. This ranking is consistent with articular surface conformity of these devices. Clearly, there is a trade-off between stability and mobility; a more conforming design has potential to hinder range-of-motion and affect the functionality of the joint [95]. Hence, in this study we selected natural knee motions as our target joint motions for each device; implants which better match natural constraint have potential to create more natural mechanics and reduce incidences of instability in patients during high demand activities with large out-of-plane loads.

This study serves as a preliminary investigation into whether joint motion can be controlled through adaptation of compressive joint via a PI controller. Having demonstrated the efficacy of the approach here, subsequent work will aim to evaluate the specific muscle force and synergy adaptations required to achieve stability during high-demand dynamic activities on a design-specific basis.

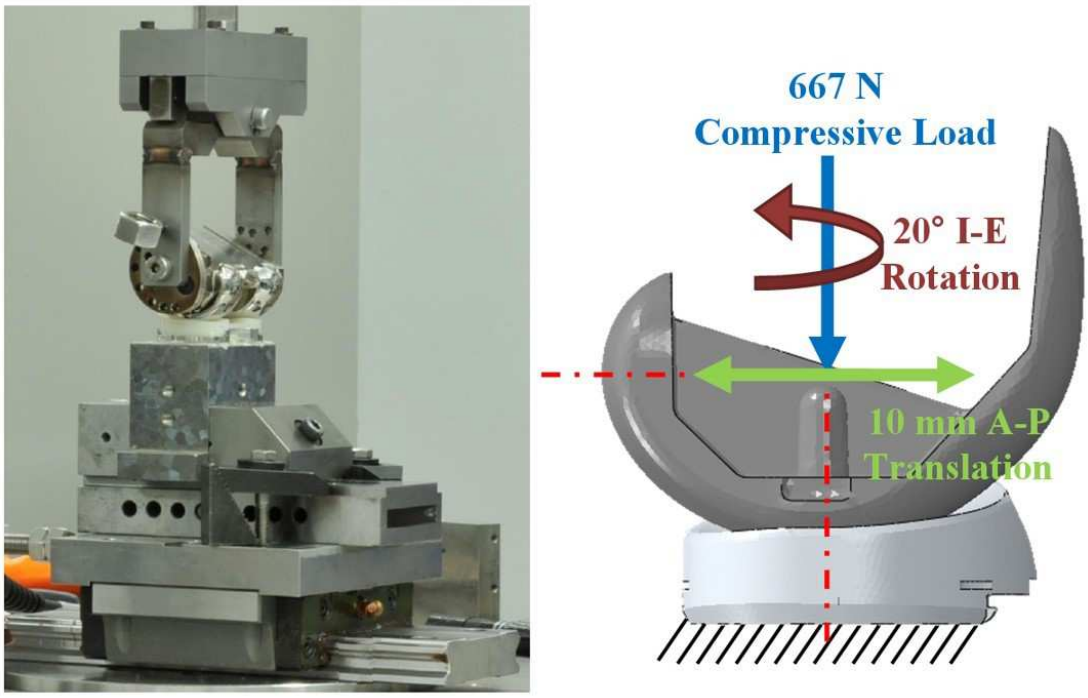

Figure 4.1: Experimental stability testing (left), and finite element model representation of anterior-posterior (AP) and internal-external (IE) testing with constant compressive load (right).

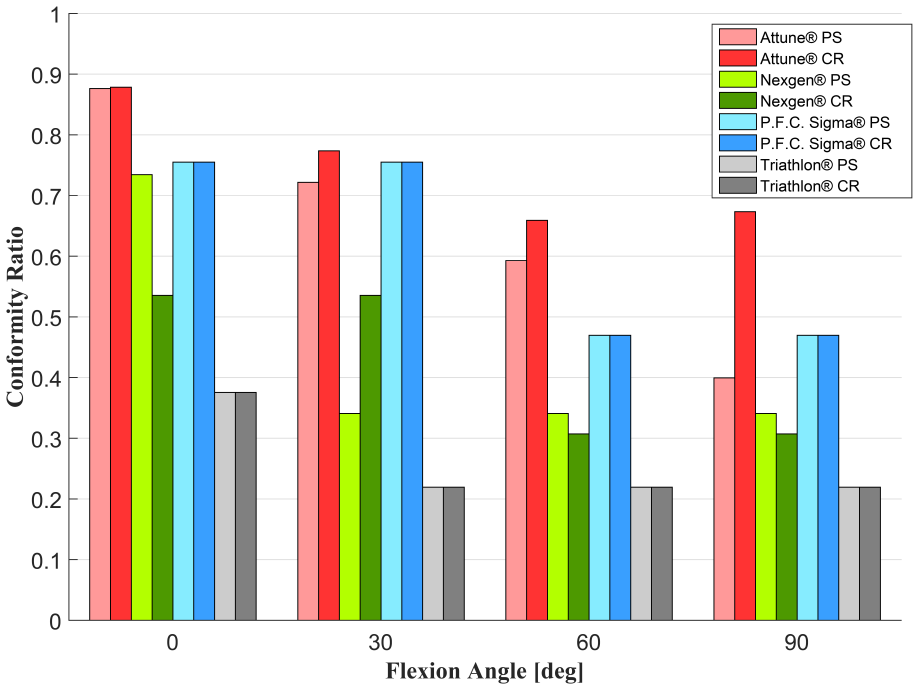

Figure 4.2: Conformity ratios of the implants at various flexion angles. Conformity ratio was calculated by dividing the femoral sagittal radius of curvature by the insert radius of curvature at the dwell point.

Figure 4.3: Finite element model of the tibiofemoral joint with posterior-stabilized implant and soft-tissue constraint.

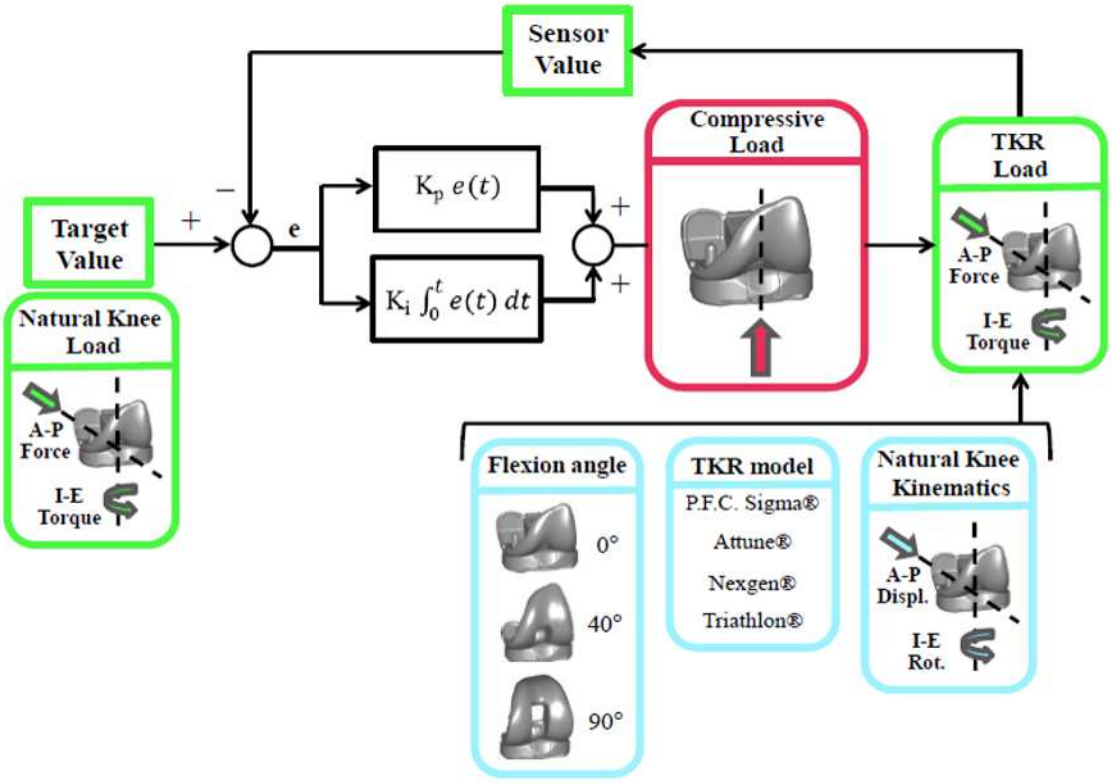

Figure 4.4: Workflow. The PI feedback controller is coded in FORTRAN and linked to the model in Abaqus/Explicit as a user-defined subroutine. Measurement from the sensor in the FE model, tracking the TKR load (AP force/IE torque) is compared to the target profile and then the actuator load required to match this target profiles is fed back to the FE simulation.

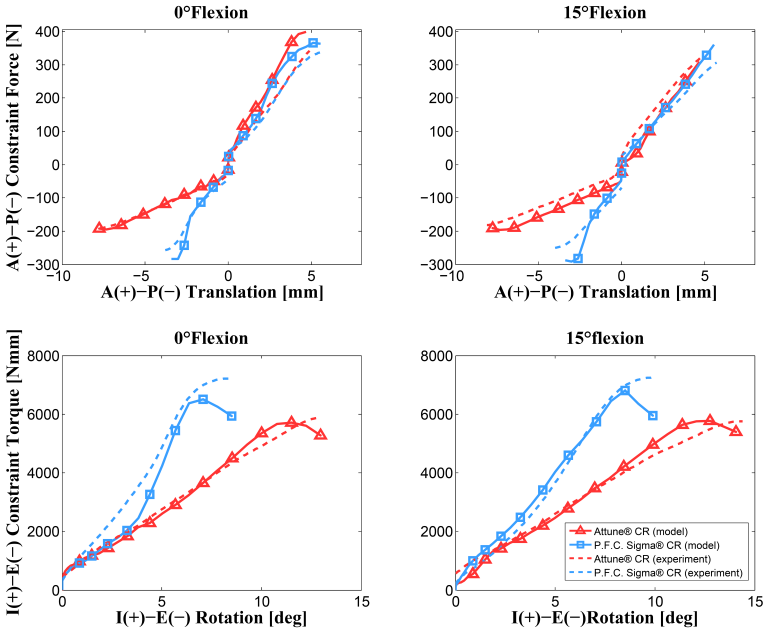

Figure 4.5: Experimental and model-predicted anterior-posterior (AP) force-displacement (above) and internal-external (IE) torque-rotation (below) data at full extension and 15° of flexion with constant compressive load. Kinematics of femoral component with respect to tibial insert is shown. Only data from the internal rotation tests are shown because the implant is symmetric with respect to the sagittal plane.

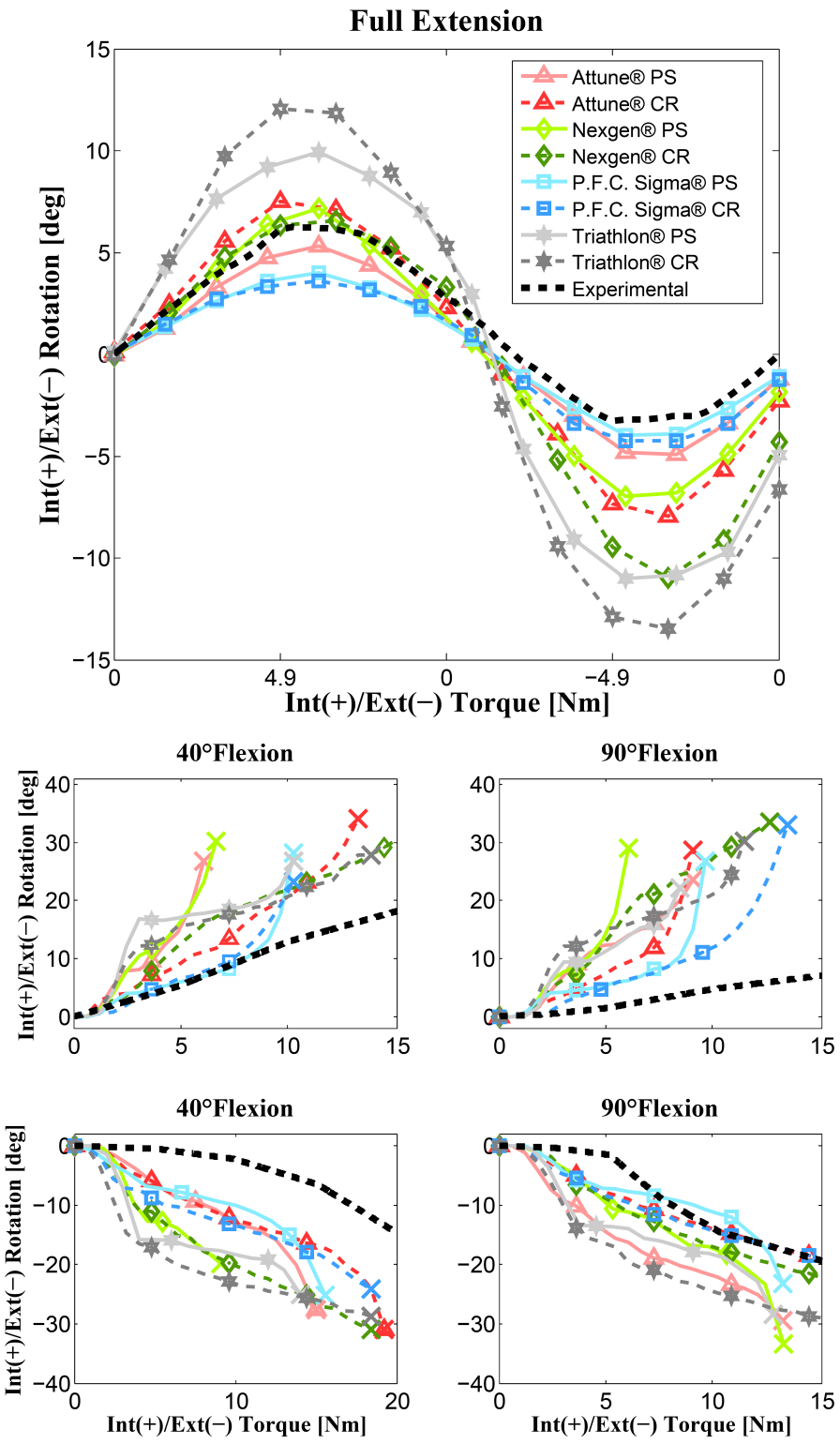

Figure 4.6: TKR laxity when the same compressive force from the natural knee testing [2, 50] is applied. IE rotation at full extension (above), at 40° and 90° of flexion (below). Dislocation occurred when the plot is interrupted with a cross.

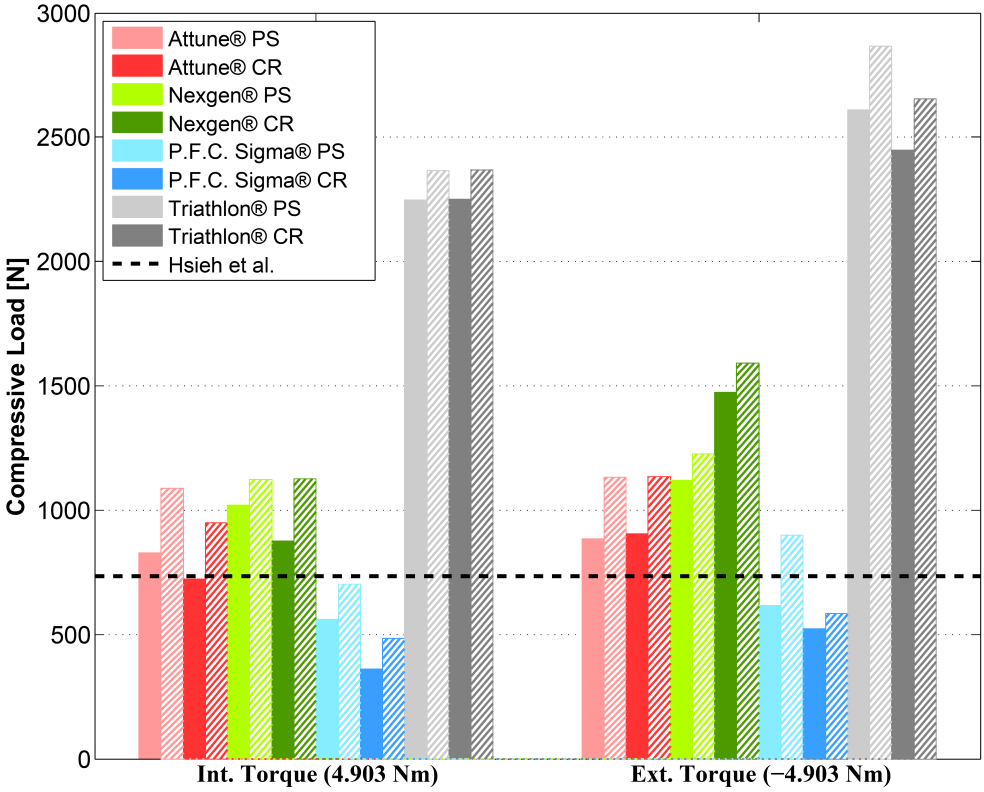

Figure 4.7: Compressive force required by the TKR to match the natural knee laxity at full extension under a tibial torque of 4.903 Nm [50] with ligaments (solid bars) and without ligaments (dashed bars).

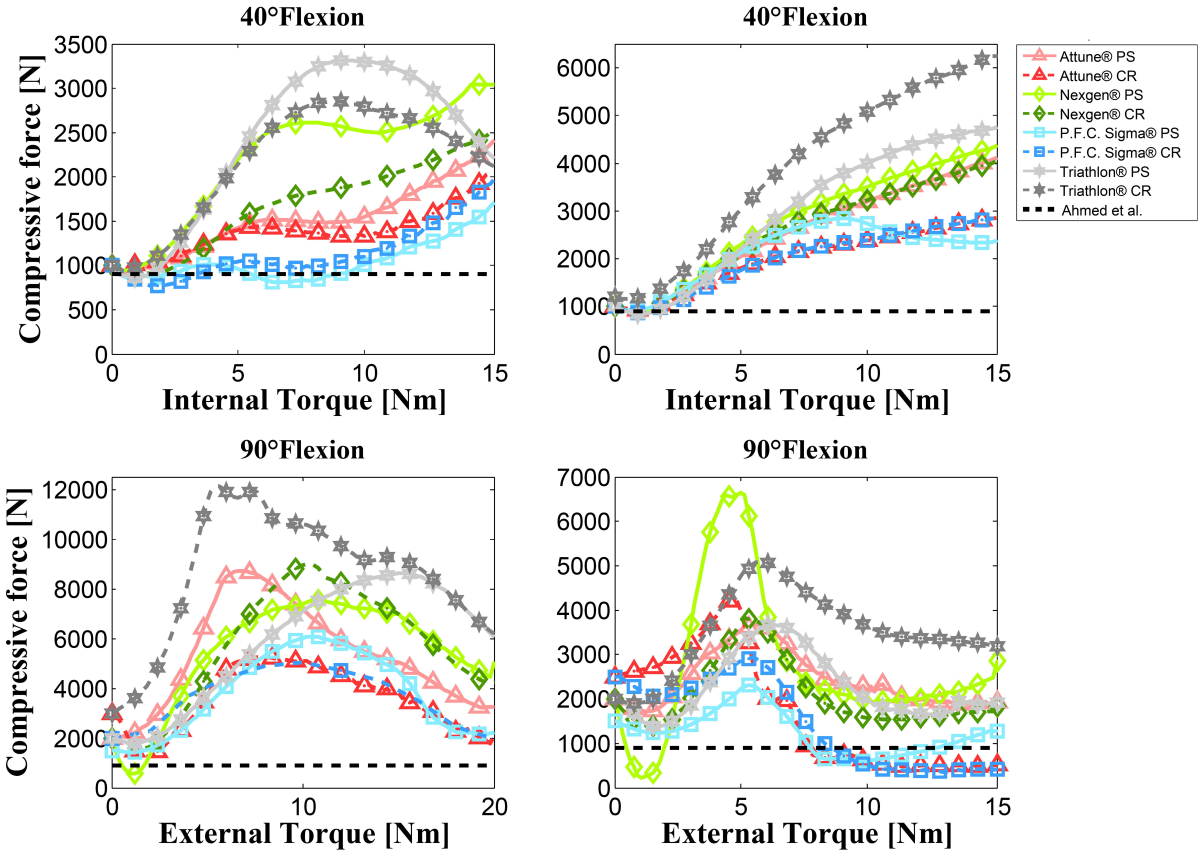

Figure 4.8: Compressive force required by the TKR to match the natural knee laxity throughout an IE torque cycle [2].

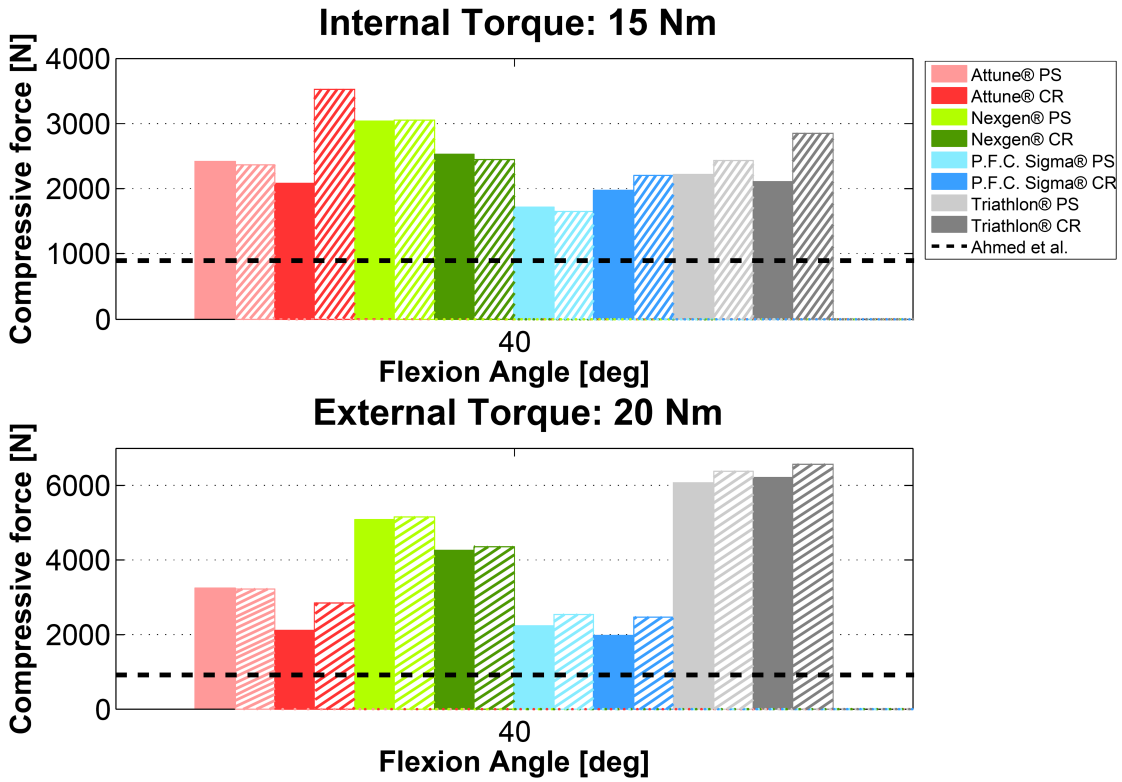

Figure 4.9: Compressive force required by the TKR to match the natural knee laxity at 40° of flexion under an IE torque [2], with ligaments (solid bars) and without ligaments (dashed bars).

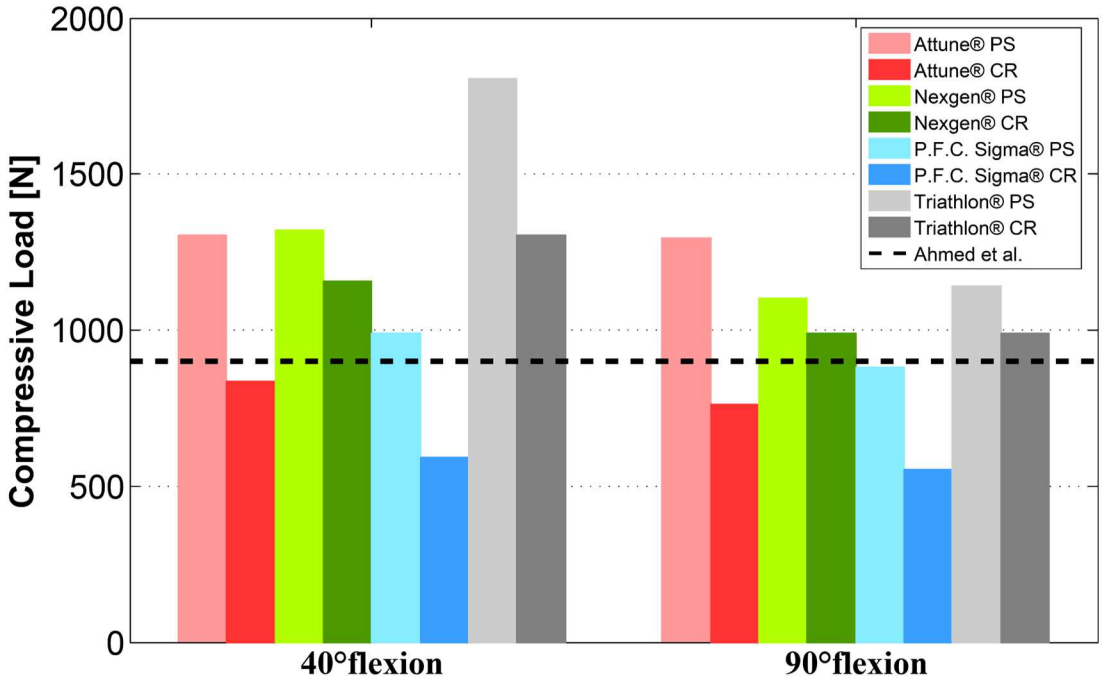

Figure 4.10: Compressive force required by the TKR to match the natural knee laxity at 40° and 90° of flexion under an AP force of 200 N [2].

Chapter 5

Conclusion

Estimates of musculoskeletal loading conditions, soft tissue stress and strain, and relative motion between the bones at the knee joint during dynamic activities can significantly benefit orthopaedic medicine by providing the necessary insights to improve prosthetic design and surgical and rehabilitation procedures planning. With the current technology, some of this information can be gathered using either *in vivo* or *in vitro* experimental techniques. It is the case of the relative motion between the bones, measurable *in vivo* by means of marker-based motion capture or fluoroscopy instrumentation; ground reaction forces, measurable with force platforms; muscular activity data, measurable with EMG signals; TKR joint loads, measurable with instrumented implants. Moreover, the most advanced imaging techniques, such as MRI and CT scans, allow for a three-dimensional view of the bones and all the soft tissue surrounding them. *In vitro* experiments can instead provide information regarding the behavior of the joint under specific loading conditions, by means of laxity tests, or the force-length relationship of ligaments or tendons, by means of tensile tests. Although beneficial to biomechanical research, experiments are expensive and time-consuming and their results are affected by numerous sources of errors, like the soft tissue artifact in motion capture techniques. Furthermore, not all the quantities of

interest can be experimentally measured in a non-invasive way with the current technology. Such is the case of the muscular forces, that are not currently measurable *in vivo*. For these reasons, the experimental approach needs to interface with the computational modeling, which offers an inexpensive, repeatable and easily adaptable way to investigate the biomechanics of the knee as well as of other parts of the human body. Holistic and reliable computational models of the static and dynamic behavior of the knee joint remain a great challenge for biomechanical researchers, given the intrinsic complex nature of the joint itself.

This dissertation presented novel and efficient computational frameworks to assess the knee behavior for both the natural (Chapter 2 and 3) and implanted joint (Chapter 4), in static and dynamic loading conditions. Regarding the healthy joint, the present work advances the state-of-the-art in the modeling of the human knee joint by implementing and validating an efficient approach for the optimization of its mechanical properties. Specifically, the first two studies (Chapter 2 and 3) successfully apply a sequential procedure for the definition of a model able to replicate the passive and loaded motion of the knee, optimizing the parameters that affect the knee laxity, i.e. ligaments stiffness and attachment areas, against experimental data. The procedure presented in Chapter 2 is computationally efficient thanks to the spherical representation of the joint contact surface, which are substituted by their anatomical representation only after the optimization. The first study proves that this process is successful and the surface substitution does not deteriorate the optimization results, as long as a detailed representation of all the main ligamentous structures is included in the model and the anatomical contact surfaces are properly adjusted in order to provide, together with the isometric ligaments, the same constraint as the kinematic model in passive motion. The last step of the sequential procedure is the implementation of the dynamic model of the joint, which is a model that includes muscles. The computational framework developed in this dissertation (Chapter 3) allows for

this last step to be performed, using two state-of-the-art techniques in biomechanics, i.e. finite element modeling and multibody musculoskeletal modeling, to replicate an *in vitro* dynamic experiment in which the previously developed knee model could be tested. The computational framework can be easily adapted to replicate *in vivo* experiments, which is the ultimate goal for a model that aims to accurately estimate muscular forces. The third Chapter 4 presents an innovative and efficient way to assess laxity in the currently available TKR geometries and provides a broad comparison between various designs, identifying the conformity of the femoral component with respect to the tibial insert as the key factor that influences the implant mechanics and therefore the muscle loading state. This study advances the traditional approach in the evaluation of the TKR laxity, suggesting that the objective of the implant should be to provide for the same stability of the healthy joint, in order to avoid the antagonistic muscular activity commonly registered in TKR patients when they perceive joint instability. In this study, the effect of the muscular co-contraction is represented as a compressive load across the joint: this representation allows for a simple but effective way to model the main effect of the muscles on the knee joint.

In conclusion, this dissertation presented novel and efficient procedures to model and evaluate the behavior of the natural and implanted knee under the effect of static and dynamic loading conditions, extending the current knowledge in the field of musculoskeletal computational modeling.

Appendix A

An exhaustive description of both the geometrical and mechanical characteristics of each ligamentous fiber of the model presented in Chapter 2 is reported in Tab. A.1.

Ligament	Origin ($\mathcal{S}_f$) $[mm]$	Insertion ($\mathcal{S}_t$) $[mm]$	K $[N]$	L_0 $[mm]$
ACL AMa	(-5.398, 2.264, 6.768)	(15.722, -2.650, -1.524)	5805	34.922
ACL AMp	(-10.741, 4.188, 9.742)	(9.703, 0.955, -6.318)	1512	32.097
ACL PLa	(-9.517, 0.547, -9.315)	(8.205, -1.229, 2.630)	1884	26.775
ACL PLp	(-12.744, 1.895, 9.769)	(2.187, 2.377, -2.164)	1560	24.499
ACL iso	(-9.104, 0.040, 9.853)	(22.896, 4.614, -3.251)	2667	34.823
PCL ALa	(1.056, -4.748, -2.392)	(-17.304, -6.777, -4.125)	4094	35.592
PCL ALp	(-1.711, -10.979, -5.812)	(-17.009, -6.595, -8.117)	4094	37.895
PCL PMa	(-5.843, 0.957, -3.199)	(-21.417, -12.838, -2.607)	4094	37.843
PCL PMp	(-8.611, -5.275, -6.619)	(-21.122, -12.656, -6.599)	4094	36.976
PCL iso	(-4.941, -2.378, -1.787)	(-32.175, -6.396, -0.048)	4094	37.933
MCL ant	(12.099, 5.094, -40.160)	(11.599, -9.675, -40.308)	3319	47.958
MCL post	(1.038, 0.358, -40.646)	(3.299, -15.223, -41.959)	3319	39.877
MCL prox	(12.098, 5.093, -40.162)	(15.077, -80.078, -15.753)	3319	120.096
MCL inter	(5.196, 10.745, -43.374)	(11.851, -89.083, -17.349)	3319	125.385
MCL dist	(1.038, 0.357, -40.646)	(7.998, -98.677, -18.076)	3319	126.630
MCL iso	(0.714, 3.778, -50.733)	(8.817, -105.708, -20.877)	3319	133.916

LCL ant	(-0.636, 5.115, 42.454)	(-18.555, -20.784, 36.386)	756	51.919
LCL post	(-3.882, 4.727, 43.269)	(-21.592, -20.110, 35.994)	756	50.708
LCL dist	(-0.688, 0.889, 42.448)	(-18.368, -22.233, 38.492)	756	49.481
PT ant	(2.000, -9.500, 40.000)	(-27.204, -12.416, 30.219)	1459	43.870
PT post	(2.000, -11.500, 40.000)	(-27.412, -10.427, 33.454)	1459	42.710
POL ant	(-3.500, 11.000, -43.000)	(-13.837, -13.690, -37.145)	1274	45.034
POL post	(-6.500, 11.000, -43.000)	(-16.809, -13.998, -36.883)	1274	45.034
CAP med	(-21.000, 28.000, -26.000)	(-18.018, -14.035, -27.744)	6780	59.400
CAP inter	(-21.000, 26.000, 0.000)	(-16.306, -8.575, -1.893)	3381	52.470
CAP lat	(-21.000, 26.000, 26.000)	(-17.045, -8.396, 24.269)	1261	52.554
MLCL Aa	(10.000, 6.000, 40.000)	(10.346, -6.442, 33.917)	200	51.833
MLCL Ap	(8.000, 6.000, 40.000)	(8.365, -6.648, 34.092)	200	49.087
MLCL Pa	(-10.500, 12.500, 38.000)	(-7.165, -8.278, 33.453)	200	40.390
MLCL Pp	(-11.500, 12.500, 38.000)	(-8.156, -8.381, 33.540)	200	40.390
FFL med	(-26.000, 8.000, 23.000)	(-28.225, -3.484, 29.155)	1835	30.466
FFL lat	(-26.000, 8.000, 25.000)	(-28.397, -3.522, 27.163)	1835	30.466
OPL Mp	(-22.000, 8.000, 21.000)	(-20.855, -12.270, -23.516)	3963	56.839
OPL Md	(-24.000, 8.000, 21.000)	(-22.837, -12.485, -23.341)	3963	56.845
OPL lat	(-25.000, 8.000, 21.000)	(-18.530, -11.773, 3.379)	3963	40.831

Table A.1: Geometrical and mechanical characteristics of the ligamentous fibers of M2 and M2s model (right leg). Namely, the ligamentous fibers are: two anteromedial (ACL AMa, ACL AMp), two posterolateral (ACL PLa, ACL PLp) and one isometric (ACL iso) fibers for the ACL; two anterolateral (PCL ALa, PCL ALp), two posteromedial (PCL PMa, PCL PMp) and one isometric (PCL iso) fibers for the PCL; two fibers (MCL ant, MCL post) in the deep boundle, three fibers (MCL prox, MCL inter, MCL dist) in the superficial boundle and one isometric fiber (MCL iso) for the MCL; one anterior (LCL ant), one posterior (LCL post) and one distal (LCL dist) fibers for the LCL; one anterior (PT ant) and one posterior (PT post) fibers for the PT; one anterior (POL ant) and one posterior (POL post) fibers for the POL; one medial (CAP med), one intermedial (CAP inter) and one lateral (CAP lat) fibers for the CAP; two anterior (MLCL Aa, MLCL Ap) and two posterior (MLCL Pa, MLCL Pp) fibers for the MLCL; one lateral (FFL lat) and one medial (FFL med) fibers for the FFL; two medial (OPL Mp, OPL Md) and one lateral (OPL lat) fibers for the OPL.

Appendix B

Appendix B shows the Matlab functions for the loop closure equations of the TF and PF mechanisms, the nonlinear constraints, the objective functions and the equilibrium equations used for the optimization of the TF kinetostatic model in Chapter 3.

```
function [eq]=closure_55(x,fes,side,a,b,l)

% fes is the flexion angle, x(1) is ab/add, x(2) is IE Ű
   Grood and Suntay notation.
% Ges2r builds the tibiofemoral transformation matrix.
% a-R*b-p are the closure equations of the mechanism (Sancisi
    2011)

feaaie=[fes,x(1),x(2)];
R=ges2r(feaaie,side);
P=[x(3);x(4);x(5)];
p=P*ones(1,5);
d=a-R*b-p;
eq=diag(d'*d)-l.^2;

end
```

```
function [C, Ceq]=constr_tf(s,r_lig,r_contact,s0)
% new variables
a(1:3,1)=s(1:3);
a(1:3,2)=s(4:6);
a(1:3,3)=s(7:9);
a(1:3,4)=s(10:12);
a(1:3,5)=s(13:15);
b(1:3,1)=s(16:18);
b(1:3,2)=s(19:21);
b(1:3,3)=s(22:24);
b(1:3,4)=s(25:27);
b(1:3,5)=s(28:30);
l(1:5)=s(31:35);
% previous variables
a0(1:3,1)=s0(1:3);
a0(1:3,2)=s0(4:6);
a0(1:3,3)=s0(7:9);
a0(1:3,4)=s0(10:12);
a0(1:3,5)=s0(13:15);
b0(1:3,1)=s0(16:18);
b0(1:3,2)=s0(19:21);
b0(1:3,3)=s0(22:24);
b0(1:3,4)=s0(25:27);
b0(1:3,5)=s0(28:30);
l0(1:5)=s0(31:35);
```

```
% C<0
% a
C(1)=norm(a(1:3,1)-a0(1:3,1))-r_lig;
C(2)=norm(a(1:3,2)-a0(1:3,2))-r_lig;
C(3)=norm(a(1:3,3)-a0(1:3,3))-r_lig;
C(4)=norm(a(1:3,4)-a0(1:3,4))-r_contact;
C(5)=norm(a(1:3,5)-a0(1:3,5))-r_contact;
% b
C(6)=norm(b(1:3,1)-b0(1:3,1))-r_lig;
C(7)=norm(b(1:3,2)-b0(1:3,2))-r_lig;
C(8)=norm(b(1:3,3)-b0(1:3,3))-r_lig;
C(9)=norm(b(1:3,4)-b0(1:3,4))-r_contact;
C(10)=norm(b(1:3,5)-b0(1:3,5))-r_contact;
% lengths
C(11)=norm(l(1)-l0(1))-2*r_lig; %iso
C(12)=norm(l(2)-l0(2))-2*r_lig; %iso
C(13)=norm(l(3)-l0(3))-2*r_lig; %iso
C(14)=norm(l(4)-l0(4))-2*r_contact; %contact
C(15)=norm(l(5)-l0(5))-2*r_contact; %contact
%
Ceq = [];
%
end


function   err=objfun_tf(s,side,exp_mot,excursions)
% ------------------------
```

```
size_exp_mot=size(exp_mot,2);
matrix_excursions=excursions(2:6)*ones(1,size_exp_mot);
x1=zeros(5,size_exp_mot);
fes=exp_mot(1,:);
aaie_xyz_s=exp_mot(2:6,:);
x0=exp_mot(2:6,1);
% ------------------------
a(1:3,1)=s(1:3);
a(1:3,2)=s(4:6);
a(1:3,3)=s(7:9);
a(1:3,4)=s(10:12);
a(1:3,5)=s(13:15);
b(1:3,1)=s(16:18);
b(1:3,2)=s(19:21);
b(1:3,3)=s(22:24);
b(1:3,4)=s(25:27);
b(1:3,5)=s(28:30);
l(1:5,1)=s(31:35);

% closure equations
indconv=1;
i=0;
opts=optimset('Display','Off','Jacobian','Off');
while i<size(exp_mot,2) && indconv==1
    i=i+1;
    [x1(:,i),~,sisconv]=fsolve(@closure_55,x0,opts,fes(i),
        side,a,b,l);
```

```
    x0=x1(:,i);
    if sisconv<=0
        indconv=indconv*0;
    end
end

% error
if indconv == 0
    err=100000;
else
    err=sum(sum(((x1-aaie_xyz_s)./matrix_excursions).^2));
end

end


function [ eq ] = closure_patella(xp,fes,TF_motion,side,s_p)
%
TFGS_mot = [fes;TF_motion]; % Flexion and the other 5 DoFs of
    femur wrt tibia from the 55 optimized mechanism
%
% fem-tib kinematics
% TFGS_mot is the motion of the TF mechanism
feaaie_tf = TFGS_mot(1:3);
Ptf = [TFGS_mot(4),TFGS_mot(5),TFGS_mot(6)]';
% pat-fem kinematics
feaaie_fp = [xp(1),xp(2),xp(3)];
```

```
Pfp = [xp(4),xp(5),xp(6)]';  % origin of patella in femoral
    anatomical ref system
%
Rfp=ges2r(feaaie_fp,side);
Rtf = ges2r(feaaie_tf(1:3),side);
%
%
% parameters
eta1  =s_p(1,1);
delta1 = s_p(2,1);
Q1 = s_p(3:4,1);
eta2  =s_p(5,1);
delta2=  s_p(6,1);
Q2=  s_p(7:8,1);
C1  =  s_p(9:11,1);
D1 =  s_p(12:14,1);
l_pl =  s_p(15,1);
lambda=  s_p(16,1);
%
n1 = [cos(delta1)*sin(eta1) sin(delta1)*sin(eta1) cos(eta1)
    ]';
n2 = [cos(delta2)*sin(eta2) sin(delta2)*sin(eta2) cos(eta2)
    ]';
%
% closure equations (Sancisi 2011)
% 6 unknows: GS angles and position of patella wrt femur
dist=Rtf*(Rfp*D1+Pfp)+Ptf-C1; % calculate distance in Sta
```

```
eqt(1)=norm(dist)-l_pl;
eqt(2:4)=Rfp*n2-n1;  % the last one (eqt(4) can be neglected
   because there are only 6 unknows
eqt(5:7)=Rfp*[Q2; 0]+Pfp-(lambda*n1+[Q1; 0]);
eq = [eqt(1);eqt(2);eqt(3);eqt(5);eqt(6);eqt(7)];
%
%
%
end


function [ C, Ceq ] = constr_pf(xp,r_ligP,inc_max,dist_max,
   s0_p)

% fmincon: C<0

% xp are the actual parameters
% s0_p are the initial parameters

% s0_p(1:2,1)   = [eta1; delta1];
% s0_p(3:4,1)   = Q1_p(1:2);
% s0_p(5:6,1)   = [eta2; delta2];
% s0_p(7:8,1)   = Q2_p(1:2);
% s0_p(9:11,1)  = C1;
% s0_p(12:14,1) = D1;
% s0_p(15,1)    = l_pl;
% s0_p(16,1)    = lambda;
```

```
C1_actual = xp(9:11);
D1_actual = xp(12:14);

C1 = s0_p(9:11);
D1 = s0_p(12:14);

C(1) = dot(C1_actual-C1,C1_actual-C1)-r_ligP; %ligament
    insertion tib
C(2) = dot(D1_actual-D1,D1_actual-D1)-r_ligP; %ligament
    insertion pat

Q1 = [s0_p(3:4); 0];
Q1_actual = [xp(3:4); 0];
Q2 = [s0_p(7:8); 0];
Q2_actual = [xp(7:8); 0];

n1 = [cos(s0_p(2))*sin(s0_p(1)) sin(s0_p(2))*sin(s0_p(1)) cos
    (s0_p(1))]';
n1_actual = [cos(xp(2))*sin(xp(1)) sin(xp(2))*sin(xp(1)) cos(
    xp(1))]';
n2 = [cos(s0_p(6))*sin(s0_p(5)) sin(s0_p(6))*sin(s0_p(5)) cos
    (s0_p(5))]';
n2_actual = [cos(xp(6))*sin(xp(5)) sin(xp(6))*sin(xp(5)) cos(
    xp(5))]';
```

```
P1 = Q1+n1;
P1_actual = Q1_actual+n1_actual;
P2 = Q2+n2;
P2_actual = Q2_actual+n2_actual;

C(3) = acos(dot(n1,n1_actual))-inc_max; %axis inclination
C(4) = acos(dot(n2,n2_actual))-inc_max; %axis inclination

C(5) = dist_axis(P1,Q1,P1_actual,Q1_actual)-dist_max; %axis
    distance
C(6) = dist_axis(P2,Q2,P2_actual,Q2_actual)-dist_max; %axis
    distance

Ceq = [];

end



function   err=objfun_pf(s_p,exp_motP,mech_motTF,excursionsP,
    side)


y0=exp_motP(1:6,1);
y1=zeros(6,length(exp_motP));
indconv=1;
i=0;
```

```
options=optimset('Display','Off','Jacobian','Off');
fes = mech_motTF(1,:);
TF_motion = mech_motTF(2:6,:);



%
RPAFA = ges2r(exp_motP(1:3,1),1);

% indipendent variable is still TF flexion
while i<size(exp_motP,2) && indconv==1
    i=i+1;
    [y1(:,i),fval,sisconv]=fsolve(@closure_patella,y0,options
        ,fes(i),TF_motion(:,i),side,s_p);
    y0=y1(:,i);
    if sisconv<=0
        indconv=indconv*0;
    end
end

exc_matP=excursionsP*ones(1,length(exp_motP));


        if indconv == 0
            err=200000;
        else
            err=sum(sum(((y1-exp_motP(:,1:size(y1,2)))./
                exc_matP(:,1:size(y1,2))).^2));
        end
```

```
end



function [eq]=equilibrium_M2(x,flex,K,tibia_weight,epsilon_l,
    L_0,contact_parameters,exp_forces,application_points,
    exp_moments,tibia_MC,insertions_Sta,origins_Sfa,side)

% The equilibrium equations of the femur are numerically
    solved at all
% flexion angles and for each loading condition
% Fext and Mext are for a specific test at a specific flexion
     angle
% x contains the GS parameters of the femur wrt tibia (Sfa
    wrt Sta)
% FEMURAL_position = [x(3) x(4) x(5)];
% FEMURAL_orientation = [flex x(1) x(2)];

Rtf_a=eye(4);
feaaie=[flex; x(1); x(2)];
Rtf_a(1:3,1:3)=ges2r(feaaie,side);
Rtf_a(1:3,4)=[x(3); x(4); x(5)];
%invert matrix to have Sta wrt Sfa (Rft_a)
Rft_a=inv(Rtf_a);
```

```
%
    ------------------------------------------------------------------------

%
    ------------------------------------------------------------------------

CL_tib=contact_parameters(1:3);
CL_fem=contact_parameters(4:6);
CM_tib=contact_parameters(7:9);
CM_fem=contact_parameters(10:12);
l0_CL=contact_parameters(13);
l0_CM=contact_parameters(14);
K_contact=contact_parameters(15);
%-----------------------------------------------Initialization
    ------------------------

Flig_Sfa=zeros(length(origins_Sfa),3); %ligament force in Sfa
l_Sfa=zeros(3,length(origins_Sfa));
insertions_Sfa=zeros(3,length(origins_Sfa));
Mlig_Sfa=zeros(length(origins_Sfa),3); %moments that Flig
    generates about the origin of Sfa
Flig_n=zeros(length(origins_Sfa),1); %norm of the force
l_SfaNorm=zeros(length(origins_Sfa),1);
rligSfa=zeros(length(origins_Sfa),3);%moment arm in Sfa
epsilon=zeros(length(origins_Sfa),1);
poleSfa = [0; 0; 0]; %origin of Sfa in Sfa ref system
```

```
%
    ------------------------------------------------------------------

%------------ Compute forces in the ligaments and their
    moments ------------
for i=1:length(origins_Sfa)
    insertions_Sfa(:,i)= Rft_a(1:3,1:3)*insertions_Sta(:,i) +
        Rft_a(1:3,4);
    l_Sfa(:,i) =  origins_Sfa(:,i)- insertions_Sfa(:,i);
    l_SfaNorm(i)=norm(l_Sfa(:,i));
    epsilon(i)=(l_SfaNorm(i)-L_0(i))/L_0(i);
    %  lig forces
    if epsilon(i)>0
        if epsilon(i)<2*epsilon_l
            Flig_n(i) = 0.25*K(i)*epsilon(i)^2/epsilon_l;
        else
            Flig_n(i) = K(i)*(epsilon(i)-epsilon_l);
        end
    else
        Flig_n(i)=0;
    end
     l_Sfa(:,i) = origins_Sfa(:,i) - insertions_Sfa(:,i);
     Flig_Sfa(i,:) = Flig_n(i)*l_Sfa(:,i)/l_SfaNorm(i);
     rligSfa(i,:) = insertions_Sfa(:,i)-poleSfa;
     Mlig_Sfa(i,:) = cross(rligSfa(i,:),Flig_Sfa(i,:));
end
```

```
%
    ------------------------------------------------------------------------

%---------- Compute contact forces and moments ----------
% lateral contact
CL_tib_Sfa=Rft_a(1:3,1:3)*CL_tib+Rft_a(1:3,4);
l_CL = CL_fem-CL_tib_Sfa;
l_CLnorm=norm(l_CL);
epsilonCL=(l_CLnorm-l0_CL)/l_CLnorm;
if epsilonCL<0 % negative epsilon
    F_CL_n = -K_contact*epsilonCL^2;
else
   F_CL_n =0;
end
% Sfa
F_CL_Sfa = F_CL_n*l_CL/l_CLnorm;
rcl_Sfa = CL_tib_Sfa - poleSfa;
Mcl_Sfa = cross(rcl_Sfa,F_CL_Sfa);
%
% medial contact
CM_tib_Sfa=Rft_a(1:3,1:3)*CM_tib+Rft_a(1:3,4);
l_CM = CM_fem-CM_tib_Sfa;
l_CMnorm=norm(l_CM);
epsilonCM=(l_CMnorm-l0_CM)/l_CMnorm;
if epsilonCM>0 % negative epsilon
    F_CM_n = K_contact*epsilonCM^2;
else
```

```
    F_CM_n =0;
end
% Sfa
F_CM_Sfa = F_CM_n*l_CM/l_CMnorm;
rcm_Sfa = CM_tib_Sfa - poleSfa;
Mcm_Sfa = cross(rcm_Sfa,F_CM_Sfa);
%
%---------------------------------- Compute weight force and moment
    ----------------
% Sfa
Fp_Sfa = [0; -(9.81*tibia_weight); 0]; %always along global y
    axis (Sfa y axis)
weight_applicationSfa=Rft_a*[tibia_MC;1]; %transform tibia
   center of mass in Sfa
rp_Sfa=weight_applicationSfa(1:3)-poleSfa;
Mp_Sfa=cross(rp_Sfa,Fp_Sfa);
%
   ------------------------------------------------------------------------------------------------------------------------------------------------------


%-------------------External Forces
   ------------------------------------------------
% Sfa
Fext_Sfa=Rft_a(1:3,1:3)*exp_forces; % exp_forces are
   expressed in Sta reference system
fext_applicationSfa=Rft_a*[application_points;1]; %rotate and
    translate the application point of the force
rext_Sfa=fext_applicationSfa(1:3)-poleSfa;
```

```
Mext_Sfa=cross(rext_Sfa,Fext_Sfa);
%
    ------------------------------------------------------------------------------


%
%-------------------- F counter Sta
    ------------------------------------------------------
%
% find the force that balances MZ, i.e. the moment about the
    femoral mediolateral axis of Sta (fixed flexion)
% Fc is directed as x axis of Sta and it is applied at the
    tibial center of mass
%
% Sfa
exp_moments_Sfa = Rft_a(1:3,1:3)*exp_moments; % exp_moments
    are expressed in Sta reference system
Mfinal_Sfa=[Mlig_Sfa;Mcm_Sfa';Mcl_Sfa';Mp_Sfa';Mext_Sfa';
    exp_moments_Sfa'];
Fc_application_Sfa = Rft_a*[tibia_MC;1];
Fc_direction_Sfa = Rft_a(1:3,1:3)*[1;0;0]; %x axis of Sta
rc_Sfa = Fc_application_Sfa(1:3)-poleSfa;
%from the matrix form of the cross product determine the norm
     of the
%force that balances Mz, i.e. sum(Mfinal_Sfa(:,3))
F_counter_norm = (-sum(Mfinal_Sfa(:,3))/(rc_Sfa(1)*
    Fc_direction_Sfa(2)-rc_Sfa(2)*Fc_direction_Sfa(1)));
F_counter_Sfa = F_counter_norm*Fc_direction_Sfa;
```

```
Mc_Sfa = cross(rc_Sfa,F_counter_Sfa);
%
%
%
%------------------ Final F and M
    ------------------------------------------------------
% Sfa
Ftot_Sfa=[Flig_Sfa;Fp_Sfa';F_CM_Sfa';F_CL_Sfa';F_counter_Sfa
    ';Fext_Sfa'];
F_Sfa =sum(Ftot_Sfa);
M_tot_Sfa=[Mfinal_Sfa;Mc_Sfa'];
M_Sfa =sum(M_tot_Sfa);
%
    ------------------------------------------------------------------------------------


eq =[F_Sfa M_Sfa(1:2)];

end
```

Appendix C

Appendix C shows an example of Abaqus user-written subroutine that instantaneously computes the compressive force to apply to the tibial insert in order to replicate the healthy knee kinematics (Chapter 4).

```
      SUBROUTINE VUAMP(
     *     ampName, time, ampValueOld, dt, nprops, props, nSvars,
     *     svars, lFlagsInfo, nSensor, sensorValues, sensorNames,
     *      jSensorLookUpTable,
     *     AmpValueNew,
     *     lFlagsDefine,
     *     AmpDerivative, AmpSecDerivative, AmpIncIntegral)

       INCLUDE 'VABA_PARAM.INC'

       parameter (iStepTime         = 1,
     *            iTotalTime        = 2,
     *            nTime             = 2)
       parameter (iInitialization    = 1,
     *            iRegularInc       = 2,
     *            ikStep            = 3,
     *            nFlagsInfo        = 3)
       parameter (iComputeDeriv      = 1,
     *            iComputeSecDeriv  = 2,
     *            iComputeInteg     = 3,
     *            iStopAnalysis     = 4,
     *            iConcludeStep     = 5,
     *            nFlagsDefine      = 5)
       dimension time(nTime), lFlagsInfo(nFlagsInfo),
     *           lFlagsDefine(nFlagsDefine),
```

```
*           sensorValues(nSensor),
*           props(nprops),
*           sVars(nSvars)

      character*80 sensorNames(nSensor)
      character*80 ampName
      dimension jSensorLookUpTable(*)


      REAL(8) IErotationsCUR1
      REAL(8) tfIEload
      REAL(8) tfIEloadmax

      REAL(8) tStart
      REAL(8) tEnd
      REAL(8) svars

      REAL(8) outputDT
      REAL(8) controlDT
      REAL(8) subDT
      REAL(8) forceDefault


      REAL(8) IE_Cp, IE_Ci, IE_Cd
      REAL(8) IE_Cpout, IE_Ciout, IE_Cdout, IE_Ctotal

      REAL(8) cie_target cie_curr cie_error, error


      character*256 jobOutDir, jobName, outFile,
*                   targetdata
      integer  lenJobOutDir, lenJobName


      forceDefault = 2000.0
      maxTorque = 20000.0
      stepLength = 0.5

      tfIELoad = vGetSensorValue('IE_LOAD_SENSOR',jSensorLookUpTable,
*                                sensorValues)
```

```
       open(unit=102,
* file= "C:\\Users\\Alessandro\\Desktop\\irene\\implicit\\INT_TORQU
&E_40_RESULTS_explicit.txt",
*  status='UNKNOWN', action='WRITE')

 if (ampName(1:14) .eq. 'AMP_COMPR_USER' ) then

 if ((lFlagsInfo(iInitialization).eq.1).AND.(lFlagsinfo(ikStep).eq.2)) then

       ampValueNew = forceDefault
       svars(1) = ampValueOld
       svars(2) = ampValueNew

    else


       tStart = tim - dt
       tEnd   = tim


         if (lFlagsinfo(ikStep).eq.2) then

          cie_target = maxTorque/stepLength*tim
           tim = time(iStepTime)
           cie_target = 40000*(tim-dt)
           cie_curr = tfIELoad

           error = -(cie_target - cie_curr)


            IE_Cp = -0.000000000001
            IE_Ci = -0.01

           IE_Cpout = IE_Cp*error

           svars(1) = (error*dt) + svars(1)
           IE_Ciout = IE_Ci*(svars(1))
           IE_Ctotal = (IE_Cpout + IE_Ciout)

         svars(2) = forceDefault + forceDefault*IE_Ctotal
```

```
    if (svars(2) .le. 0) then
     svars(2) = 0.0
    end if

       ampValueNew = svars(2)

    WRITE(102,'(F18.6,F18.6,F18.6,F18.6,F18.6,F18.6)')
*error,tim,cie_target,cie_curr, svars(2)


       end if

    end if

 end if


 return
 end
```

Bibliography

[1] E. M. Abdel-Rahman and M. S. Hefzy. Three-dimensional dynamic behaviour of the human knee joint under impact loading. *Med Eng Phys*, 20(4):276–90, 1998.

[2] A. M. Ahmed, A. Hyder, D. L. Burke, and K. H. Chan. In-vitro ligament tension pattern in the flexed knee in passive loading. *J Orthop Res*, 5(2):217–30, 1987.

[3] A. A. Ali, S. S. Shalhoub, A. J. Cyr, C. K. Fitzpatrick, L. P. Maletsky, P. J. Rullkoetter, and K. B. Shelburne. Validation of predicted patellofemoral mechanics in a finite element model of the healthy and cruciate-deficient knee. *J Biomech*, 49(2):302–9, 2016.

[4] F. C. Anderson and M. G. Pandy. Static and dynamic optimization solutions for gait are practically equivalent. *J Biomech*, 34(2):153–61, 2001.

[5] M. A. Baldwin, C. W. Clary, C. K. Fitzpatrick, J. S. Deacy, L. P. Maletsky, and P. J. Rullkoetter. Dynamic finite element knee simulation for evaluation of knee replacement mechanics. *J Biomech*, 45(3):474–83, 2012.

[6] Mark A. Baldwin, Chadd W. Clary, Clare K. Fitzpatrick, James S. Deacy, Lorin P. Maletsky, and Paul J. Rullkoetter. Dynamic finite element knee simulation for evaluation of knee replacement mechanics. *Journal of Biomechanics*, 45:474–483, 2012.

[7] Mark A. Baldwin, Peter J. Laz, Joshua Q. Stowe, and Paul J. Rullkoetter. Efficient probabilistic representation of tibiofemoral soft tissue constraint. *Computer Methods in Biomechanics and Biomedical Engineering*, 12(6):651–659, 2009.

[8] S. A. Banks, M. K. Harman, J. Bellemans, and W. A. Hodge. Making sense of knee arthroplasty kinematics: news you can use. *J Bone Joint Surg Am*, 85-A Suppl 4:64–72, 2003.

[9] M. G. Benedetti, P. Bonato, F. Catani, T. D'Alessio, M. Knaflitz, M. Marcacci, and L. Simoncini. Myoelectric activation pattern during gait in total knee replacement: relationship with kinematics, kinetics, and clinical outcome. *IEEE Trans Rehabil Eng*, 7(2):140–9, 1999.

[10] M. G. Benedetti, F. Catani, T. W. Bilotta, M. Marcacci, E. Mariani, and S. Giannini. Muscle activation pattern and gait biomechanics after total knee replacement. *Clin Biomech*, 18(9):871–6, 2003.

[11] L. Blankevoort and R. Huiskes. Ligament-bone interaction in a three-dimensional model of the knee. *J Biomech Eng*, 113(3):263–9, 1991.

[12] L. Blankevoort, J. H. Kuiper, R. Huiskes, and H. J. Grootenboer. Articular contact in a three-dimensional model of the knee. *J Biomech*, 24(11):1019–31, 1991.

[13] K. H. Bloemker, T. M. Guess, L. Maletsky, and K. Dodd. Computational knee ligament modeling using experimentally determined zero-load lengths. *Open Biomed Eng J*, 6:33–41, 2012.

[14] J. J. Cherian, B. H. Kapadia, S. Banerjee, J. J. Jauregui, K. Issa, and M. A. Mont. Mechanical, anatomical, and kinematic axis in tka: Concepts and practical applications. *Curr Rev Musculoskelet Med*, 7(2):89–95, 2014.

[15] R. R. da Silva, A. A. Santos, J. de Sampaio Carvalho Junior, and M. A. Matos. Quality of life after total knee arthroplasty: systematic review. *Rev Bras Ortop*, 49(5):520–7, 2014.

[16] B. S. Davidson, D. L. Judd, A. C. Thomas, R. L. Myzner, D. G. Eckhoff, and J. E. Stevens-Lapsley. Muscle activation and coactivation during five-time-sit-to-stand movement in patients undergoing total knee arthroplasty. *Journal of Electromyography and Kinesiology*, 23(6):1485–1493, 2013.

[17] J. Dawson, R. Fitzpatrick, D. Murray, and A. Carr. Questionnaire on the perceptions of patients about total knee replacement. *J Bone Joint Surg Br*, 80(1):63–9, 1998.

[18] S. Delp. *Surgery simulation: A computer-graphics system to analyze and design musculoskeletal reconstructions of the lower limb*. PhD thesis, Stanford University, 1990.

[19] S. L. Delp, F. C. Anderson, A. S. Arnold, P. Loan, A. Habib, C. T. John, E. Guendelman, and D. G. Thelen. Opensim: open-source software to create and analyze dynamic simulations of movement. *IEEE Trans Biomed Eng*, 54(11):1940–50, 2007.

[20] J. D. DesJardins, P. S. Walker, H. Haider, and J. Perry. The use of a force-controlled dynamic knee simulator to quantify the mechanical performance of total knee replacement designs during functional activity. *J Biomech*, 33(10):1231–42, 2000.

[21] R. Di Gregorio and V. Parenti-Castelli. A spatial mechanism with higher pairs for modelling the human knee joint. *J Biomech Eng*, 125(2):232–7, 2003.

[22] R. Di Gregorio, V. Parenti-Castelli, J. J. O'Connor, and A. Leardini. Mathematical models of passive motion at the human ankle joint by equivalent spatial parallel mechanisms. *Med Biol Eng Comput*, 45(3):305–13, 2007.

[23] A. Diamantopoulos, Tzurbakis M. Tokis, A., I. Patsopoulos, and A. Georgoulis. The posterolateral corner of the knee: evaluation under microsurgical dissection. *Journal of Arthrostopic and Related Surgery*, 21(7):826âĂŞ833, 2005.

[24] A. Erdemir, T. M. Guess, J. Halloran, S. C. Tadepalli, and T. M. Morrison. Considerations for reporting finite element analysis studies in biomechanics. *J Biomech*, 45(4):625–33, 2012.

[25] H. R. Fallah-Yakhdania, H. Abbasi-Bafghi, O. G. Meijer, S. M. Bruijn, N. van den Dikkenberg, M. G. Benedetti, and J. H. van Dieen. Determinants of co-contraction during walking before and after arthroplasty for knee osteoarthritis. *Clin Biomech*, 27(5):485–494, 2012.

[26] J. D. Feikes, J. J. O'Connor, and A. B. Zavatsky. A constraint-based approach to modelling the mobility of the human knee joint. *J Biomech*, 36(1):125–9, 2003.

[27] C. K. Fitzpatrick, M. A. Baldwin, C. W. Clary, L. P. Maletsky, and P. J. Rullkoetter. Evaluating knee replacement mechanics during adl with pid-controlled dynamic finite element analysis. *Comput Methods Biomech Biomed Engin*, 17(4):360–9, 2014.

[28] M. Forlani, N. Sancisi, M. Conconi, and V. Parenti-Castelli. A new test rig for static and dynamic evaluation of knee motion based on a cable-driven parallel manipulator loading system. *Meccanica*, pages 11–11, 2015.

[29] R. Franci, V. Parenti-Castelli, C. Belevedere, and A. Leardini. A new one-dof fully parallel mechanism for modelling passive motion at the human tibiotalar joint. *Journal of Biomechanics*, 42:1403ï£¡–1408, 2009.

[30] R. Franci and N. Parenti-Castelli; V., Sancisi. A three-step procedure for the modelling of human diarthrodial joints. *International Journal of Mechanics and Control*, 10(2), 2009.

[31] M. T. Galloway, E. S. Grood, J. N. Mehalik, M. Levy, S. C. Saddler, and F. R. Noyes. Posterior cruciate ligament reconstruction. an in vitro study of femoral and tibial graft placement. *Am J Sports Med*, 24(4):437–45, 1996.

[32] F.G. Girgis, J.L. Marshall, and A. Monajem. The cruciate ligaments of the knee joint. anatomical, functional and experimental analysis. *Clinical Orthopaedics and Related Research*, 106:216–231, 1975.

[33] A. C. Godest, M. Beaugonin, E. Haug, M. Taylor, and P. J. Gregson. Simulation of a knee joint replacement during a gait cycle using explicit finite element analysis. *J Biomech*, 35(2):267–75, 2002.

[34] J.P. Goldblatt and J.C Richmond. Anatomy and biomechanics of the knee. *Operative Techniques in Sports Medicine*, 11(3):172–186, 2003.

[35] J. Goodfellow and J. O'Connor. The mechanics of the knee and prosthesis design. *J Bone Joint Surg Br*, 60-B(3):358–69, 1978.

[36] O. Gothesen, B. Espehaug, L. Havelin, G. Petursson, S. Lygre, P. Ellison, G. Hallan, and O. Furnes. Survival rates and causes of revision in cemented primary total knee replacement: a report from the norwegian arthroplasty register 1994-2009. *Bone Joint J*, 95-B(5):636–42, 2013.

[37] H. Gray. *Anatomy of the Human Body*. Lea and Febiger, Philadelphia, PA, 1985.

[38] J.E. Greenleaf. The anatomy and biomechanics of the lateral aspect of the knee. *Operative Techniques in Sports Medicine*, 4(3):141–147, 1996.

[39] C. J. Griffith, C. A. Wijdicks, R. F. LaPrade, B. M. Armitage, S. Johansen, and L. Engebretsen. Force measurements on the posterior oblique ligament and superficial medial collateral ligament proximal and distal divisions to applied loads. *Am J Sports Med*, 37(1):140–8, 2009.

[40] Chad J. Griffith, Coen A. Wijdicks, Robert F. La Prade, Bryan M. Armitage, Steinar Johansen, and Lars Engebretsen. Force measurements on the posterior oblique ligament and superficial collateral ligament proximal and distal divisions to applied loads. *The American Journal of Sports Medicine*, 10(10):1–9, 2008.

[41] E. S. Grood, S. F. Stowers, and F. R. Noyes. Limits of movement in the human knee. effect of sectioning the posterior cruciate ligament and posterolateral structures. *J Bone Joint Surg Am*, 70(1):88–97, 1988.

[42] E. S. Grood and W. J. Suntay. A joint coordinate system for the clinical description of three-dimensional motions: application to the knee. *J Biomech Eng*, 105(2):136–44, 1983.

[43] T. M. Guess and A. Stylianou. Simulation of anterior cruciate ligament deficiency in a musculoskeletal model with anatomical knees. *The Open Biomedical Engineering Joirnal*, 6(23):23–32, 2012.

[44] Y. Guo, X. Zhang, A. Meiwen, and W. Chen. Determination of quadriceps forces in squat and its application in contact pressure analysis of knee joint. *Acta Mechanica Solida Sinica*, 25(1):53–60, 2011.

[45] H. Haider and P. S. Walker. Measurements of constraint of total knee replacement. *J Biomech*, 38(2):341–8, 2005.

[46] J. P. Halloran, A. J. Petrella, and P. J. Rullkoetter. Explicit finite element modeling of total knee replacement mechanics. *J Biomech*, 38(2):323–31, 2005.

[47] S. Harish, P. O'Donnell, D. Connell, and A. Saifuddin. Imaging of the posterolateral corner of the knee. *Clin Radiol*, 61(6):457–66, 2006.

[48] C. D. Harner, G. H. Baek, T. M. Vogrin, G. J. Carlin, S. Kashiwaguchi, and S. L. Woo. Quantitative analysis of human cruciate ligament insertions. *Arthroscopy*, 15(7):741–9, 1999.

[49] M.S. Hefzy and T.D.V Cooke. Review of knee models: 1996 update. *Applied Mechanics Reviews*, 49(10-2):187–193, 1996.

[50] H. H. Hsieh and P. S. Walker. Stabilizing mechanisms of the loaded and unloaded knee joint. *J Bone Joint Surg Am*, 58(1):87–93, 1976.

[51] H. Huber and C. Mattheck. The cruciate ligaments and their effect on the kinematics of the human knee. *Med Biol Eng Comput*, 26(6):647–54, 1988.

[52] J. C. Hughston and A. F. Eilers. The role of the posterior oblique ligament in repairs of acute medial (collateral) ligament tears of the knee. *J Bone Joint Surg Am*, 55(5):923–40, 1973.

[53] K. E. Keenan, S. Pal, D. P. Lindsey, T. F. Besier, and G. S. Beaupre. A viscoelastic constitutive model can accurately represent entire creep indentation tests of human patella cartilage. *Journal of Applied Biomechanics*, 29(3):292–302, 2013.

[54] A.M. Kiapour, V. Kaul, A. Kiapour, C.E. Quatman, S.C. Wonderman, T.E. Hewett, C.K. Demetropoulos, and V.K. Goel. The effect of ligament modeling techniques on knee joint kinematics: a finite element study. *Applied Mathematics*, 4(5A):91–97, 2013.

[55] E. Kondo, A. M. Merican, K. Yasuda, and A. A. Amis. Biomechanical analysis of knee laxity with isolated anteromedial or posterolateral bundle-deficient anterior cruciate ligament. *Arthroscopy*, 30(3):335–43, 2014.

[56] S. Kurtz, K. Ong, E. Lau, F. Mowat, and M. Halpern. Projections of primary and revision hip and knee arthroplasty in the united states from 2005 to 2030. *J Bone Joint Surg Am*, 89(4):780–5, 2007.

[57] R. F. LaPrade, A. H. Engebretsen, T. V. Ly, S. Johansen, F. A. Wentorf, and L. Engebretsen. The anatomy of the medial part of the knee. *J Bone Joint Surg Am*, 89(9):2000–10, 2007.

[58] R. F. LaPrade, T. V. Ly, F. A. Wentorf, and L. Engebretsen. The posterolateral attachments of the knee: a qualitative and quantitative morphologic analysis of the fibular collateral ligament, popliteus tendon, popliteofibular ligament, and lateral gastrocnemius tendon. *Am J Sports Med*, 31(6):854–60, 2003.

[59] R. F. LaPrade, P. M. Morgan, F. A. Wentorf, S. Johansen, and L. Engebretsen. The anatomy of the posterior aspect of the knee. an anatomic study. *J Bone Joint Surg Am*, 89(4):758–64, 2007.

[60] Z. F. Lerner, M. S. DeMers, S. L. Delp, and R. C. Browning. How tibiofemoral alignment and contact locations affect predictions of medial and lateral tibiofemoral contact forces. *J Biomech*, 48(4):644–50, 2015.

[61] G. Li, J. Gil, A. Kanamori, and S. L. Woo. A validated three-dimensional computational model of a human knee joint. *J Biomech Eng*, 121(6):657–62, 1999.

[62] E. Luger, S. Sathasivam, and P. S. Walker. Inherent differences in the laxity and stability between the intact knee and total knee replacements. *The Knee*, 4(1):7–14, 1997.

[63] H. L. Lunderberg, I. L. Rojas, and Wimmer; M. A. Foucher; K. C. Comparison of antagonist muscle activity during walking between total knee replacement and control subjects using unnormalized electromyography. *The Journal of Arthroplasty*, 1(1-9), 2016.

[64] R. F. La Prade, T. S. Bollom, F. A. Wentorf, N. J. Wills, and K. Meister. Mechanical properties of the posterolateral structures of the knee. *American journal of sports medicine*, 33(9):1386–1391, 2005.

[65] Claude T. Moorman III and R. F. La Prade. Anatomy and biomechanics of the posterolateral corner of the knee. *The Journal of Knee Surgery*, pages 137–145, 2005.

[66] G. McCluskey and T.A Blackburn. Classification of knee ligament instabilities. *Journal of the American Physical Therapy Association*, 60(12):1575–1577, 1980.

[67] T. Minowa, G. Murakami, H. Kura, D. Suzuki, S. H. Han, and T. Yamashita. Does the fabella contribute to the reinforcement of the posterolateral corner of the knee by inducing the development of associated ligaments? *J Orthop Sci*, 9(1):59–65, 2004.

[68] K. Mitchell, S. Banks, J. Rawlins, S. A. Wood, and W. A. Hodge. Strength of intrinsically stable tka during stair-climbing. 51st Annual Meeting of the Orthopaedic Research Society, 2005.

[69] R. L. Mizner and L. Snyder-Mackler. Altered loading during walking and sit-to-stand is affected by quadriceps weakness after total knee arthroplasty. *J Orthop Res*, 23(5):1083–90, 2005.

[70] F. Moissenet, L. Cheze, and R. Dumas. A 3d lower limb musculoskeletal model for simultaneous estimation of musculo-tendon, joint contact, ligament and bone forces during gait. *J Biomech*, 47(1):50–8, 2014.

[71] T. J. Mommersteeg, L. Blankevoort, R. Huiskes, J. G. Kooloos, and J. M. Kauer. Characterization of the mechanical behavior of human knee ligaments: a numerical-experimental approach. *J Biomech*, 29(2):151–60, 1996.

[72] T. J. A. Mommersteeg, L. Blankevoort, R. Huiskes, J. G. M. Kooloos, and J. M. G. Kauer. Characterization of the mechanical behavior of human knee ligaments: a numerical-experimental approach. *Journal of Biomechanics*, 29(2):151–160, 1996.

[73] V. C. Mow, G. A. Ateshian, and R. L. Spilker. Biomechanics of diarthrodial joints: a review of twenty years of progress. *J Biomech Eng*, 115(4B):460–7, 1993.

[74] D. Nam, R. M. Nunley, and R. L. Barrack. Patient dissatisfaction following total knee replacement: a growing concern? *Bone Joint J*, 96-B(11 Supple A):96–100, 2014.

[75] A. Navacchia, C. A. Myers, P. J. Rullkoetter, and K. B. Shelburne. Prediction of in vivo knee joint loads using a global probabilistic analysis. *J Biomech Eng*, 138(3), 2016.

[76] P. C. Noble, M. J. Gordon, J. M. Weiss, R. N. Reddix, M. A. Conditt, and K. B. Mathis. Does total knee replacement restore normal knee function? *Clin Orthop Relat Res*, (431):157–65, 2005.

[77] J. J. O'Connor, T. L. Shercliff, D. FitzPatric, E. Biden, and J. W. Goodfellow. Mechanics of the knee. In D. Daniel et al., editor, *Knee Ligaments: Structures, Function, Injury and Repair*, pages 201–237. Raven Press, 1990.

[78] A. Ottoboni, V. Parenti-Castelli, N. Sancisi, C. Belvedere, and A. Leardini. Articular surface approximation in equivalent spatial parallel mechanism models of the human knee joint: an experiment-based assessment. *Proc Inst Mech Eng H*, 224(9):1121–32, 2010.

[79] M. G. Pandy and K. B. Shelburne. Theoretical analysis of ligament and extensor-mechanism function in the acl-deficient knee. *Clin Biomech*, 13(2):98–111, 1998.

[80] M.G. Pandy, K. Sasaki, and S. Kim. A three-dimensional musculoskeletal model of the human knee joint. part 1: theoretical construction. *Computer Methods in Biomechanics and Biomedical Engineering*, 1:87–108, 1997.

[81] V. Parenti-Castelli and R. Di Gregorio. *Parallel mechanisms applied to the human knee passive motion simulation.* Advances in Robot Kinematics. 2000.

[82] V. Parenti-Castelli and N. Sancisi. Synthesis of spatial mechanisms to model human joints. In M. McCarthy, editor, *21th Century Kinematics*, pages 49–84. Springer, 2012.

[83] E. Pena, B. Calvo, M. A. Martinez, and M. Doblare. A three-dimensional finite element analysis of the combined behavior of ligaments and menisci in the healthy human knee joint. *J Biomech*, 39(9):1686–701, 2006.

[84] W. Petersen, S. Loerch, S. Schanz, M. Raschke, and T. Zantop. The role of the posterior oblique ligament in controlling posterior tibial translation in the posterior cruciate ligament-deficient knee. *Am J Sports Med*, 36(3):495–501, 2008.

[85] A. Race and A. A. Amis. Pcl reconstruction: in vitro biomechanical comparison of 'isometric' versus single and double-boundled 'anatomic' grafts. *Journal of Bone and Joint Surgery*, 80B(1):173–179, 1998.

[86] H. H. Rachmat, D. Janssen, T. van Tienen, R. L. Diercks, B. Verkerke, and N. Verdonschot. Material properties of the human posterior knee capsule. *Journal of Biomechanics*, 45(S1):S380, 2012.

[87] J. A. Reinbolt, M. D. Fox, M. H. Schwartz, and S. L. Delp. Predicting outcomes of rectus femoris transfer surgery. *Gait and Posture*, 30(1):100–5, 2009.

[88] V. I. Roberts, C. N. Esler, and W. M. Harper. A 15-year follow-up study of 4606 primary total knee replacements. *J Bone Joint Surg Br*, 89(11):1452–6, 2007.

[89] J. R. Robinson, A. M. Bull, and A. A. Amis. Structural properties of the medial collateral ligament complex of the human knee. *J Biomech*, 38(5):1067–74, 2005.

[90] N. Sancisi, B. Baldisserri, V. Parenti-Castelli, C. Belvedere, and A. Leardini. One-degree-of-freedom spherical model for the passive motion of the human ankle joint. *Med Biol Eng Comput*, 52(4):363–73, 2014.

[91] N. Sancisi and V. Parenti-Castelli. A 1-dof parallel spherical wrist for the modelling of the knee passive motion. *Mechanism and Machine Theory*, 45:658–665, 2010.

[92] N. Sancisi and V. Parenti-Castelli. On the role of ligaments in the guidance of the human knee passive motion. In *Proceedings of Euromech Colloquium 511, Ponta Delgada, Azores, Portugal, March 09–12*, pages 1–9, 2011.

[93] N. Sancisi and V. Parenti-Castelli. A sequentially-defined stiffness model of the knee. *Mechanism and Machine Theory*, 46:1920–1928, 2011.

[94] S. Sathasivam and P. S. Walker. A computer model with surface friction for the prediction of total knee kinematics. *J Biomech*, 30(2):177–84, 1997.

[95] S. Sathasivam and P. S. Walker. The conflicting requirements of laxity and conformity in total knee replacement. *J Biomech*, 32(3):239–47, 1999.

[96] L. C. Schmitt and K. S. Rudolph. Influences on knee movement strategies during walking in persons with medial knee osteoarthritis. *Arthritis Rheum*, 57(6):1018–26, 2007.

[97] K. B. Shelburne and M. G. Pandy. A musculoskeletal model of the knee for evaluating ligament forces during isometric contractions. *J Biomech*, 30(2):163–76, 1997.

[98] K. B. Shelburne, M. R. Torry, and M. G. Pandy. Muscle, ligament, and joint-contact forces at the knee during walking. *Medicine and Science in Sports and Exercise*, 37(11):1948–1956, 2005.

[99] M. A. Sherman, A. Seth, and S. L. Delp. What is a moment arm? calculating muscle effectiveness in biomechanical models using generalized coordinates. *Proc ASME Des Eng Tech Conf*, 2013, 2013.

[100] I. Sintini, N. Sancisi, and V. Parenti Castelli. A sequentially-defined kinetostatic model of the knee with anatomical surfaces. In *Interdisciplinary Applications of Kinematics*, volume 26 of *Mechanism and Machine Science*, pages 109–117.

[101] G. C. Terry and R. F. La Prade. The posterolateral aspect of the knee. Anatomy and surgical approach. *American Journal of Sports Medicine*, 24(6):732–739, 1996.

[102] D. G. Thelen, F. C. Anderson, and S. L. Delp. Generating dynamic simulations of movement using computed muscle control. *J Biomech*, 36(3):321–8, 2003.

[103] D. G. Thelen, K. Won Choi, and A. M. Schmitz. Co-simulation of neuromuscular dynamics and knee mechanics during human walking. *J Biomech Eng*, 136(2):021033, 2014.

[104] A. C. Thomas, D. L. Judd, B. S. Davidson, D. G. Eckhoff, and J. E. Stevens-Lapsley. Quadriceps/hamstrings co-activation increases early after total knee arthroplasty. *The Knee*, 21(6):1115–1119, 2014.

[105] P. S. Walker. Application of a novel design method for knee replacements to achieve normal mechanics. *Knee*, 21(2):353–8, 2014.

[106] P. S. Walker. The design and pre-clinical evaluation of knee replacements for osteoarthritis. *J Biomech*, 48(5):742–9, 2015.

[107] P. S. Walker, J. S. Rovick, and D. D. Robertson. The effects of knee brace hinge design and placement on joint mechanics. *J Biomech*, 21(11):965–74, 1988.

[108] D. R. Wilson, J. D. Feikes, and J. J. O'Connor. Ligaments and articular contact guide passive knee flexion. *J Biomech*, 31(12):1127–36, 1998.

[109] D. R. Wilson, J. D. Feikes, A. B. Zavatsky, and J. J. O'Connor. The components of passive knee movement are coupled to flexion angle. *J Biomech*, 33(4):465–73, 2000.

[110] D.R. Wilson and J.J.: OâĂŹConnor. A three-dimensional geometric model of the knee for the study of joint forces in gait. *Gait and Posture*, 5(2):108–115, 1997.

[111] H. Xu, D. Bloswick, and Merryweather. An improved opensim gait model with multiple degrees of freedom knee joint and knee ligaments. *Computer Methods in Biomechanics and Biomedical Engineering*, 18(11):1216–1224, 2014.

[112] G. T. Yamaguchi and F. E. Zajac. A planar model of the knee joint to characterize the knee extensor mechanism. *J Biomech*, 22(1):1–10, 1989.

[113] F. E. Zajac. Muscle and tendon: properties, models, scaling, and application to biomechanics and motor control. *Crit Rev Biomed Eng*, 17(4):359–411, 1989.